



Durham E-Theses

Structural and electrical properties of magnesium oxide powders

Johnson, A P

How to cite:

Johnson, A P (1986) *Structural and electrical properties of magnesium oxide powders*, Durham theses, Durham University. Available at Durham E-Theses Online: <http://etheses.dur.ac.uk/7037/>

Use policy

The full-text may be used and/or reproduced, and given to third parties in any format or medium, without prior permission or charge, for personal research or study, educational, or not-for-profit purposes provided that:

- a full bibliographic reference is made to the original source
- a [link](#) is made to the metadata record in Durham E-Theses
- the full-text is not changed in any way

The full-text must not be sold in any format or medium without the formal permission of the copyright holders.

Please consult the [full Durham E-Theses policy](#) for further details.

Structural and Electrical Properties
of Magnesium Oxide Powders.

by

A. P. Johnson, B.Sc. (Dunelm)
St. Mary's College.

A thesis submitted to the University of Durham
in candidature for the degree of Master of Science

November, 1986

The copyright of this thesis rests with the author.
No quotation from it should be published without
his prior written consent and information derived
from it should be acknowledged.



19 JUL 1987

To: A.F.J, F.A.J.

CONTENTS

	Pages
ACKNOWLEDGEMENTS	i
ABSTRACT	ii
CHAPTER 1 INTRODUCTION	1
CHAPTER 2 X-RAY CHARACTERISATION OF MgO POWDERS	9
2.1 Crystal Structure of MgO	9
2.2 X-Ray Diffractometry	12
2.3 EDAX analysis	15
2.3.1 Techniques	15
2.3.2 Results	16
2.4 Detailed Analysis of XRD Data	17
2.4.1 Method of Approach	17
2.4.2 Results and Discussion	19
CHAPTER 3 MAGNETIC SUSCEPTIBILITY STUDIES	24
3.1 The Gouy Balance Technique	25
3.2 Experimental Techniques	28
3.3 Results for Pure MgO	29
3.4 Results from Commercial MgO Powders	30
3.4.1 Results from fusion stage	31
3.4.2 Results from post-fusion stages of processing	33
3.5 Results from Chromium Doped MgO and Magnesiochromite	36
3.6 Results from Iron Doped MgO and Magnesioferrite/MgO Mixtures	38
3.7 Further Studies using the Gouy Magnetometer	44

	Pages	
CHAPTER 4	PRINCIPLES OF ELECTRON SPIN RESONANCE	50
	4.1 General	51
	4.2 Theory of the Single Free Electron	53
	4.3 The Paramagnetic Ion in the Crystalline Environment	55
	4.4 The Spin Hamiltonian and Energy Levels	56
	4.5 Microwave Power Absorption	59
	4.6 Paramagnetic Relaxation	60
	4.7 Experimental	61
	4.8 Reference Spectra	63
	4.8.1 ESR spectra of Fe/MgO	63
	4.8.2 ESR spectra of Cr/MgO	66
	4.8.3 ESR spectrum Mn/MgO	67
	4.8.4 ESR spectra of Ni/MgO	68
	4.9 Conclusions	69
CHAPTER 5	ELECTRON SPIN RESONANCE - RESULTS AND DISCUSSION	72
	5.1 Method of Identifying Impurities	72
	5.2 Results from Commercial MgO Powders	73
	5.3 Results from Chromium Doped MgO and Magnesiochromite	76
	5.4 Results from Iron Doped MgO	77
CHAPTER 6	DISCUSSION AND CONDITIONS	80
	6.1 Magnetic Phases in MgO	80
	6.2 Electrical Properties of MgO	83
	6.2.1 Conductivity mechanisms in single crystals	83
	6.2.2 Measurements on MgO powders	88
	6.2.3 The dielectric properties of magnesioferrite	92
	6.3 Suggestions for further work	93
APPENDIX		95

ACKNOWLEDGEMENTS

I shall always be most grateful to Dr. J.S.Thorp without whom this work would not have been started, continued or completed. He has given time, encouragement and accurate and careful guidance freely, and I have relied on his generosity and patience throughout.

My thanks are due to Professor G.C.Roberts and latterly to Dr.J.Woods for allowing me to use the facilities of the Department, and to Mr. C.Savage, Mr. W. Mounsey and Mr. P.Richardson for technical help.

I am grateful to Thermal Syndicate Limited for financial support and to Mr.J.Allen and Mr.J.Dodd for their time and assistance. I should also like to thank my present employers, the partners of Abel and Imray for encouragement and practical help and to Mrs.S.Mellanby for typing the manuscript.

A. P. Johnson,
September, 1986.

ABSTRACT

Commercial magnesium oxide powders have been examined before and after electrofusion and subsequent stages of the manufacturing process to evaluate the effect of these stages on the impurity content. Particular emphasis has been paid to the identification of magnetic phases as some of these have been found to have deleterious effects on the insulating properties of the powder which is widely used, as "electrical grade magnesia" as the refractory dielectric filler in heating elements.

X-ray diffractometry was used for structural phase analysis supplemented by energy dispersive analysis by X-rays to aid interpretation of the more complex X-ray diffraction results. Iron, magnesioferrite, manganese oxide, aluminium silicate, iron II oxide (and many other impurities at less than 2% abundance) were detected. Reference standards were also obtained from powdered doped MgO single crystals of known composition. Measurements of magnetic susceptibility, made with a Gouy magnetometer, showed that during the fusion stage of the commercial process, the magnetic impurities diffused towards the centre of the melt, accumulating in a distinct band bounded on either side by less magnetic material, ($K \sim + 450 \text{ J T}^{-2} \text{ m}^{-3}$ for the former, $K \sim + 50 \text{ J T}^{-3} \text{ m}^{-3}$ for the latter compared with $-20 \text{ J T}^{-2} \text{ m}^{-3}$ for pure MgO). Control experiments were made on heat treated Fe/MgO, obtained from ground single crystals, to establish details of the formation and properties of the magnesio-ferrite phase precipitated in the MgO matrix. These studies also established that in the commercial powders the annealing type heat treatment increased the susceptibility of the resultant material whilst the quenching-type heat treatment and especially the magnetic separation stages reduced it.

Electron Spin Resonance spectra of the commercial samples showed a broad line (80 mT, $g \approx 2.00$) superimposed on the isolated ion lines for Cr^{3+} and Mn^{2+} . No evidence of Fe^{3+} transitions was observed. Comparison with single crystal reference spectra for Fe/MgO, Cr/MgO and Mn/MgO showed that the broad line was very similar to that seen for heat treated Fe/MgO, especially as regards its dependence on iron concentration and heat treatment. Further studies using the Gouy Magnetometer confirmed that the magnetic phases present in the commercial powders were not purely paramagnetic and strongly indicated, in support of the ESR data, that superparamagnetic or ferrimagnetic phenomena were involved.

A review is given of measurements and data on the dielectric properties and conductivity mechanisms in MgO, Fe/MgO and Cr/MgO and some suggestions are made for future work.

CHAPTER ONEINTRODUCTION

Magnesium oxide is a material whose properties make it attractive in at least three rather distinct senses, first in its own right, as an engineering material, secondly as a constituent used in the preparation of other materials, and thirdly as a medium in which many of the phenomena and problems of solid state physics and chemistry may be encountered and studied. Direct applications of magnesium oxide have for many years included its use as the insulator in heating elements, (Niedhart and Scheider, 1.1), where the combination of good electrical insulation properties at high temperatures and the favourable flow characteristics of the powdered material cannot easily be matched by any alternative material ; over the past three decades its uses have been extended to the nuclear power industry which may impose the additional requirement of compatibility with radiation conditions. From the second point of view one may mention the use of magnesia in glass manufacture, where one of the most important groups of glasses are those based on the magnesia - alumina - silica glass forming system, leading for example to the more specialised groups of cordierite glasses and glass-ceramics for electronic insulators and dielectrics. In this area the amount of magnesia added is high, as it is a major constituent of the glass. In other engineering materials, particularly those formed by sintering or hot-pressing, e.g. silicon nitride or the sialons, a small amount of magnesia may be added to facilitate densification, leading to increased strength of the product. In the third sense, that of examining physical phenomena, magnesium oxide owes some of its attractiveness to the facts



that it can be obtained in good quality single crystal form both pure and doped with a variety of transition group or rare earth group ions and that it possesses a relatively simple cubic crystal structure which is a beneficial feature in the interpretation of experimental data.

The most widely used technique for the production of both high purity single crystal material and for commercial magnesia powders is carbon arc fusion. Although there are detailed differences in the design and scale of the furnaces involved they all operate on the same basic principle, namely that an arc is struck (between graphite electrodes) so as to make a pool of molten magnesium oxide in the centre of a larger volume of powdered magnesia which in turn is held in a steel or stainless steel water cooled container. For the growth of high purity and doped magnesium oxide single crystals crystal growth apparatus similar to that shown in Fig 1.1 has generally been used, (Abraham, Butler and Chen 1.1, W.C.Spicer Ltd., 1.3). This comprises a water cooled stainless steel tub with a hollow depression in the form of an inverted tetrahedron with chamfered edges and a truncated bottom. Three graphite electrodes are inserted parallel to the chamfered edges (only one being shown in Fig 1.1). Power for the arc was obtained from a three phase supply controlled by a saturable reactor and to initiate operation of the furnace a fourth, electrically inactive, graphite rod serving as a bridging electrode provides a convenient means of ensuring good initial contact between adjacent electrodes. This type of furnace is suitable for melts of mass up to a few kilogrammes and has a long history of use in the preparation of high quality, optically clear crystals such as magnesium oxide, calcium oxide and zirconia in sizes of up to approximately 25 cc. During fusion, growth of MgO crystals was started at arc powers of 50 kW for about an hour and a half, which formed an aggregate of large single crystals beneath the arc ; the power

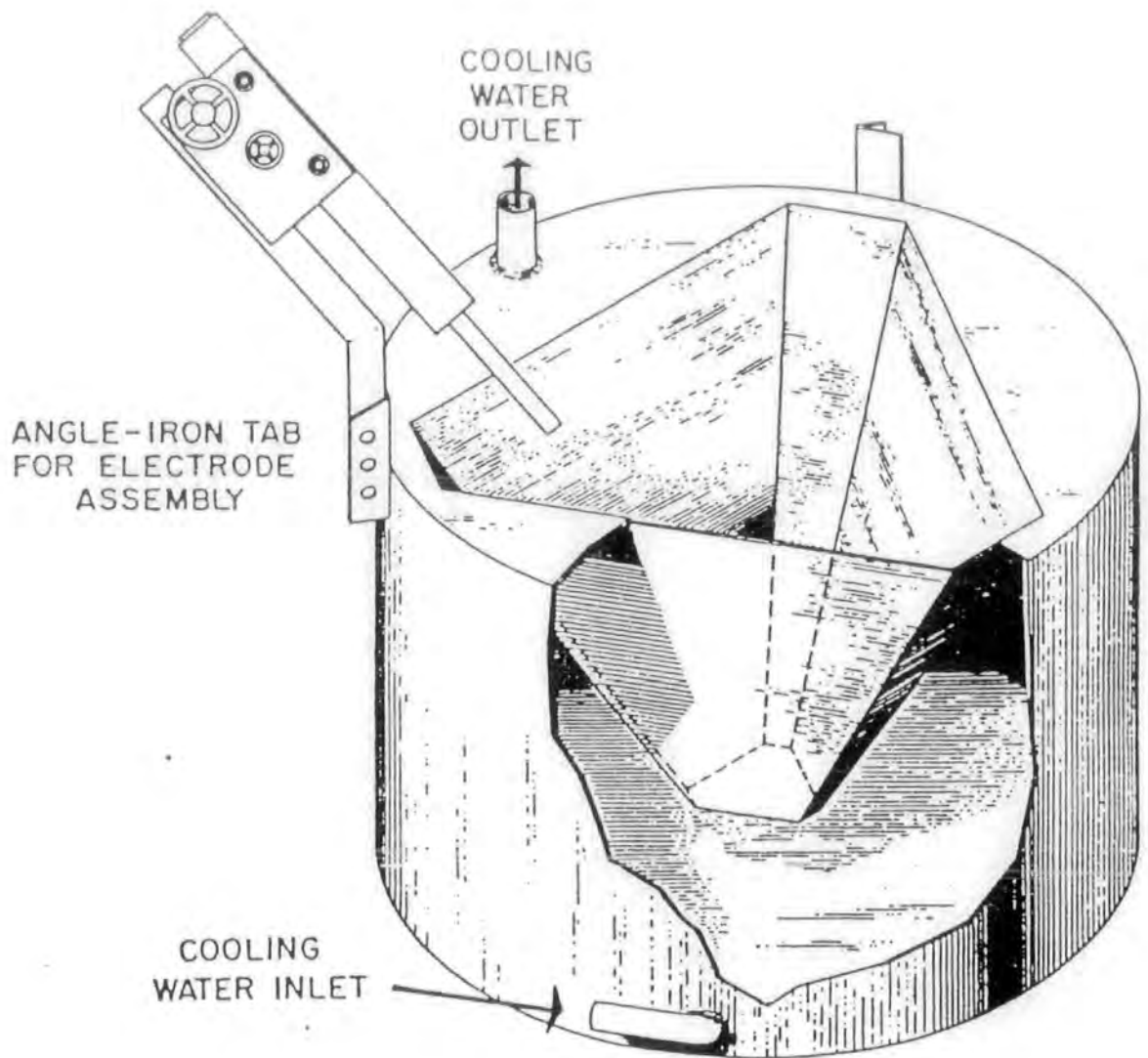


Figure 1.1. Schematic drawing of the stainless-steel water-cooled tub for the three-phase arc-fusion apparatus. Only one of the three graphite electrode assemblies is shown inserted.

was then lowered and maintained at about 20 kW for about ten hours providing an opportunity for bubbles (a source of cloudiness in early attempts to grow clear single crystals) to diffuse to exterior surfaces. It is possible by these methods also to produce doped magnesium oxide single crystals and quite a wide variety containing either the rare earth ions or the transition group ions can be obtained from suppliers. An illustration of part of this range is given by Table 1.1 which reproduces a section of W.C.Spicers catalogue of single crystals of magnesia and calcia ; this Table also shows that two accepted methods of analysis at these doping levels (of up to several hundred ppm) are atomic emission spectroscopy and x-ray fluorescent analysis, further reference to both of which will be made later. There is a very large literature on various aspects of solid state physics which have been investigated using this type of pure or specially doped single crystal. Two areas of these extensive researches are of particular relevance to this thesis - they are the literature on electron spin resonance in magnesium oxide (e.g. Thorp et al, 1.4, 1.5, 1.6, 1.7) and the published papers on the conductivity mechanisms, permittivity and dielectric loss of iron doped and chromium doped magnesium oxide (Thorp et al, 1.8, 1.9). More detailed reference to these topics is made as they are discussed in greater depth in following chapters.

The commercial manufacture of electrical grade powdered magnesia presents a very different picture despite its being based, like single crystal production, on the arc fusion process. As regards the fusion stage, the main difference perhaps is one of scale since it is not uncommon for quantities of up to 20 tons to be fused in a single operation using powers of up to several megawatts. Fig 1.2 gives an impression of a large scale fusion technique (Stoyell et al, 1.10). An

MgO	4N	Clear White	Ni	370	A
MgO	4N	Clear White	Ni	130	A
MgO	4N	Pale Green with 'cloud'	Ni	1,400	X
MgO	4N	Clear to Pink	Mn	840	X
MgO	4N	Deep Amber	Mn	1,400	X
MgO	4N	Dark Amber	Mn	2,900	X
MgO	4N	Amber	Mn	4,800	X
MgO	4N	"	Mn	3,100	X
MgO	4N	Dark Blue	Ti	2,900	-
MgO	3N	Clear Green	V	450	X
MgO	4N	Black	V	15,000	X
MgO	4N	Olive Green	V	1,000	X
MgO	4N	Medium to Dark Green, transparent	Cr	740	X
MgO	4N	Green Clear	Cr	800	A
MgO	4N	Green Clear	Cr	1,300	A
MgO	4N	Dark Green	Cr	7,400	X
MgO	4N	" "	Cr	15,100	X
MgO	4N	" "	Cr	3,600	X
MgO	4N	" "	Cr	5,000	X
MgO	4N	" "	Cr	6,200	X
MgO	4N	" "	Cr	9,500	X
MgO	4N	Green Transparent	Cr	760	X
MgO	4N	Very Dark Green	Cr	4,400	X
MgO	4N	" " "	Cr	4,200	X
MgO	3N	Green Clear, some crystals banded	Fe & V	150 & 300	C
MgO	3N	Light Amber	Fe	300	C
MgO	3N	Amber	Fe	710	X
MgO	4N	Clear Pale Yellow	Fe	310	X
MgO	4N	Clear Amber to Green	Fe	2,300	X
MgO	4N	Dark Clear Green	Fe	4,300	X
MgO	4N	" " "	Fe	8,500	X
MgO	4N	Dark Brown to Black	Fe	11,900	X
MgO	4N	" " "	Fe	12,900	X
MgO	4N	Pale Green	Fe & Cr	2,900 & 1,000	X
MgO	4N	Dark Green	Fe & Cr	1,900 & 800	X
MgO	4N	Pale Green	Fe & Cr	1,900 & 1,000	X
MgO	4N	Green	Fe & Cr	1,500 & 1,100	X
MgO	4N	"	Fe & Cr	2,100 & 800	X
MgO	4N	Clear Dark Brown	Fe & Cr	500 & 1,500	X
MgO	4N	" " "	Fe & Cr	1,700 & 3,000	X
MgO	4N	" " "	Fe & Cr	2,300 & 5,300	X
MgO	4N	" " "	Fe & Cr	1,100 & 2,900	X
MgO	4N	Clear Pink	Co	310	A
MgO	4N	Deep Clear Pink	Co	1,900	X
MgO	4N	Deep Pink	Co	3,300	X
MgO	4N	" "	Co	9,900	X
MgO	4N	" "	Co	8,200	X
MgO	4N	Deep Pink (cloudy)	Co	4,800	X
MgO	4N	Clear Pink	Co	1,250	X

TABLE 1.1: Data for doped magnesium oxide single crystals.

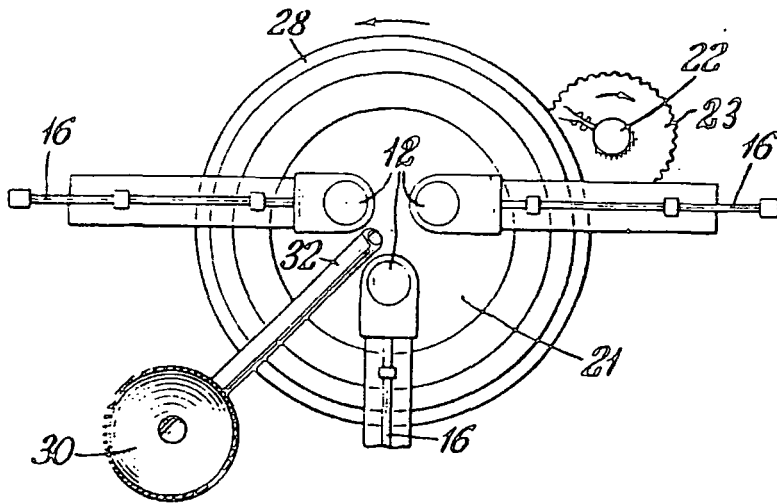
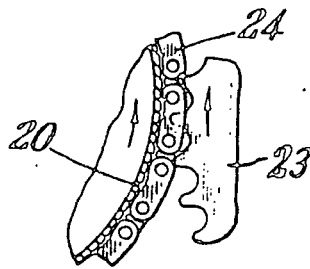
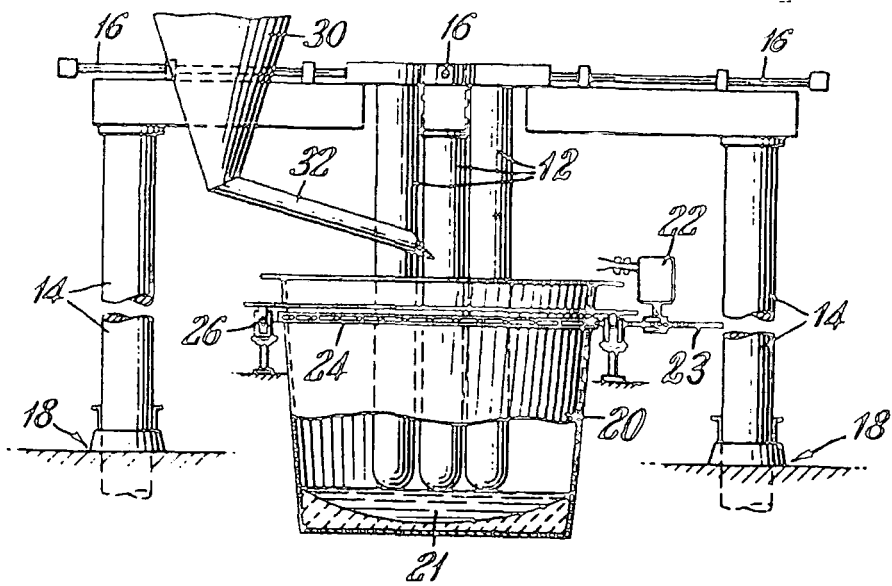


Figure 1.2. Large scale furnace for magnesia fusion.
 Key: graphite electrode, 12; electrode support, 14;
 busbars, 16; hydraulic lift, 18; steel shell, 20;
 melt, 21; rotation motor, 22; gear, 23; chain, 24;
 rollers, 26; hopper, 30; chute, 32.

immediate corollary of this increase in scale is apparent in the choice of the starting material ; the costs alone of providing high quality pure magnesia in the quantities required would be prohibitive, quite apart from considerations of availability. In the bulk production of fused magnesium oxide the starting material is often a magnesite or a calcined caustic magnesite, which, being a naturally occurring mineral extracted by quarrying, contains impurities. Fusion is often undertaken using a very large water-cooled container. It is filled with the crushed starting material (magnesite) and by striking an arc between massive carbon electrodes the central part of the powder mass is melted; this molten pool of fused magnesium oxide is contained since the low thermal conductivity of magnesium oxide enables the outer parts of the mass to remain as either partially-fused or, at the extreme edges, completely unfused powder. Some general characteristics of the fused melt, which have important consequences in determining the electrical quality of the product, may be noted here. The fused melt has a very large mass and cools slowly. The centre, when molten, is at a temperature of about 2900°C and so both during the fusion itself and the subsequent cooling to room temperature (a process which may take several days) there is a large temperature gradient, in the radial direction, across the mass. Consequently, impurity segregation may occur and in fact it is often quite marked. Thus the central region of the melt is hard, highly crystalline and typically of pale green colour while towards the edges the degree of polycrystallinity increases to give quite a friable material with associated colour changes to an off-white or even light yellow-brown. Occasionally near the centre of a fusion some regions of grey or black material are found and it is generally felt that the "black magnesia" has undesirable electrical properties. The conditions under which the formation of this "black

magnesia" may occur or be prevented have not, to the author's knowledge, been fully ascertained though there have been suggestions that it may be associated with carbon. In the production of electrical grade magnesia powders the solid fused melt is first broken up and may then be separated into fractions corresponding to the different regions of the fusion. Each fraction then proceeds to various stages of milling and subsequent heat treatment. Iron contamination may arise from tools used in the initial breaking and crushing of the melt and it is customary to employ magnetic separation techniques to remove major inclusions of iron or other extraneous ferrous material, (Mills, 1.11, Jones, 1.12, Iannicelli, 1.13). An indication of the overall purity of some commercial fused magnesia powders is given by the chemical analysis data (Thermal Syndicate, 1.14), shown in Table 1.2 ; from this, which may be taken to be reasonably representative of this type of product, it can be seen that the major impurities present at fractions of a percent level are iron (or iron oxide), calcia, alumina, silica and zirconia with other impurities, notably the transition group elements nickel, cobalt chromium and manganese, present at levels of a few tens of ppm.

The work described in this Thesis has been primarily directed towards characterising the impurities, particularly magnetic impurities, present in commercial, electrical grade magnesia powders. Consequently, attention has been given to the assessment of techniques suitable for quality control and impurity identification in commercial powders, to the provision of reference standards (which involved the use of single crystal magnesium oxide) and to the isolation of those impurities which show particularly high conductivity or dielectric loss.

Chapter 2 describes the application of x-ray diffraction techniques (XRD) to the problem of impurity identification in commercial magnesia powders and shows how analysis of the complex spectra obtained may be

Impurity	CENTRE				OUTER			
	A	B	C	D	E	F	G	H
SiO ₂	1.43%	1.61%	1.94%	2.79%	3.23%	4.35%	2.82%	4.32%
TiO ₂	2.3	7.0	5.3	14.5	<0.5	<0.5	1.0	<0.5
Cr ₂ O ₃	40	42	40	39	36	41	42	41
MnO	15	19	20	20	26	29	29	29
Fe ₂ O ₃	0.109%	0.091%	0.103%	0.100%	0.138%	0.156%	0.167%	0.160%
Co ₂ O ₃	30	30	30	31	30	31	33	33
NiO	253	265	280	250	420	470	500	470
CuO	4.0	4.0	4.0	5.0	7.0	7.5	8.5	9.0
ZnO	2.0	2.0	2.0	1.0	5.0	5.0	6.0	6.0
ZrO ₂	0.18%	0.36%	0.26%	0.19%	0.25%	0.70%	0.54%	0.23%
Al ₂ O ₃	0.08%	0.33%	0.18%	0.15%	0.08%	0.18%	0.13%	0.15%
CaO	0.58%	0.65%	0.83%	0.99%	1.40%	1.63%	1.24%	1.40%
Na ₂ O	4.5	4.0	7.5	8.0	33.5	34.0	30.0	34.0
K ₂ O	20.5	20.5	22.5	22.5	36.0	36.0	31.5	40.5
Li ₂ O	1.2	1.4	1.6	1.9	2.9	3.4	1.7	4.0
S ₂ O ₃	11.6	8.6	11.8	12.1	15.6	11.6	12.7	13.7
SO ₂	25.2	24.0	45.0	40.0	160	147	126	170
MgO-by difference	97.48%	96.92%	96.64%	95.74%	94.82%	92.90%	95.02%	93.65%
	All results are expressed as p.p.m. unless shown as percentage							

TABLE 1.2: Chemical analysis of fused magnesia ; samples (A, B, C, D) and (E,F,G,H) refer to specimens taken from the central and outer parts of the fused melt respectively.

simplified by the acquisition of additional X-ray information, in this instance from Energy Dispersive Analysis by X-rays (EDAX). The magnetic nature of some of the impurity phases is introduced in Chapter 3 which first discusses the principles of magnetic susceptibility measurement by Gouy balance methods and then outlines their use in following the formation of ferrimagnetic magnesio-ferrite precipitates in heat-treated iron-doped magnesium oxide. In Chapter 4 the general principles and theory of another magnetic method of analysis, Electron Spin Resonance (ESR), are given together with a discussion of some single crystal reference spectra and the methods used for identifying features in esr powder spectra. Chapter 5 describes the application of these esr methods to the study of a selection of magnesia powders both before and after various heat treatments and the results confirm that the presence of ferromagnetic or ferrimagnetic phases is an important effect in some commercial magnesia powders. Finally, Chapter 6 correlates the data obtained by the different techniques adopted, reviews their significance in relation to conductivity and dielectric loss measurements, and makes some suggestions for future work.

CHAPTER ONEREFERENCES

- 1.1 M.M.Abraham, C.T.Butler, Y.Chen
Jour.Chem.Phys.55, (1971), 3752.
- 1.2 W.C.Spicer Ltd., Cheltenham, U.K.
-private communications.
- 1.3 W.C.Spicer Ltd., Cheltenham, U.K.
-product catalogues.
- 1.4 J.S.Thorp, R.A.Vasquez, C.Adcock, W.Hutton.
Jour.Mater.Sci.11, (1976), 89.
- 1.5 J.S.Thorp, M.D.Hossain, L.J.C.Bluck.
Jour.Mater.Sci.14, (1979), 2853.
- 1.6 J.S.Thorp, M.D.Hossain, L.J.C.Bluck, T.G.Bushell.
Jour.Mater.Sci.15, (1980), 903.
- 1.7 A.D.Inglis, J.S.Thorp.
Jour.Mater.Sci.16, (1981), 1887.
- 1.8 J.S.Thorp, N.Enayati-Rad.
Jour.Mater.Sci.16, (1981), 255.
- 1.9 J.S.Thorp, B.L.J.Kulesza, N.E.Rad, S.V.J.Kenmuir.
Jour.Mater.Sci.16, (1981), 1052.
- 1.10 L.A.Stoyell, H.S.Redline
U.S.Patent No, 3328183, (1967).
- 1.11 C.Mills.
Industrial Minerals, 8, (1977), 41.
- 1.12 G.H.Jones.
U.S.Patent No, 3346116, (1977).

1.13 J.Iannicelli.

Inst.Elect. & Electron.Eng.(Trans. on Magnetics)

MAG-12, (1976), 436.

1.14 Thermal Syndicate Ltd., Wallsend, U.K.

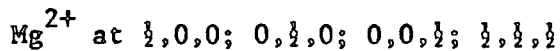
-private communication.

CHAPTER TWO

X-RAY CHARACTERISATION OF MAGNESIUM OXIDE POWDERS

2.1 The Crystal Structure of Magnesium Oxide

Magnesium oxide is an ionic solid which crystallizes with the "sodium chloride" or "rocksalt" structure (2.1). This structure may be described as a cubic close packed array of oxygen ions with magnesium ions occupying all the octahedral interstices. The Mg^{2+} ions are arranged in a face-centred cubic (F.C.C.) pattern as are the o^{2-} ions; the two interpenetrating F.C.C. sublattices are aligned but one is displaced from the other along a reference $\langle 100 \rangle$ axis of the cubic unit cell by a distance equal to half the lattice parameter, a . Thus each Mg^{2+} ion is octahedrally surrounded by six o^{2-} ions and similarly each o^{2-} ion is octahedrally surrounded by six Mg^{2+} ions to form a regular three-dimensional array (the co-ordination number for both ions is therefore six). In terms of atomic co-ordinates the MgO structure has ions at the following locations:



where the atomic co-ordinates are expressed as fractions of the unit cell length (lattice parameter) along three mutually perpendicular $\langle 100 \rangle$ type directions. A pictorial representation of the MgO unit cell is shown in Figure 2.1.

The ratio of the radius of the cation to that of the anion is often the most important factor in determining the structure of an ionic compound. If it is assumed that the anions and cations are hard spheres

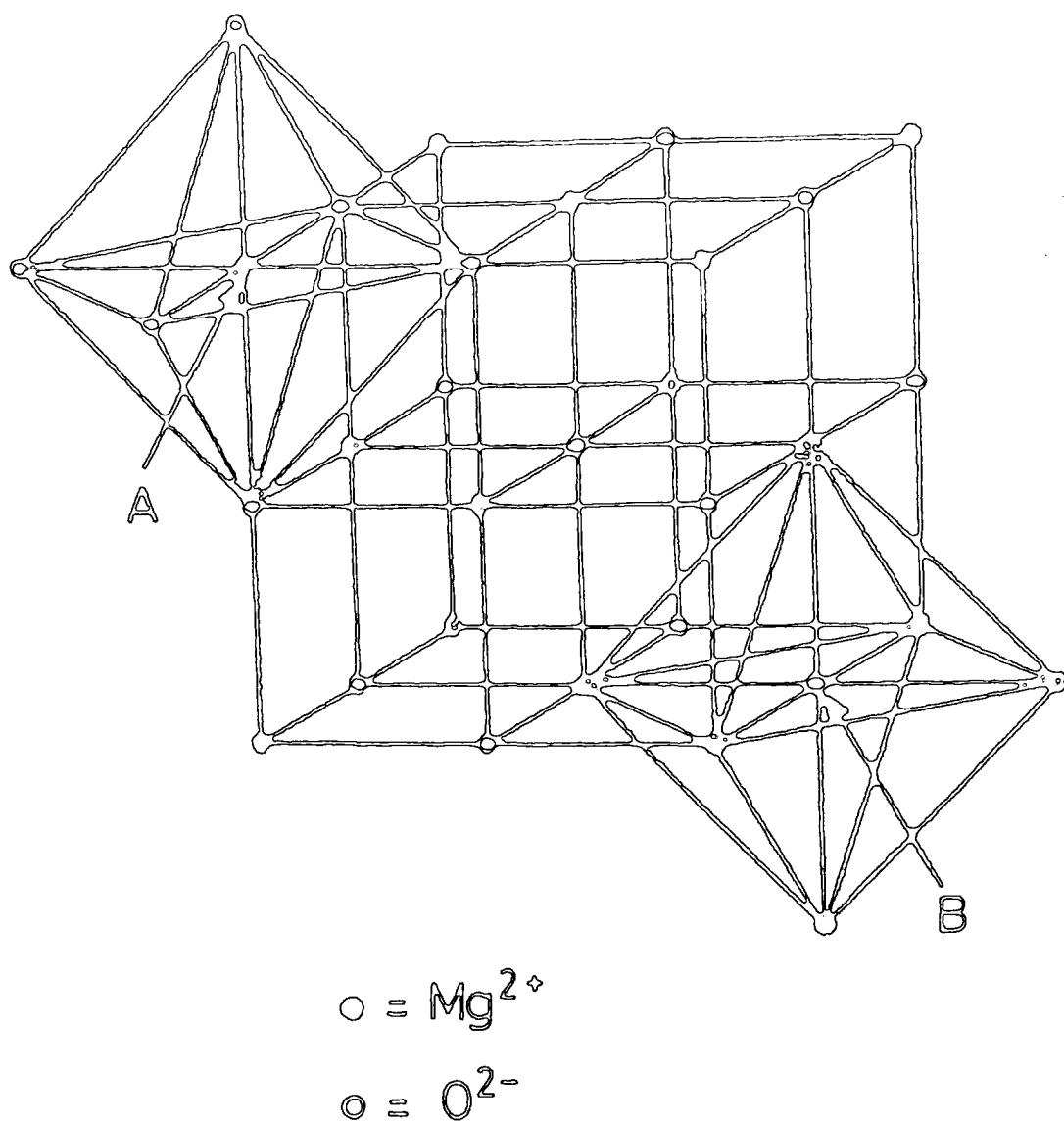


Figure 2.1. The crystal structure of MgO showing the octahedral co-ordination of the Mg (A) and O (B) ions.

of fixed radii and that the coordination number will be as high as possible, the crystal structure can be predicted from the value of this ratio (2.2). An ionic solid will have an "idealized" rocksalt structure if the anions are in mutual contact as well as in contact with the cations. For such a compound, as Figure 2.2(a) shows, $r_+/r_- = (\sqrt{2} - 1)$ where r_+ & r_- are, respectively, the cationic and anionic radii. If the ratio r_+/r_- is less than 0.414 ($\sqrt{2} - 1$), the anions will be in contact with each other but not with the cations. Compounds for which $r_+/r_- < 0.414$ will not adopt the sodium chloride structure because this would result in large electrostatic forces of repulsion between the anions. Such materials tend to adopt the zinc blende (cubic ZnS) structure, even though the coordination number of the cations is reduced to four, because this structure allows the anions to be in mutual contact as well as in contact with the cations when the radius ratio, r_+/r_- , is much less than 0.414 (2.2). On the other hand, if the radius ratio exceeds 0.414 the rocksalt structure is still favoured but the anions become separated from each other although they remain in contact with the cations. When r_+/r_- reaches a value of 0.732 however the caesium chloride structure becomes favourable because at this high value of the radius ratio adoption of the CsCl structure increases the cation coordination number to eight whilst at the same time allowing the anions to remain in mutual contact as well as in contact with the cations (2.2). Thus compounds of the type MX (where M is a cation and X is an anion) will tend to adopt the sodium chloride structure if the ratio r_+/r_- lies between 0.414 and 0.732. If $r_+/r_- = 0.414$ then the compound has the "idealized" rocksalt structure (Figure 2.2(a)); if $0.732 > r_+/r_- > 0.414$ then the compound still has the sodium chloride structure but the anions, although in contact with the cations, are separated from each other (see Figure 2.2(b)).

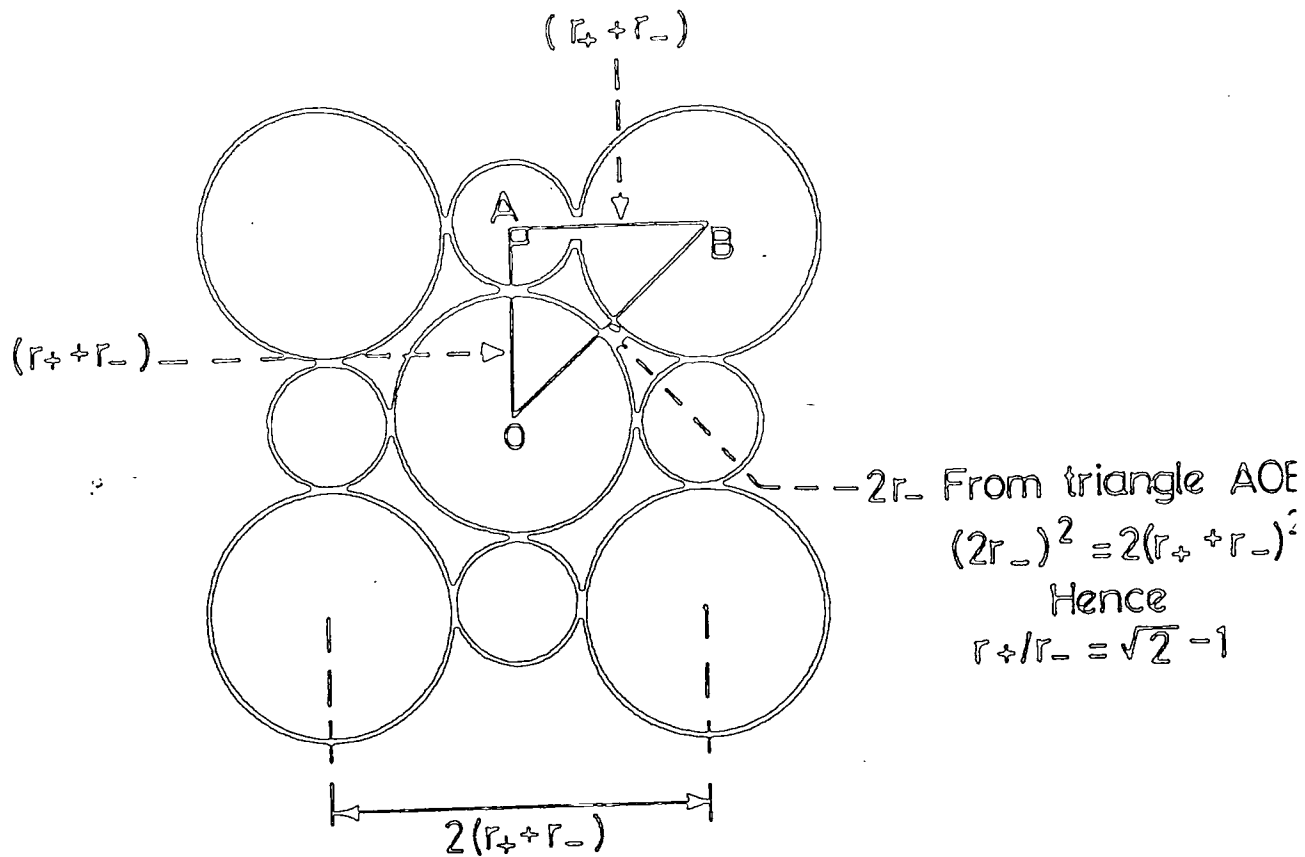


Figure 2.2(a). A cross-section of the unit cell of a compound having the idealised rocksalt structure.

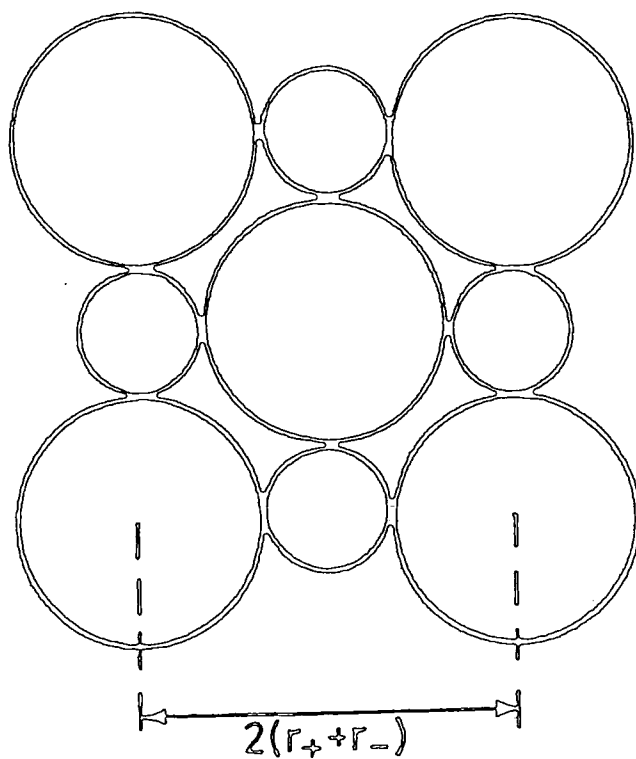


Figure 2.2(b). A cross-section of the unit cell of MgO showing the separation of the anions.

Reference to Figures 2.2(a) and (b) shows that if a compound crystallizes with the rocksalt structure, the lattice parameter, a , is given by:

$$a = 2 (r_+ - r_-) \quad (2.1)$$

If the assumption of hard, incompressible ions with fixed radii is valid substituting appropriate values of r_+ ($= r(\text{Mg}^{2+})$) and r_- ($= r(\text{O}^{2-})$) into equation 2.1, should give a value for the lattice parameter of magnesium oxide for comparison with that measured experimentally using x-ray diffraction methods ($a_{\text{exp}} = 4.211 \text{ \AA}$ at 21°C (2.1)).

The ionic radii have been estimated using several methods of approach and much of the work in this area has been reviewed by Shannon and Prewitt (2.3). They considered a large number of reported experimental observations of interatomic distances and assumed a linear relationship between ionic volume and unit cell volume for a series of isotopic oxides and fluorides. Shannon and Prewitt deduced that the ionic radii of Mg^{2+} and O^{2-} in six-fold coordination are:

$$r(\text{Mg}^{2+}) = 0.72\text{\AA}; \quad r(\text{O}^{2-}) = 1.40\text{\AA}$$

Substitution of these values into equation 2.1 yields a value for the lattice parameter, a , of 4.24\AA . Bearing in mind the empirical nature of the methods used to determine ionic radii, this value is in remarkably good agreement with that found experimentally (4.2112\AA). It is likely that the measured value of a is slightly smaller than that suggested by equation 2.1 because of the effects of covalent bonding, which causes the inter-ionic distances to be less than those calculated

assuming that the ions are hard spheres. Using Shannon and Prewitt's values of $r(\text{Mg}^{2+})$ and $r(\text{O}^{2-})$ the radius ratio, r_+/r_- for MgO is 0.514. It may be concluded from this that MgO does not have the "idealized" rocksalt structure (Figure 2.2(a)); instead it adopts the structure shown in Figure 2.2(b) which has the anions in contact with the cations but separated from each other.

2.2 X-Ray Diffractometry

A number of factors are considered likely to influence the performance of Magnesium Oxide as the electrical insulator in a heating element, but there is strong evidence that the electrical properties are adversely influenced by some impurities (2.4,2.5). To determine which such impurities are present in commercial magnesia a technique is required which can reveal the impurity phases present in the powders.

Many analytical systems can detect impurities only of a certain class, (for example, electron spin resonance, though extremely powerful in certain circumstances, can detect only paramagnetic species) but a method capable of identifying all phases is necessary for useful analysis of the commercial magnesia. The best method available is x-ray diffractometry (X.R.D.) which analyses via crystallographic structure. It can detect impurities down to about 2% abundance and is very suitable for powders.

Diffractometer traces were obtained from the flat bed of a Phillips P.W.1130 diffractometer operating with a cobalt target emitting $K\alpha$ radiation of wavelength 1.791Å. An iron filter designed to give a ratio of integrated intensities of $K\beta_1:K\alpha$ better than 1:100 was used.

The emitted monochromatic X-radiation passes through a divergence slit which broadens the beam to the size of the sample surface (about 1 cm x 1.5 cm) as shown in Fig.2.3. The powder sample (about 1 gram of MgO) having been placed in a special container and mounted in the path

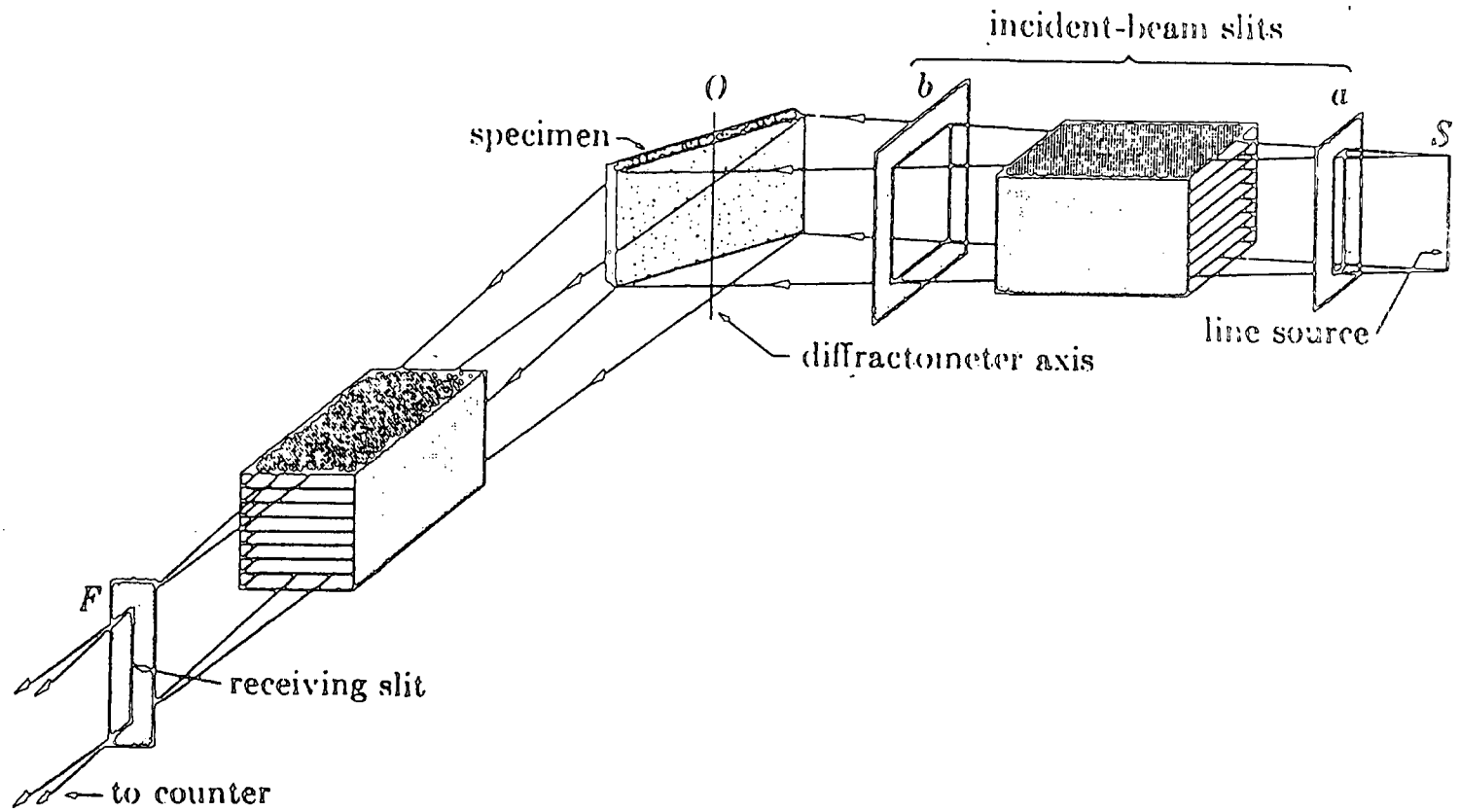


Figure 2.3. Arrangement of slits in a diffractometer.

of the beam, diffracts and reflects the x-rays. The waves of the reflected radiation interfere constructively where the Bragg condition is satisfied, i.e. at Bragg angles characteristic of the crystallographic structures in the sample. The reflected radiation is collected by a series of slits and is focussed by a crystal whose surface is curved to ensure that the beam is focussed in the locus of the detector ; (see Fig 2.4). The angles of the incident beam, sample surface, and the receiving and detecting means are controlled and monitored by an angle programmer and this information together with the detector signal is processed by a system, shown in the block diagram of Fig 2.5, to produce the trace of intensity of reflected radiation against 2θ where θ is the Bragg angle.

The accuracy of the d-values calculated for the 2θ readings varies from about 0.005\AA for high θ values to $\pm 0.01\text{\AA}$ at low values of θ . However, many of the peaks appearing on the trace, particularly those at low intensity, are not very distinct because noise peaks or peaks of other impurities of nearly the same d-value are superimposed and are too close to be resolved. In practice peaks of low intensity were accurate only to about 0.02\AA or more.

The information is a great deal less accurate than the d-value data and interpretation is difficult. The low intensity of the peaks of many of the impurities present in the commercial magnesia makes quantitative analysis impossible because the signal-to-noise ratio is so low. Furthermore, the signal-to-noise ratio was sensitive to small changes in the power supply, and although much of the work was done at night, the noise level was not sufficiently constant from one spectrum to the next to yield much information about the variation in intensity of particular peaks for different samples.

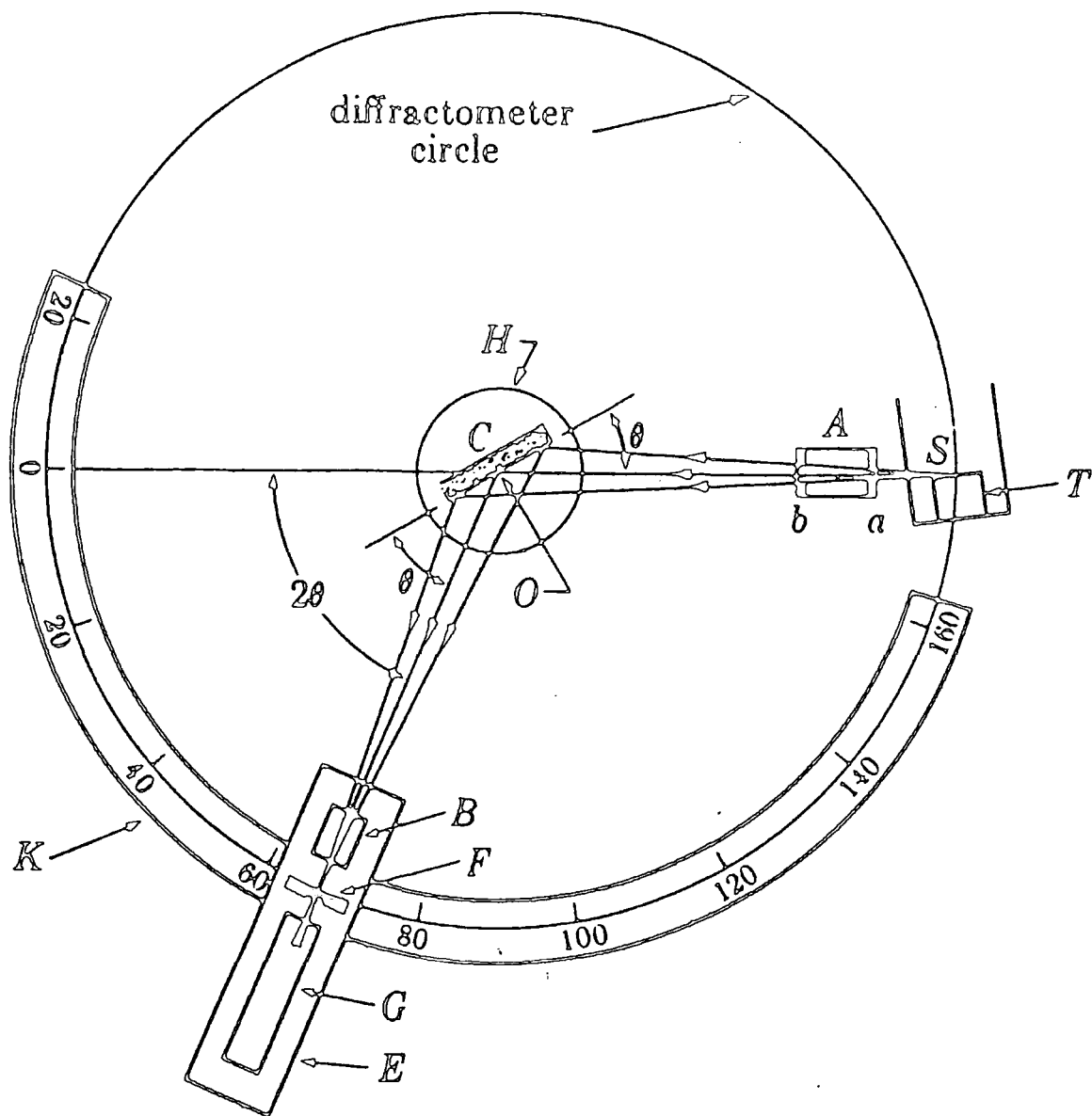


Figure 2.4. Schematic diagram of an X-ray diffractometer.

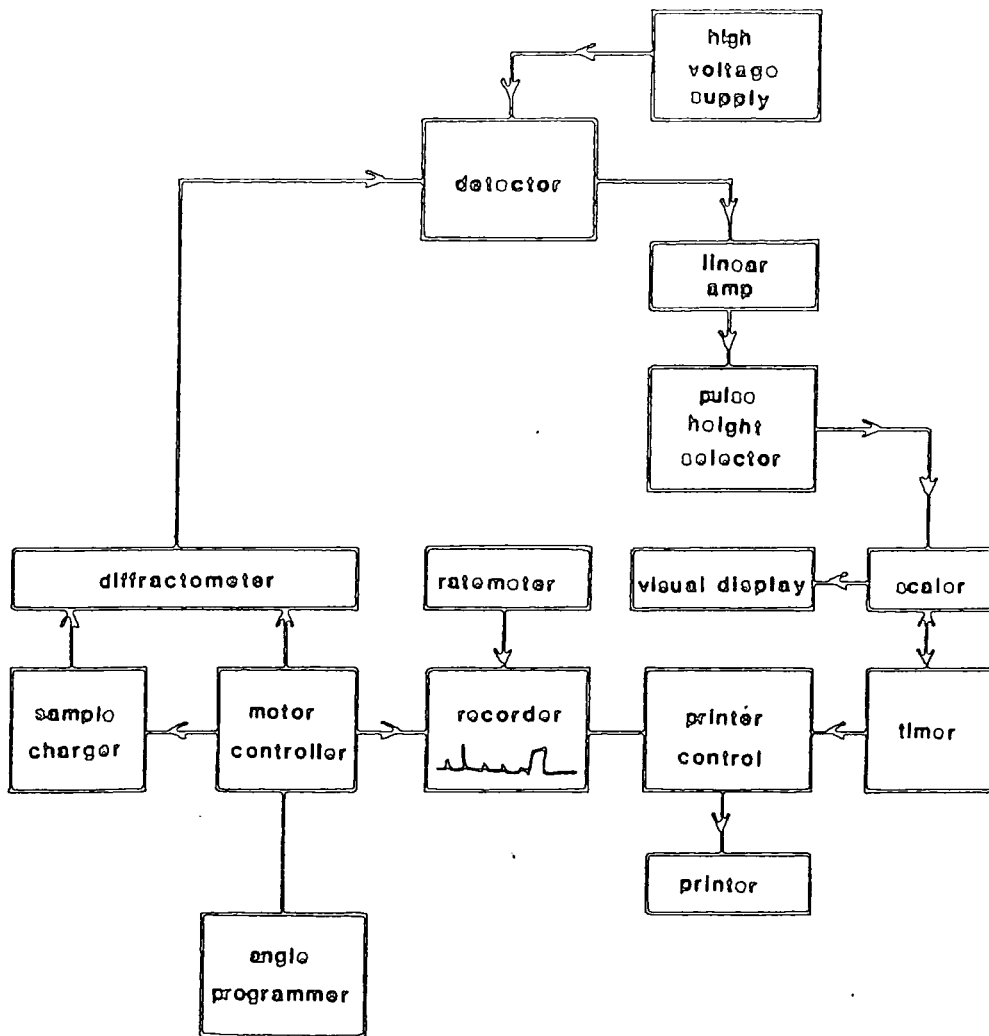


Figure 2.5. Block diagram of the XRD system.

The form of an X.R.D. powder spectrum is shown in Fig.2.6, which refers to pure MgO (Koch-Light 99.998% pure Magnesium Oxide). The spectrum is relatively simple, containing only seven lines, and the fit between the d-values observed experimentally and those expected from the A.S.T.M. data for MgO (periclase) is shown in Table 2.1 to be very close. As would be expected (with the pure sample material) no lines are present in the spectrum which cannot be accounted for by the A.S.T.M. listing: (note the diffractometer has recorded only in the range $10^\circ < 2\theta < 100^\circ$).

Examination of a typical good commercial grade MgO, Fig. 2.7, illustrates the difficulties immediately encountered with impure material. In addition to the seven very strong periclase lines there are more than forty extra lines. Such powder spectra are too complex for successful interpretation, since the pattern of impurity peaks could be caused by very many possible combinations of superimposed impurity patterns: in fact there are so many plausible interpretations of such a spectrum that virtually no useful conclusion can be drawn. The problem is aggravated where the peak height is of the order of the height of noise peaks, since the ASTM's relative intensity information - is rendered useless, and indeed, for some impurities it may be only the strongest peak of the characteristic pattern which is readily detectable above the noise.

It was clear that some further information had to be obtained to reduce the number of possible interpretations. In this instance the "energy dispersive analysis by x-rays, (EDAX)" facility of a scanning electron microscope (S.E.M) was used. This facility collects the characteristic x-rays induced in the atoms bombarded by the electrons of the S.E.M. beam and thus gives an elemental analysis of surface atoms of a sample. The information gained from these measurements together with

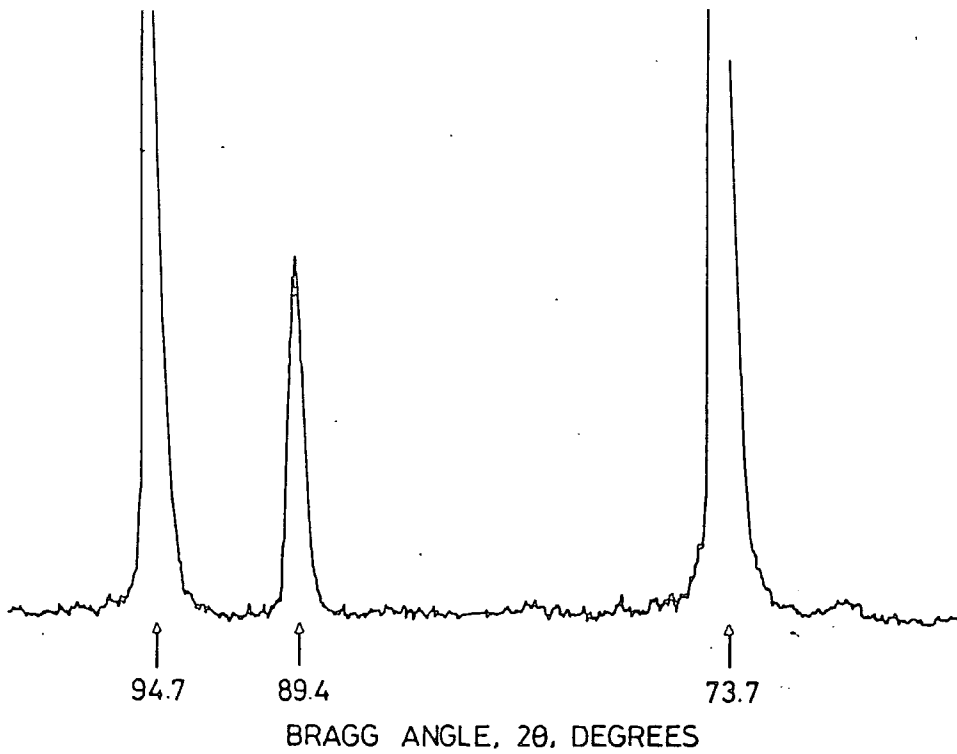
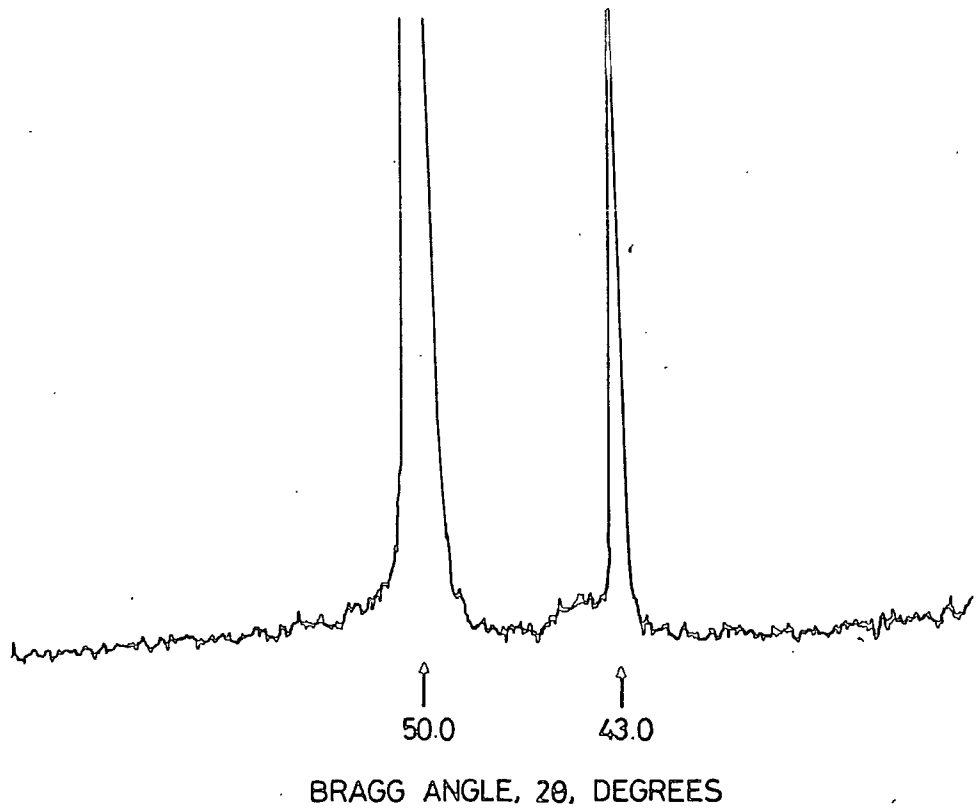


Figure 2.6. XRD spectrum of pure MgO.

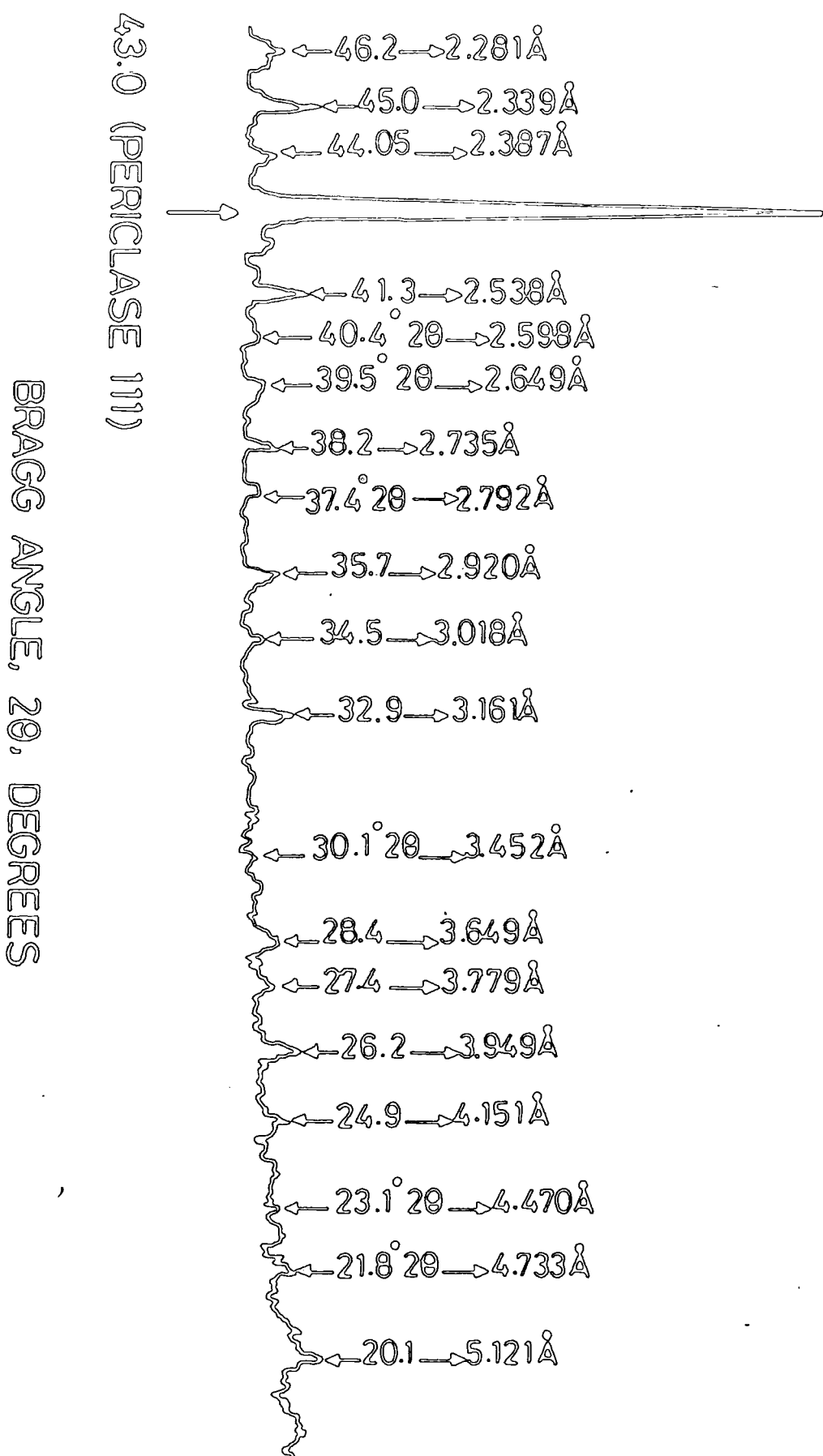


Figure 2.7. XRD spectrum of good commercial magnesia; 2θ range from 20° to 43°.

the chemical analysis of commercial magnesias proved essential for the analysis of the more complex X.R.D. spectra.

2.3 Edax Analysis

2.3.1 Techniques

The EDAX facility available was a Cambridge Instruments Steroscan 600 S.E.M., and this was employed to produce the information necessary for analysis of XRD powder spectra.

This EDAX technique is difficult for powders and so was used here for examining bulk samples from the fusion. The electron beam could be focussed to diameters down to about 1 μm and on striking the atoms of the sample surface the electrons induced the emission x-rays of frequencies characteristic of the atoms (see Fig 2.8). These x-rays impinged on the surface of a lithium drifted silicon detector causing it to produce an electrical output proportional to the energies of the x-rays incident. This signal was analysed by a Linksystems 860 analyser employing standard computer memories and an energy spectrum showing the elements present was then produced.

Magnesium oxide, being a good electrical insulator would tend to become electrostatically charged by the electron beam. The resulting field would deflect the electron beam and destroy the S.E.M. image of the sample (sight of which is essential for selecting a target region for each EDAX spectrum). Hence, after being mounted on an aluminium stub with silver dagenum paste, the sample (which is about 1-5 mm^3) together with the mount is plated with gold to insure that such charge may conduct away. The gold layer should be so thin (about \AA) as to be translucent to the electron beam. To achieve this the sputtering method of coating was employed.

However, the EDAX equipment could not detect atoms of mass number less than 20, and more particularly, because of the overall sensitivity

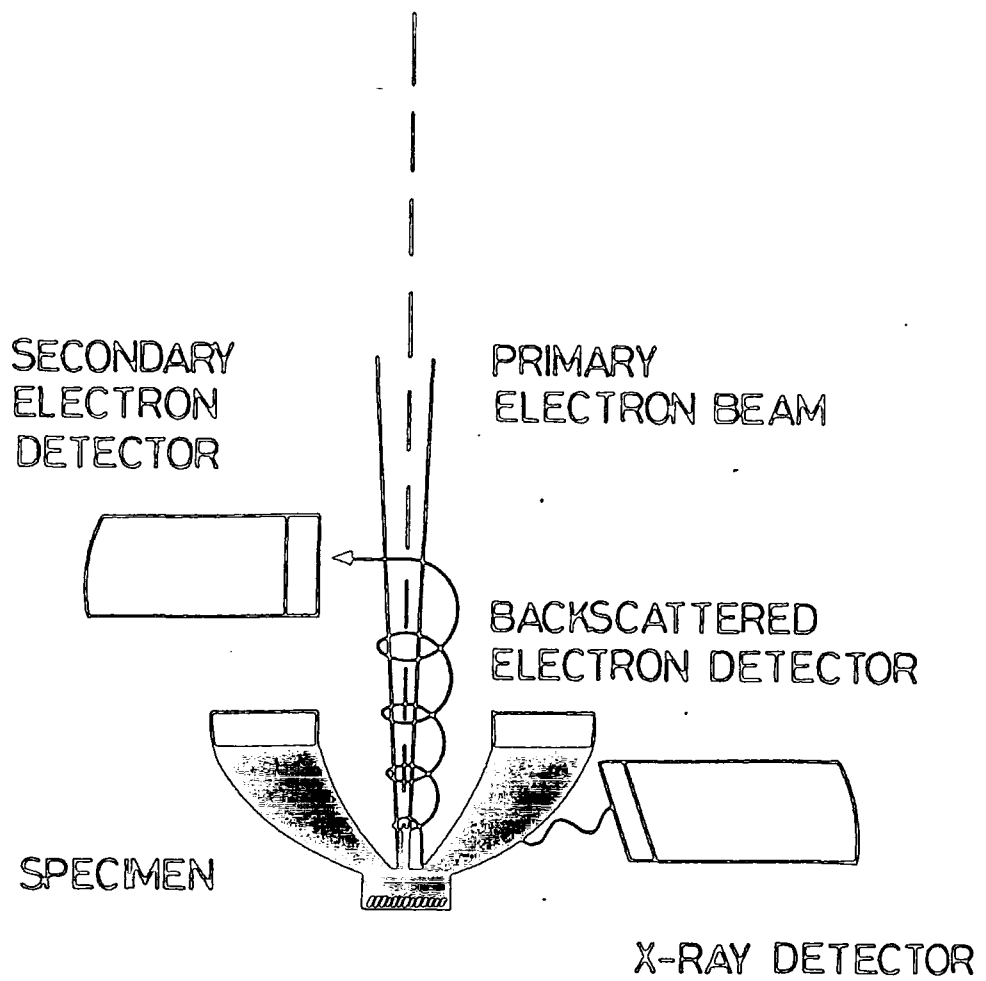


Figure 2.8. Principles of the EDAX technique.

any element present at less than about 2% abundance remained undetected. Since the purity of commercial magnesiias is typically 92 to 98%, many of the impurities would be expected to be present in much lower proportions than this. Referring to the chemical analysis of the impurities listed all but silicon and calcium are found to be present at undetectable abundances. Hence the sample seems likely to contain many atoms from the undetectable classes.

2.3.2 Results from EDAX Study

The results from the EDAX study are summarised in Table 2.2, and typical spectra are shown in Figs 2.9 and 2.10.

Figure 2.9 shows a typical EDAX spectrum obtained when the electron beam scanned about 0.5 mm^2 of the surface of a centre of fusion crystalline sample. As expected the $K\alpha$ lines of silicon and calcium are just detectable, and are seen with the $k\alpha$ line of magnesium and the μ line for gold (caused by the gold plating). Also shown on Fig 2.9 (clear and dotted) is a spectrum obtained when the electron beam scanned $\sim 1.0 \text{ }\mu\text{m}^2$. In this region the silicon and calcium peaks are significantly greater than those from the spectrum of the wider areas implying significant inhomogeneity of impurity concentration in the fused sample.

Figure 2.10 shows spectra from one such inhomogeneous region. Here, even scanning most of the surface of the sample relatively high levels of supposedly undetectable atoms were found, i.e. Aluminium, Sulphur, Iron and Nickel. On focussing the beam to its minimum diameter ($\sim 1 \text{ }\mu\text{m}^2$) a region of this sample was found which revealed only aluminium sulphur and nickel. (The silver peak appearing in the spectrum is caused by the silver dagenum paste). In similar studies of local inhomogeneities Titanium, Phosphorous Chlorine and Potassium were also found (See Table 2.2).

d-values of spectrum peaks $\text{\AA} \pm 0.015 \text{\AA}$	d-values from A.S.T.M. index for MgO (4.0829) \AA
2.442	2.431
2.110	2.106
1.493	1.489
1.271	1.270
1.217	1.216

TABLE 2.1: Analysis of spectrum of Pure MgO (Koch-Light).

Figure	Sample	Impurities
3.2	Batch Ia, Centre of fusion	Al, Si, Ca, (Au)
3.3	Batch Ic, Near centre of fusion	Mg, Si, Cl, K, Ca, (Au)
3.4	Batch II Cover	Mg, Si, Ca, (Au)
3.5	Batch III Particles	Mg, Si, Ca, Ti, (Au)
3.6 & 7	Batch V Black region	Mg, Al, Si, P, S, Ca, (Au) Fe, Ni, (Ag).

TABLE 2.2: Results of E.D.A.X. Study on Commercial Fusion Products.

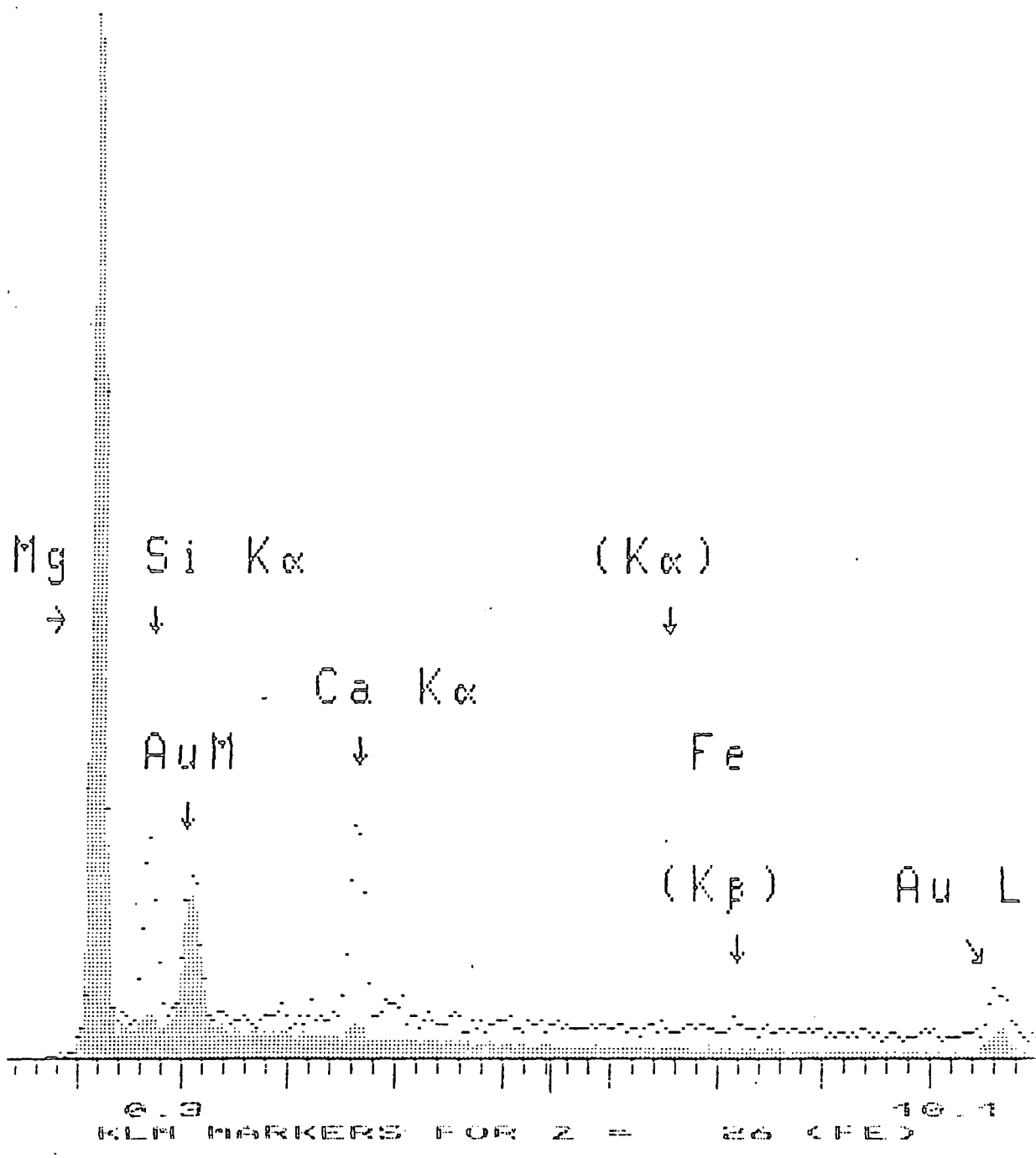


Figure 2.9. EDAX trace for material from the centre of the fusion, (scanning 0.5 mm² of the surface "----" scanning 1.0 mm² of the surface ".....").

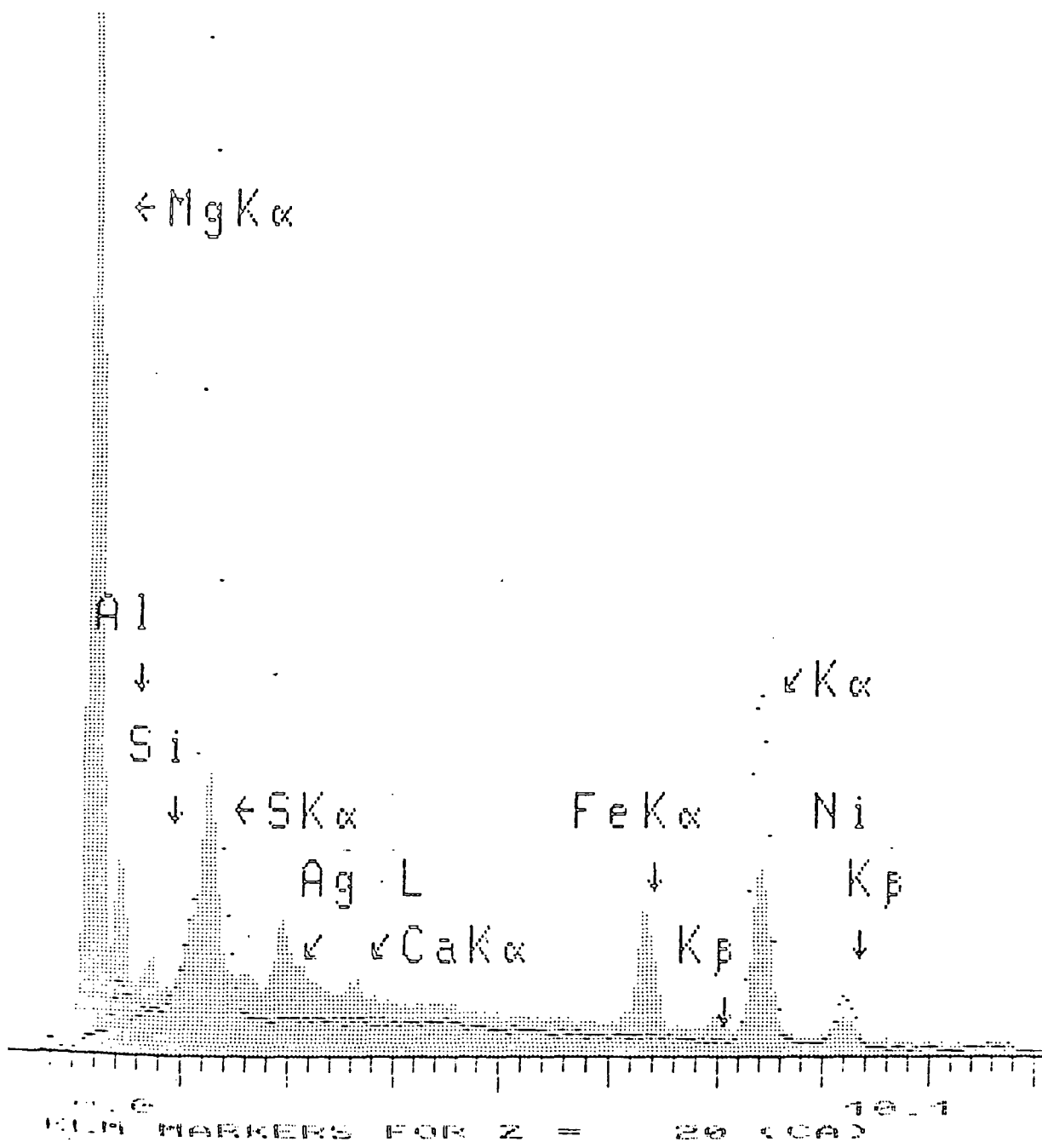


Figure 2.10. EDAX trace for material of the black region of the fusion, (scanning 0.5 mm² of the surface "----" scanning 1.0 mm² of the surface ".....").

These results, together with the chemical analysis were used to aid analysis of the results from the x-ray diffraction spectroscopy study.

2.4 Detailed Analysis of XRD Data

2.4.1 Method of Approach

Even with the additional information from the EDAX study and the chemical analysis, interpretation of the spectra is not straightforward. The method used was first to calculate the d-values of the impurity peaks from the reading on the 2 θ scale of the trace. The A.S.T.M. (American Society for Testing Materials) Search Manual for Common Inorganic Phases 2.6) was then consulted. The selection criteria for the common phases used by the A.S.T.M. for this manual was based on the classification of all elements into three groups ; common elements, less common elements and uncommon elements. A phase included in the manual contains :

- (a) up to four "common" elements;
- or (b) fewer elements one of which may be "less common" but not "uncommon";
- or (c) the phase is a frequently encountered mineral phase.

The elements revealed by the elemental analysis of the commercial magnesia (EDAX, and Chemical Analysis) are all "common" elements except for zirconium and lithium which are classed by the A.S.T.M. as "less common". The search manual also includes phases which, whilst stable at room temperatures, are created at higher temperatures. Thus, the manual is very likely to list all the phases which could possibly be present as impurities in the commercial magnesia.

The 2,300 phases listed in the search manual are grouped and ordered according to d-values of the three strongest lines of the diffraction pattern, whereas the full A.S.T.M. index lists the phases alphabetically. The d-value listing greatly eases the task of finding

patterns which fit the peaks of the spectrum, but only the eight strongest lines of each pattern are listed. However, since the majority of the impurities are at low abundances this does not seem likely to introduce significant inaccuracy.

The method of analysis is now described with reference to the spectrum of a good grade magnesia part of which is shown in Fig 2.7. First the d -value of the strongest distinct impurity peak was taken, and the search manual list of phases having this value for any one of the three strongest lines of the pattern was examined. Phases where the two other strongest lines have d -values where a peak appears on the spectrum were noted. Those phases containing ions not revealed by the elemental analysis (e.g. Arsenic) were deleted. The d -values of the remaining five lines of each phase were then compared with those of peaks on the spectrum. If there were peaks on the diffractometer spectrum at all of the d -values of the pattern which lay within the range of the spectrum (1.17-10.27 Å) then the phase was classed as "certain", where one or two of the peaks were not clearly defined (i.e. were barely distinguished from noise or were obscured by a larger peak) then the phase was classed as "probable". Where three or four lines of the listed pattern were not clearly defined, but the three strongest lines were well defined and one of the three strongest lines corresponded to a peak on the "spectrum" which could not be explained by another phase, then the phase was classed as "likely". In practice other factors such as the signal-to-noise ratio were taken into account in the classing of the phases detected.

Table 2.3 shows the complete analysis for the good commercial magnesia shown in Fig 2.7. For some phases identified by the above analysis direct confirmation could be achieved by obtaining a sample of the pure phase and irradiating in the diffractometer. The resulting

As Observed d-values 5.128 Å	ASTM DATA							
	MgO	MnO ₂	Mn ₂ O ₃	Mn ₃ O ₄	MgSO ₄	MnSO ₄	MgFe ₂ O ₄	MnFe ₂ O ₄
	4-829	14-644 12-716	6-540 24-508	16-454 13-162 5-10	21-546	11-88	17-964	10-319
4.181							4.87	4.91
4.934								
4.470								
4.340								
4.168					4.15			
3.949		3.96						
3.779								
3.6995								
3.649						3.70		
3.423					3.61			
3.515					3.53			
3.452						3.47		
3.340					3.35			
3.227					3.18			
3.161		3.14						
3.018								3.01
2.976								
2.920							2.96	
2.792				2.77				
2.735			2.74					
2.695			2.72					
2.649				2.63	2.64	2.70		
2.598					2.01	2.63		
2.538				2.54			2.53	2.56
2.481			2.48	2.49				
2.442					2.45			
2.430	2.43							
2.420		2.41					2.43	
		2.42						
2.387								
2.339						2.39		
2.281		2.32						
2.114	2.11							
2.042						2.08	2.09	2.12
1.985								
1.955								
1.907								
1.854						1.85		
1.812								
1.756								
1.715							1.71	1.73
1.650			1.66					
1.620		1.63					1.61	1.64
1.519								
1.506								1.50
1.493	1.49			1.49				
1.484							1.48	
1.447						1.45		
1.270	1.27							
1.216	1.23						1.213	
1.053	1.05						1.09	
1.45								1.11

TABLE 2.3: XRD Analysis of Good Commercial Magnesia (c.f Fig 2.7)

As Observed	ASTM DATA							
	Al ₂ Si ₂ O ₅ (OH) ₄ 12-447	Ca ₂ SiO ₄ 11-369	FeO 6-711	Fe ₂ O ₃ 16-895	NiC 14-20 Ni 4-850	Fe-C 8-133	FeSi ₂ 22-113	CaCl ₂ 24-223
5.128 Å								
4.181								
4.934								
4.470	4.47							4.48
4.340	4.34	4.32						
4.168	4.16							
3.949								
3.848		3.82						
3.779								
3.6995								
3.649								
3.423								
3.515								
3.452								
3.340								
3.227								
3.161				3.23				
3.018		3.01						3.05
2.976				2.98				
2.920								
2.792								2.86
2.735		2.75						
2.695		2.73						
2.649								
2.598								
2.538	2.55							
2.481	2.48		2.49					
2.442				2.46				
2.430								
2.420								
2.387							2.37	2.36
2.339	2.33							2.33
2.281	2.28			2.24				
2.114			2.15					2.24
2.042					2.04/2.03	2.08		2.08
1.985				1.98				
1.955								
1.907		1.91					1.89	1.91
1.854		1.88					1.84	
1.812		1.80				1.80		
1.756				1.74	1.77/1.76		1.78	
1.715							1.70	
1.650								
1.620								
1.519			1.52	1.52				
1.506			1.51					
1.493								
1.484	1.48							
1.447				1.47				
1.270			1.29		1.26/1.25	1.27		
1.216			1.24					
1.053			1.08		1.07/1.06	1.08	1.08	
1.45					1.02			
			0.96		0.79	1.04		
			0.99		0.81	0.9	1.34	
			1.30		0.88	0.00		
						0.00		

TABLE 2.3 Con'd...

spectrum could then be compared with those for the commercial magnesia to confirm whether the phase was present or not ; for example, pure Magnesioferrite (MgFe_2O_4): was obtained (from Alfa Neutron) and the spectrum compared with the good commercial magnesia of Fig 2.7. The results are shown in Fig 2.11. (The MgFe_2O_4 was found to contain low levels of copper oxide, Cu_2O).

The analysed spectrum of the good commercial grade magnesia was then compared with each spectrum in turn and the differences noted. Where new peaks appeared the above analysis was repeated to find which phases could have caused them.

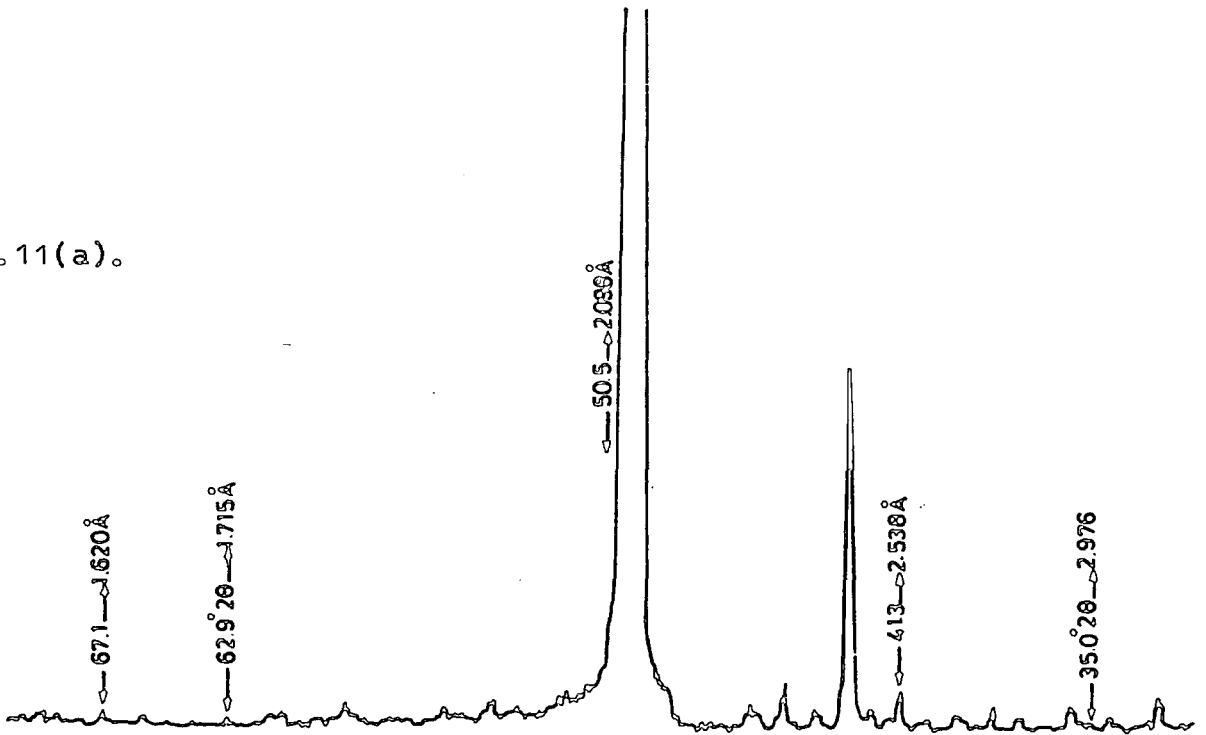
2.4.2 Results and Discussion

The results from the starting material (i.e. caustic calcined magnesia) and the fusion are summarised in Table 2.4.

The spectrum of starting material has many impurity peaks and was found to be consistent with the diffraction patterns of the compounds listed in Table 2.4. The diffraction pattern of only one element was found to fit the spectrum of this starting material, that of nickel. However, the range of d-values of this spectrum is not sufficient to allow the diffraction pattern of nickel to be distinguished from that of nickel carbide, NiC.

The patterns of all these impurities were found in the spectrum from the black region near the centre of the fusion. However, on comparing these two spectra that of the black material had many more impurity peaks than that of the starting material. Also, many of the impurity peaks which appeared in both spectra were stronger (relative to the MgO peaks) in the spectrum of the black material. The patterns of Magnesium Ferrite and/or Manganese Ferrite, Iron, Iron Silicide, Chromium Oxide and Copper Oxide fitted the pattern of new peaks in the spectrum of the black material.

2.11(a).



2.11(b).

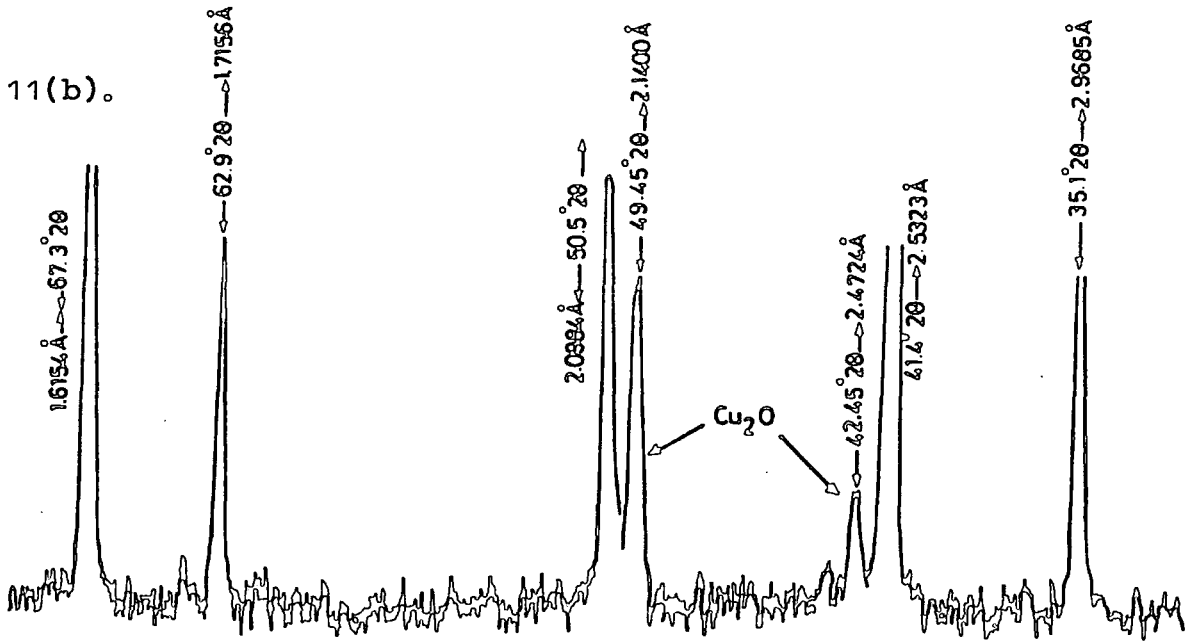


Figure 2.11. Comparison of the XRD spectra of (a) good commercial magnesia with (b) pure magnesioferrite.

Sample	Impurity Phases Detected		
	Certain	Likely	Possible
Caustic calcined magnesia	Mn oxides Al silicates	Mg Sulphate Ca Silicates Ni/NiC Iron Carbide Fe Sulphate Fe ₂ O ₃ Ca Chloride	Fe Oxide Mg Silicide Cr Silicide Zr Nitride Ni Ferrite Zr Oxide Ca Phosphide Mn SO ₄
Centre of fusion	Mn oxides Al silicates	Mg Sulphate Ca Silicates Ni/NiC Iron Carbide Mg/Mn Ferrite Mn Sulphate	FeO Fe Silicide Ca Phosphide
Outer part of fusion	Mn oxides Al silicates Fe ₂ O ₃	Mg Sulphate Mn Sulphate Ca Silicates Ni/NiC Iron Carbide Mg/Mn Ferrite	FeO Fe Silicide Mg Silicide Ni Ferrite Ca Phosphide Ca Chloride
Black region of fusion	Mn oxides Al silicates Fe ₂ O ₃	Mg Sulphate Ca Silicates Ni/NiC Iron Carbide Fe Sulphate Mn Sulphate Mg/Mn Ferrite Iron Ca Chloride Fe Silicide	Cr Oxide Cu Oxide FeO Mg Silicide Cr Silicide Zr Nitride Ni Ferrite Zr Oxide Ca Phosphide

TABLE 2.4: Summary of results of analysis of starting material and samples from fusion.

Conversely, the spectra of the other regions of the fusion had fewer peaks than the starting material, lacking peaks characteristic of Iron Sulphate, Chromium Silicide and Zirconium Nitride and Oxide. The spectrum of material from the centre of the fusion also lacked peaks characteristic of Fe_2O_3 , Magnesium Silicide, Nickel Ferrite and Calcium Chloride. However, both the outer and the centre of the fusion had gained peaks concurring with the diffraction pattern of Magnesium Ferrite and Manganese Ferrite. Generally the impurity peaks of the spectra of these regions were of lower intensity than those of the starting material and the black region, showing that the former fused regions are purified, at the expense of the black region, by the fusion process.

The introduction to the fusion of a phase which is not apparent in the starting material may occur for any of several reasons : a phase may be introduced by contact with the heating apparatus or a phase may form when ions dissolved in the molten, or indeed in the solid magnesia, form a new compound. Since the ferrite must be present in a concentration greater than $\sim 1\%$ to be detected by diffractometry, and the heating apparatus consists principally of carbon, the latter seems more likely.

The existence of peaks concurring with the patterns for Iron Sulphate, Chromium Silicide and Zirconium Oxide and Nitride in the spectra of both the starting material and the black material, but in no other spectrum of the fusion, implies that these impurities, although initially spread throughout the material in the furnace, migrate to the black region from the other areas during the fusion process. Similarly the four phases absent from the centre of the fusion but present in the starting material and the other areas of the fusion (Fe_2O_3 , Magnesium Silicide, Nickel Ferrite, and Calcium Chloride) appear to have migrated to the black region, since their characteristic peaks are stronger

relative to the MgO peaks on the spectrum for the black region than for the other regions, or the starting material. Migration to the black region may also explain the appearance of peaks in the spectrum concurring with the patterns of Chromium Oxide, Copper Oxide, Iron and Iron Silicide. These phases may have been present in the starting material in concentrations lower than 2%, but after migrating to the black region the concentrations were sufficient to allow detection.

The fused magnesia from the outer and inner regions of the fusion was ground separately and samples of the resulting powder exposed in the X-ray Diffractometer. The spectra of this ground magnesias were very similar to those of their counterparts from the fusion, except for the appearance of two new low intensity peaks at $d = 1.166 \text{ \AA}$ and $d = 1.425 \text{ \AA}$. The only pattern of the A.S.T.M. index that could be found to fit both these peaks was that of elemental Iron (A.S.T.M. pattern NO. 6.696). This pattern's six strongest lines are at d -values of 2.03, 1.17, 1.43, 0.91, 1.01 and 0.83 \AA , the last being the weakest. The last three lines lie outside the range of d -values tested by these exposures, the second and third strongest lines match the new peaks of the present spectra very well, and at $d = 2.03$ on the spectra a weak line does indeed appear. Thus elemental iron seems likely to be present, being added to both magnesias on grinding.

On comparing the spectra of powders before and after annealing-type heat treatments, very few differences could be detected, the only notable change being a drop in the height of the peaks corresponding to Fe_2O_3 , relative to the peak heights of MgO and other impurities. At the same time new peaks appeared, but could not be readily identified; thus the peaks are due either to several different phases or to one "uncommon" phase (see section 2.5).

However, the quenching treatment reduced the height of peaks attributed to Fe_2O_3 , Mn/Mg Ferrite, and to a lesser extent those of aluminium substrates and magnesium substrates. This apparent cleaning effect was more marked in material from the centre of the fusion than in the outer brown fused material. There were no new peaks, and no peaks corresponding to those that appeared after the annealing treatment.

Inspection of the spectra of the samples taken before and after magnetic separation and of samples of material swept from the magnet pole faces suggests that the magnets preferentially remove Fe, Mg/Mn Ferrite, Ni/NiC, Ni Ferrite, and Fe_2O_3 from the powders, although peaks corresponding to all the phases seen in the material taken before the separation appeared in the spectra of material swept from the magnet powders. The notable feature was that the magnets were not more efficient at removal of the magnetic phases. Even ferromagnetic iron was detectable in the spectra of material taken after separation. Surprising also was the large amount of MgO attracted to the pole faces. This material did seem to be electrostatically charged and perhaps this accounts for the unlikely degree of attraction of non-magnetic material to the magnets.

CHAPTER TWOREFERENCES

- 2.1 R.W.G. Wyckoff, "Crystal Structures", Vol.I.
Wiley-Interscience N.Y. (1965).
- 2.2 F.A.Cotton and G.Wilkinson, "Advanced Inorganic Chemistry", 3rd
edition, Wiley-Interscience N.Y. (1972).
- 2.3 R.D.Shannon and C.T.Prewitt, Acta.Cryst. B25, (1969) 925.
- 2.4 J.S.Thorp, and N.Enayati-Rad, J.Mat.Sci. 16 (1981) 255.
- 2.5 J.S.Thorp, B.L.J.Kulesza, N.E.Rad, S.V.J.Kenmuir, 16,
(1981) 1052.
- 2.6 "Powder Diffraction Search Manual", Joint Committee on Powder
Diffraction Standards, Pennsylvania U.S.A, (1976).

CHAPTER THREEMAGNETIC SUSCEPTIBILITY STUDIES

Magnetic susceptibility measurements can be made using several techniques, for example, the induction method, the force method, the vibrating sample magnetometer (V.S.M), the Curie method and the Gouy balance technique. The induction method and the force method are only of use for magnetisations of ferromagnetics, but their sensitive variants, the V.S.M. and Curie method respectively could be used to measure the much weaker magnetisations associated with ferrimagnetics, paramagnetics and even diamagnetics. The V.S.M. vibrates the sample in a magnetising field inducing an alternating signal in the pick-up coils. If a reference signal is used to eliminate errors due to spurious vibrations and temperature fluctuations then this is a very sensitive technique. However, the system is a complex one designed for plotting the hysteresis loops of crystalline samples and hence is an arduous way of obtaining a susceptibility. Furthermore, the crystalline sample must be simulated by a sintered powder and so this method was rejected in spite of its accuracy, for problems with time and availability. The Curie method measures the magnetic force exerted on a small sample suspended between the poles of an electromagnet. For maximum sensitivity the sample must rest level with the upper edge of the pole-gap, i.e. where the field gradient is maximum, but this gradient is extremely difficult to measure accurately. This measurement may be omitted if a standard is used, but only relative values of susceptibility can be obtained and often without sufficient accuracy. The sample requirements are stringent since the size must be great

enough to allow a force to register but small enough to make the field gradient approximately constant across the sample. However, the Gouy balance technique is a simple method of obtaining an absolute value of paramagnetic susceptibility and is the most appropriate for powders.

3.1 The Gouy Balance Technique

The Gouy method (Gouy, 3.1) was first used extensively by Pascal (Pascal, 3.2) and is another variant of the force method. It measures the force exerted on a sample suspended in a magnetic field gradient. The force acting on any magnetisable sample situated in a magnetic field may be calculated from the variation of its free energy with position (Crangle, 3.3). In the force method the magnetisation is uniform and the field varies with position so the force exerted is given by the tensor equation

$$\underline{F} = - \underline{VM} \cdot \underline{\nabla B} \quad 3.1$$

where V is the volume of the sample, \underline{M} the magnetisation tensor and $\underline{\nabla B}$ the gradient of the magnetic flux density due to the applied field \underline{H} .

In general $\underline{B} = \mu \underline{H}$ (where $\mu = \mu_0 \mu_r$), which for free space reduces to:-

$$\underline{B} = \mu_0 \underline{H} \quad 3.2$$

where μ_0 is the magnetic constant.

This relation holds to a

very good approximation for air. Now, writing equation 3.1 in Cartesian form gives:-

$$-\frac{1}{V} F_x = M_x \frac{\partial B_x}{\partial x} + M_y \frac{\partial B_y}{\partial x} + M_z \frac{\partial B_z}{\partial x}$$

$$-\frac{1}{V} F_y = M_x \frac{\partial B_x}{\partial y} + M_y \frac{\partial B_y}{\partial y} + M_z \frac{\partial B_z}{\partial y}$$

$$-\frac{1}{V} F_z = M_x \frac{\partial B_x}{\partial z} + M_y \frac{\partial B_y}{\partial z} + M_z \frac{\partial B_z}{\partial z}$$

In the Gouy Method the electromagnet provides a unidirectional field between the poles in the x direction making $B_y = B_z = 0$ and a long thin sample is aligned in the z direction with one end between the magnet poles and the other in a relatively field free region (see Fig 3.1). In this configuration most samples in laboratory fields have negligible force exerted in the x and y directions, so equation 3.3 become:-

$$-\frac{1}{V} F_z = M_x \frac{\partial B_x}{\partial x} \quad 3.4$$

Volume susceptibility (K) is defined:-

$$K = \frac{M_x}{B_x} \quad 3.5$$

Substituting into equation 3.4 gives:-

$$F_z = V K B_x \frac{\partial B_x}{\partial z} \quad 3.6$$

Now considering the arrangement of Fig 3.1, the small vertical force acting on the element of volume dV is given by:-

$$dF_z = dV K B_x \frac{dB_x}{dz} \quad 3.7$$

For a powder packed tube (see Fig 3.2) the elemental volume dV is given by:-

$$dV = \frac{\text{elemental mass}}{\text{density of sample material}} \quad 3.8$$

$$= \frac{a \, dz \, \rho_1}{\rho_2} \quad 3.9$$

where a is the cross-sectional area of the sample

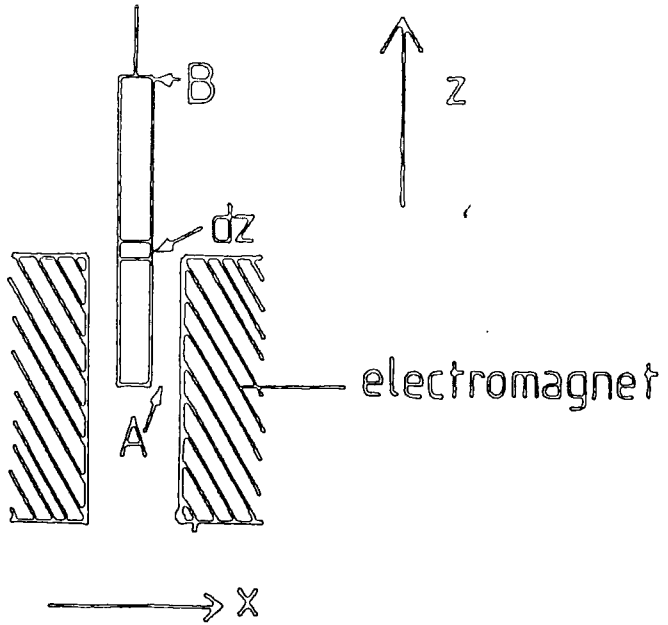


Figure 3.1. Principle of the Gouy method.

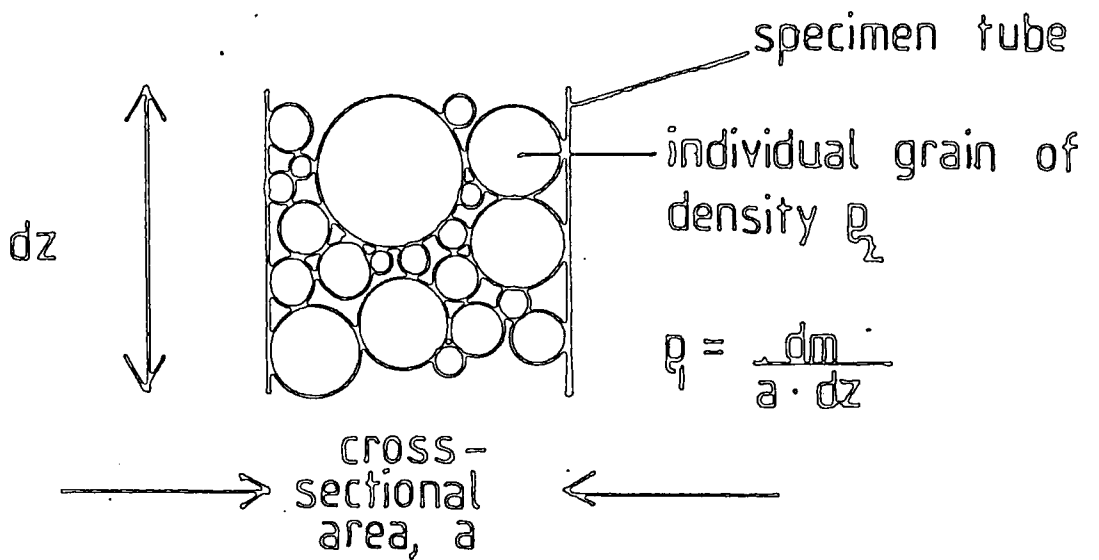


Figure 3.2. An elemental volume of powder.

ρ_1 is the packing density of the powder
and ρ_2 is the density (specific gravity of the material itself).

Substituting into equation 3.7 gives

$$dF_z = \frac{\rho_1}{\rho_2} a dz K B_x \frac{dB_x}{dz} \quad 3.10$$

and integrating from A to B (the ends of the sample column) yields finally

$$F_z = \frac{1}{2} \frac{\rho_1}{\rho_2} a K (B_{x_A}^2 - B_{x_B}^2) \quad 3.11$$

B_{x_A} and B_{x_B} can be determined via an initial calibration with a Hall probe and teslameter and since ρ_1 and ρ_2 can be measured accurately the total volume susceptibility for two sample, K_T , can be determined absolutely. $(B_{x_A}^2 - B_{x_B}^2)$ should be as large as possible to make the reading of F_z greater and hence more accurate.

If the material is a single substance the susceptibility of the substance is uniquely determined, and indeed K_T could be useful as a means of identifying the substance.

However, if the sample contains more than one magnetic component then K_T is given by Wiedemann's Law:-

$$K_T = aK_a + bK_b + cK_c + \dots \quad 3.12$$

where a, b, c, \dots are the fractional concentrations of the sample components A, B, C... whose volume susceptibilities are K_a, K_b, K_c , etc; the experimental measurement of K_T does not per se enable identification of the separate components, a task for which additional independent chemical and structural information is required.

Further, the assumption is made that K_T is a constant independent of applied field, i.e. that the sample is paramagnetic (or diamagnetic); thus this calculation applied to ferromagnetics, ferrimagnetics or superparamagnetics does not produce a true susceptibility as a result. However it is evident that a sample failing to produce the same value of susceptibility for different field values must contain some non-paramagnetic content, and also that the greater this content, the greater the force on the sample. In these cases measurement of force and calculation of susceptibilities at constant fields B_{x_A} and B_{x_B} , do provide useful comparative values which should not be regarded as "true" susceptibilities in any of the senses which this quantity is conventionally defined for hysteretic materials. Given that the magnetisations associated with ferromagnetics are about five orders of magnitude greater than the diamagnetic or paramagnetic magnetisations, the presence of such impurities should be readily detectable since their properties will dominate even at low concentrations, and in such samples force becomes a measure of relative concentration of high "susceptibility" impurity.

3.2 Experimental Techniques

The apparatus was set up as shown in Fig 3.3. After preliminary trials the optimum conditions of operation were determined. The pyrex tube was of 2mm bore and 200mm in length and was always filled to a height of 188mm (approximately 2-3 grams of MgO powder). These dimensions insured negligible magnetisation in the x and y directions and also that the upper boundary lay in a relatively field free region (7.5 mT) compared with the field at the lower boundary (360 mT). A correction was made for the small susceptibility of the glass tube.

Care was taken in packing the powder to insure homogeneity both in packing density and concentration of the various components of the powder mixtures.

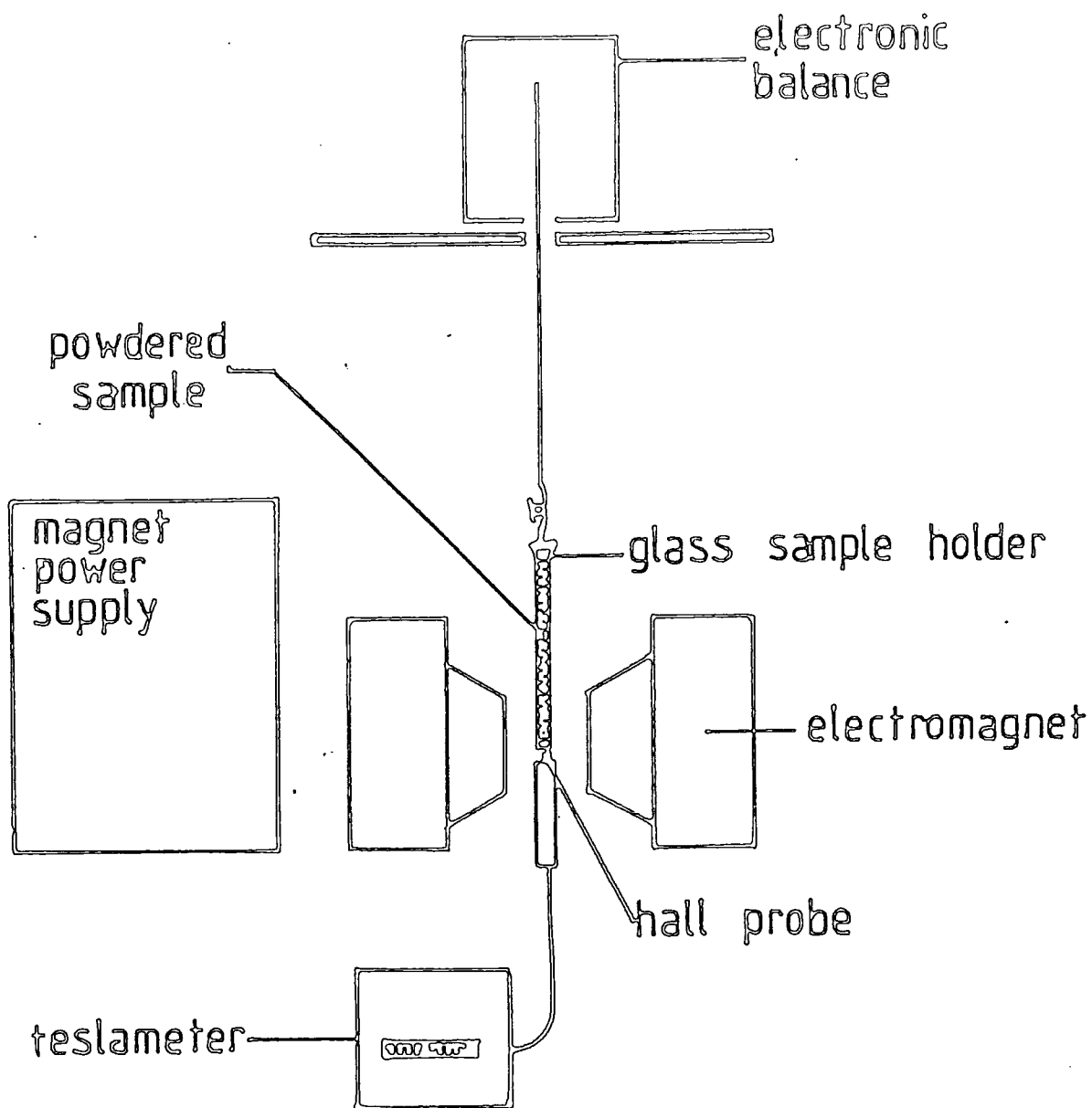


Figure 3.3. Apparatus for measuring volume susceptibility.

When the electromagnet was switched on the sample became magnetised and experienced a force measured as a mass on the electronic balance. The force (given by equation 3.11) could be measured to ± 0.05 mg implying an accuracy in volume measurement of $\pm 2 \text{ JT}^{-2} \text{ m}^{-3}$. The force due to the tube alone was measured and subtracted.

It should be noted that the volume of the sample used for measurement is small ($\sim 0.6 \text{ cm}^3$) and therefore very small changes in concentration of highly magnetic impurities may cause substantial differences in the susceptibilities of different samples taken from one, nominally homogeneous bulk specimen. Equally the successful use of the Oertling electronic balance depends on the precise maintenance of balance position and level. Any vibrations of the table on which the balance stands, or even the effects of air currents on the suspended sample introduce systematic changes in the readings. To improve accuracy the apparatus assembly was rebuilt to incorporate a very strong table, enclosure of the sample and water cooling for the magnet enabling the use of higher fields. The improved apparatus produced greater repeatability of results (in spite of variations of ferromagnetic impurity concentrations) and allowed comparison between similar low susceptibility powders.

3.3 Results for Pure Magnesium Oxide

Several brands of pure magnesium oxide were examined, the lowest susceptibility powder was assumed to contain the least (higher susceptibility) contamination and was used as the standard for control throughout the work.

Susceptibility measurements on the Koch-light (K-L) pure MgO were repeated to assess the accuracy of the apparatus. The average of the measurements was taken and the percentage error calculated from the greatest difference from the average. This gave an error of $\pm 2/5\%$.

The errors arise, primarily, from inaccuracy in measurement of weight and field. The resolution of the balance was 0.11 but six weight readings are used to calculate the susceptibility and thus a balance inaccuracy is significant, particularly for low susceptibility values. Although the effects of vibrations and air currents were minimised when the apparatus assembly was rebuilt, the errors due to these were still in excess of balance resolution.

The error in field reading is caused by inaccuracy in measurement technique (the Hall Probe must be oriented for a maximum reading), and the difficulty of taking these readings makes it impossible to assess field fluctuations with time. A different type of uncertainty in measurement is caused by inhomogeneities in packing density and, where impurities are present, because the density (specific gravity) and susceptibility are not uniform for the whole sample column. None of these effects can be assessed easily.

3.4 Results from Commercial Magnesia Powders

Two groups of materials have been examined. The first comprised solid pieces cut from a fused MgO melt in order to find its susceptibility profile, (visual examination of the cross-section of the fused melt shows marked radial differences in both colour and texture indicative of impurity segregation). Parts of each solid specimen were ground individually to provide powdered material.

The second group consisted of powdered magnesia samples, taken from stages of the manufacturing process, to assess the effects of the various treatments. Lists of the contents of each group are given with the summary of results shown later. All measurements were made at room temperature (20°C).

It became apparent that, whilst several readings taken for any given sample were well within experimental error ($\pm 2.5\%$), if the

contents of the specimen tube were exchanged for different powder taken from the same stock then the readings could differ by $\pm 5\%$. Several readings were therefore taken for different powder of the same stock and an average value calculated for each stock. Given that care was taken to assure an even mix of the powder particles it seems unlikely that this variation in susceptibility could be caused entirely by variation of the percentage of pure MgO in each sample tube. However, such variation in the susceptibility value would occur if there were even very slight variations in the concentration of a high susceptibility impurity. Impurities are known to be present in the commercial magnesias (the x-ray diffraction study revealed patterns corresponding to Iron, Magnesioferrite etc) which have high magnetisations at the high field value used to determine the susceptibility values.

3.4.1 Results from Fusion Stage

The results from the fusion are given in Table 3.2. The first point of note is that all the samples have susceptibility values greater than the value for pure MgO (-20.3 JT m^{-3}) thus all the fused samples have some impurity with a positive susceptibility value, i.e. ferroferri-, or paramagnetic impurity.

The highest susceptibility values are found for the Bloch region; the value for the centre of this region being 9 or more times greater than the values for the other regions. Thus the impurity concentrations and/or the impurities' susceptibility values here are greater.

The samples from the centre of the melt have the next highest susceptibility values and these are about twice the values recorded for samples of green material taken from the region on the outer side of the black band. The chemical analysis shows that the average MgO content of

"Pure" Magnesia Brands	Volume Susceptibility $J T^{-2} m^{-3} \pm 5\%$
Aldrich Chemicals Gold Label Pure MgO	- 5.4
Johnson-Matthey Specpure grade Magnesia	25.8
Koch-Light 99.998% pure magnesia	-20.3
Spicer's 3N pure magnesia	21

TABLE 3.1: Results from pure MgO

Sample Code	Sample Description	"Volume Susceptibility" $(J T^{-2} m^{-3} \pm 5\%)$
Batch I a	MgO nearest centre of melt	54
b	"	37
c	"	58
Batch II a	MgO near green/brown boundary	24
Batch II b	Green end of green/brown boundary	34
c) intermediate sections	26
d		14
e	brown end of green/brown boundary	10
Batch II f	MgO near green/brown boundary	-5
Batch III	MgO from outer region	-9
Batch IV A	MgO at green/black boundary	246
Batch V	Black material	465
Batch IV B	MgO at green/black boundary	245

TABLE 3.2: Susceptibility data for specimens taken from a fused melt.

the green material is 96.7%. Using Wiedemann's Law:-

$$K_{\text{sample}} = aK_{\text{MgO}} + bK_{\text{impurities}} \quad 3.13$$

where a is the fractional concentration of MgO and b is the fractional concentration of the impurities. Taking the average volume susceptibility value for MgO from the centre ($50\text{JT}^{-2} \text{m}^{-3}$), the volume susceptibility established for pure MgO and the average MgO concentration for green material, a value for the volume susceptibility of the impurities of $K_{\text{impurities}} = 2110 \text{ J T}^{-2} \text{m}^{-3}$ was obtained. This value is of the order of those obtained for strong paramagnetic materials and it suggests that some of the impurities are strongly magnetic relative to the diamagnetic MgO lattice.

The x-ray diffractometry results for the black region (see Chapter 2) show more impurity peaks, stronger in intensity than those for other regions of the fusion, suggesting that the concentration of MgO (in equation 3.13, " a ") is less in the Black region than the average 96.7% for green material, or indeed even then the average of 94.1% for brown material, and also that the value of $K_{\text{impurities}}$ is different. Thus solutions of the equation 3.13 lie along the line:-

$$465 = -20.3a + (1-a) K_{\text{impurities}} \quad 3.14$$

where 465 is the value of K_{sample} for material of the black region, -20.3 is the value of K_{MgO} . The solutions are plotted in the graph of Fig 3.4, for arbitrary values of ' a '.

The Wiedemann's Law calculation was performed for the other regions giving the $K_{\text{impurities}}$ value for the green region between the outer brown and black regions of $\sim 1,300 \text{ JT}^{-2} \text{m}^{-3}$ and a value of $171 \text{ JT}^{-2} \text{m}^{-3}$ for the outer region. This last result is the most surprising for,

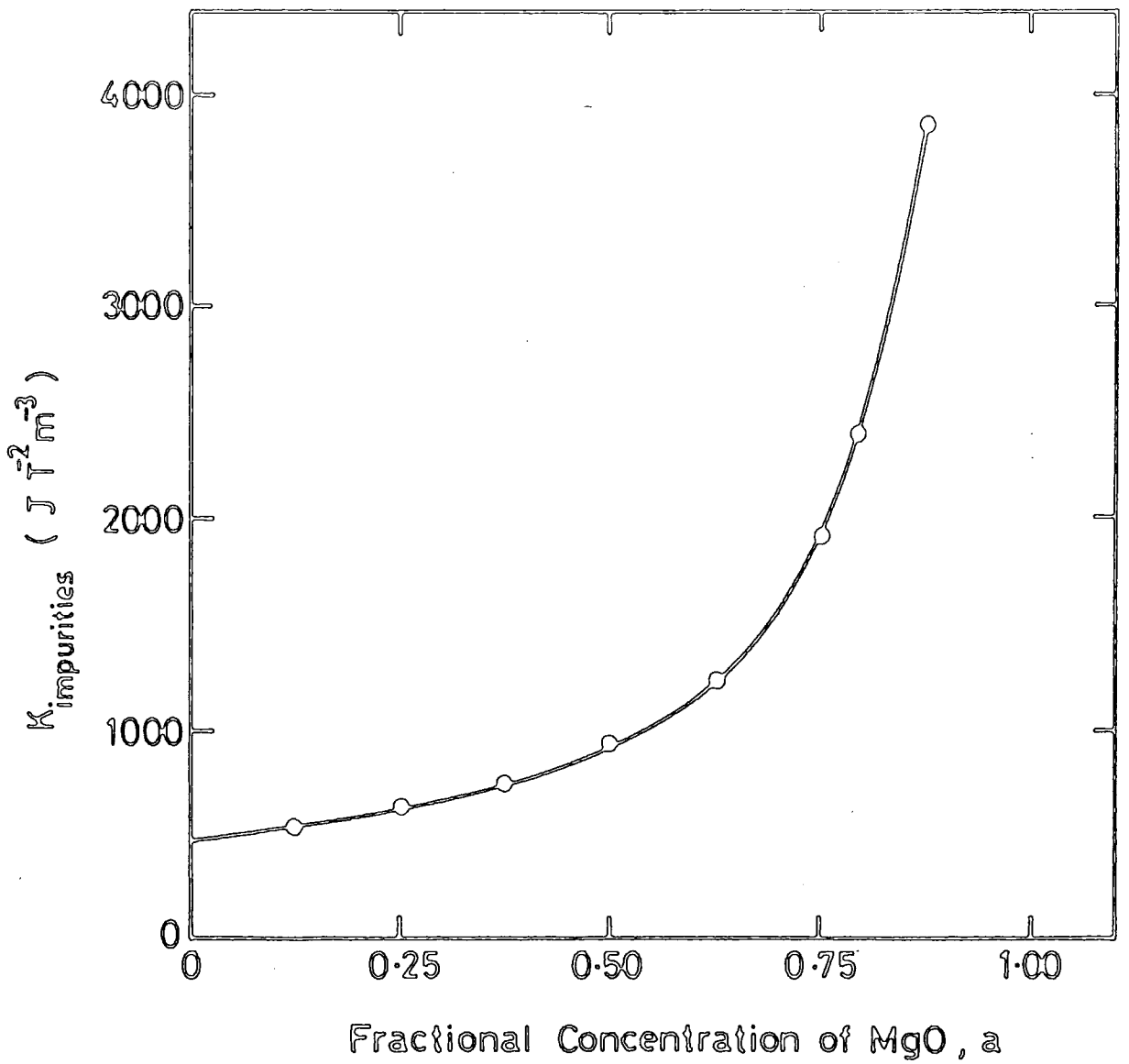


Figure 3.4. Solutions of Wiedemann's Law for material of the black region of the fusion.

whilst the fractional concentration of the impurities in the outer region is greater than that for the inner green regions (94.1% compared with 96.7% for inner region), the susceptibility of the impurities has dropped to a tenth of the values for the green regions. This shows that the magnetic impurities are concentrated in the inner region and the non-magnetic impurities in the outer region.

The same experiment was repeated, this time using lower fields : 183mT at the bottom of the sample tube (A) and 3mT at the top (B).

All the susceptibility values calculated for lower applied fields were greater than their high field counterparts, (see Table 3.3), except for those of brown MgO from the outer region, where the two values were the same. All the positive susceptibility values were not constant with applied field, the ratio of high field values to low field values being about 2:3. Thus the equation 3.5 defining susceptibility:-

$$K = \frac{M_x}{B_x} \quad 3.15$$

no longer holds, the graph of M_x against B_x is not a straight line as it would be for paramagnetics, but instead the gradient decreases with increasing applied field, implying a saturation or hysteretic effect. Given the almost certain presence of $MgFe_2O_4$ in the fusion (see Table 2.4) this effect is not so surprising since $MgFe_2O_4$ is ferrimagnetic at room temperature and likely to saturate at fields near 360 mT.

3.4.2 Results from Post-Fusion Stages of Processing

As outlined in the Introduction the manufacture of commercial magnesia has several post-fusion stages (including milling, grinding, calcining and magnetic separation) being used to aid purification, and hence improve the electrical resistivity of the material. Grinding, (apart from being essential, practically, to obtain the correct flow

Sample Code	Sample Description	"Susceptibility" at $B_A = 183 \text{ mT}$ ($J T^{-2} \text{ m}^{-3} \pm 5\%$)	"Susceptibility" at $B_A = 360 \text{ mT}$ ($J T^{-2} \text{ m}^{-3} \pm 5\%$)
Batch I a	MgO nearest centre of melt	83	54
b	"	53	37
c	"	92	58
Batch II a	green MgO near green/brown boundary	35	24
Batch II b	Green end of green/brown boundary	53	34
c)	intermediate sections	37	26
d)		23	14
e	brown end of green/brown boundary	13	10
Batch II f	brown MgO near green/brown boundary	-4	-5
Batch III	MgO from outer region	-9	-9
Batch IV A	MgO at green/black boundary	335	246
Batch V	Black region	753	465
Batch IV B	MgO at green/black boundary	325	245

TABLE 3.3: Susceptibility results using lower fields.

characteristics to permit satisfactory filling of heating elements) also influences electrical properties by introducing an additional resistivity factor between the boundaries of one particle and the next. However, the mills of the commercial plants may suffer wear, thus introducing metallic impurity to the resulting powder. This factor may not be negligible as magnesia is one of the hardest, and therefore most abrasive, materials produced commercially, and the material introduced, invariably metal, is a good electrical conductor. Magnetic separation is generally used to assist with the removal of some metals, and other highly magnetic impurities. The material is passed through the strong magnetic field and the magnetic material is attracted to the poles leaving a purer substance behind. The many different calcining processes may be divided into two broad categories : those where the material is annealed, and those where it is quenched.

The effects of some of the various stages of the commercial process were treated by taking samples from the fusion of inner (green) material and outer (brown) material and measuring their susceptibilities before and after grinding, annealing, quenching and magnetic separation. Distinctions between the inner and outer fused material could thus be investigated further. The results are shown in Table 3.4.

The grinding stage increases the susceptibility (measured at full field) for both inner and outer material of the fusion. The effect is greatly more dramatic in the outer than the inner region of the fusion. The most likely of a number of possible explanations for this feature is that the impurity in the fused outer magnesia was highly localised and thus did not feature in the earlier measurements. It seems most unlikely that the outer material could erode more metal from the mill, as it is in fact noticeably more friable than the fused inner MgO. Considering only the inner result, the impurity introduced on grinding is not greatly significant.

A. Inner (green) material from fusion

	Grinding	Annealing	Quenching	Magnetic Separation
Before	47	52	78	30
After	52	35	18	12

B. Outer (brown) material from fusion

	Grinding	Annealing	Quenching	Magnetic Separation
Before	-9	121	116	49
After	121	197	46	7.9

C. Material swept from magnet poles

Inner (green)	613
Outer (brown)	3886

TABLE 3.4: Susceptibility results from before and after the various stages of commercial MgO manufacture. (measured in $J T^{-2} m^{-3}$ at room temperature, standard full field).

The inner and outer materials again show distinct respective results in the test of the annealing heat treatment. The material, having been heated to 600–800°C was cooled gradually, over many hours, to room temperature. The inner material reduced a little in susceptibility, whilst the outer material became more magnetic. This suggests that at least some of the impurities in the two materials are quite different ; those of the outer material and containing a component (or components) that react on heating to enhance the magnetic properties, those of the inner material reducing the susceptibility.

However, the alternative calcining process, where the heated material was quenched from 1800°C to about 100°C produces the same effect in both inner and outer materials, namely dramatically to reduce the susceptibility. This suggests that the high temperature phases in both materials are less magnetic than those formed at lower temperatures during annealing. The outer material is more magnetic than the inner, again suggesting that it contained more and/or different impurities after fusion.

The magnetic separation is notably more effective on the outer material. Apart from producing a less magnetic material ($7.9 \text{ J T}^{-2} \text{ m}^{-3}$ for outer, $12 \text{ J T}^{-2} \text{ m}^{-3}$ for inner MgO), the material drawn from the poles of the magnetic pole faces is greatly more magnetic for outer than inner MgO (3896 to $613 \text{ J T}^{-2} \text{ m}^{-3}$). Thus, the impurity of the outer is much more readily separable, being of higher susceptibility than that of the inner. Inspection of the swept material shows significantly more MgO to be present amongst the separated (red/brown) material of the inner MgO than could be seen in the outer counterpart.

Of the treatments tested only the annealing heat treatment had a deleterious effect, and then only upon material from the outer parts of the fused melt.

3.5 Results from Chromium Doped MgO and Magnesiochromite

Recent electron spin resonance work [(Skinner 3.4)] carried out on single crystals of MgO doped with chromium in the range 760-9,500 p.p.m. suggested that a chromium spinel was formed after a heat treatment similar to some commercial calcining treatments, and since the commercial powders were known to contain chromium some specific investigations were made on the Cr/MgO system.

It was first necessary to characterise the spinel in terms of its susceptibility. From literature [3.5] MgCr_2O_4 is deemed to be antiferromagnetic with a Neel point of 4K. Thus at room temperatures the material is expected to be strongly paramagnetic. A pure MgCr_2O_4 powder (Alfa Chemicals 99% pure) was obtained and the susceptibility measured for various fields ; the results are shown in Table 3.5. Although there is a slight decline in value with increasing field, this is within experimental error and is possibly due to the impurities. The susceptibility could be calculated with the best accuracy from the gradient of a plot of force against $(B_A^2 - B_B^2)$; see Fig 3.5. This gave a susceptibility for chromite of $1,501 \text{ J T}^{-2} \text{ m}^{-3}$.

Skinner's work had been carried out using single crystals of MgO doped with Chromium which had been grown by electrofusion and supplied by W & C Spicer Ltd. (Cheltenham). However, since powder was required here, single crystal chippings, (taken from the edge of the single crystal fusion) were obtained from W & C Spicer Ltd. and were crushed to form powder suitable for the Gouy magnetometer. The chromium concentrations were determined by X-ray fluorescent analysis, as were the typical concentrations of the impurities, (Table 3.6).

The samples were heated for $\frac{1}{2}$ hour to 800°C , the typical temperature of a hot heating element, and then quench cooled to room temperature. The susceptibility was measured again at half the full

Current to magnet poles (A)	$B_a^2 - B_b^2$ (T ²) ± 2%	Volume Susceptibility (J T ⁻² m ⁻³) ± 2.5%
0	0	-
5.0	0.072	1580
6.0	0.097	1597
7.0	0.129	1543
8.0	0.161	1525
9.0	0.193	1501
10.0	0.222	1995

TABLE 3.5: Susceptibility data on 99% pure HgCr_2O_4

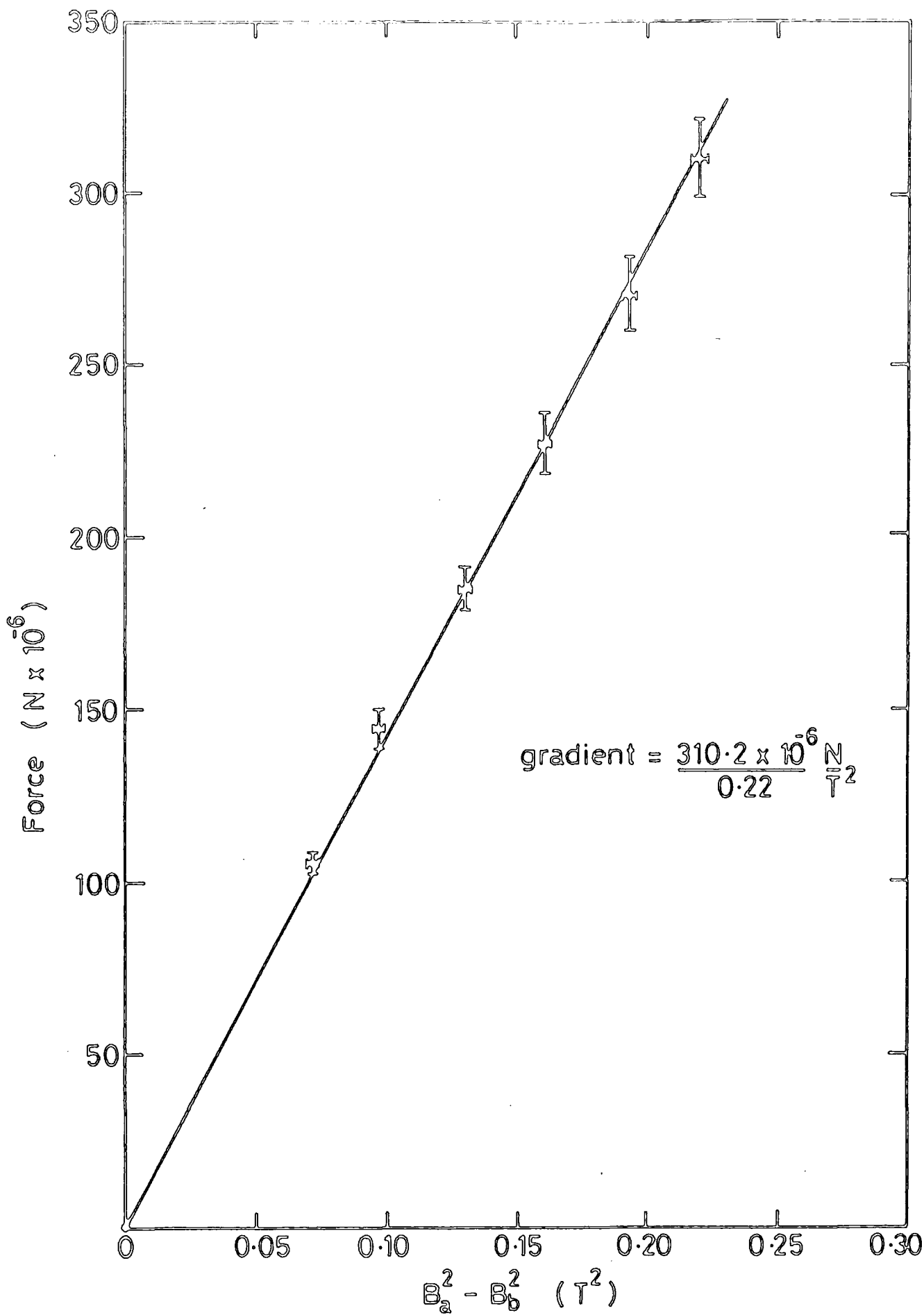


Figure 3.5. Variation of Gouy force on Mg Cr₂ O₄ with varying applied field.²

Impurity	ppm.vt. present
Aluminium	35
Calcium	20
Silicon	15
Iron	3
Nickel	2
Manganese	0.1
Phosphorus	2
Lead	< 1
Sulphur	5
Copper	< 1
Zinc	5
Vanadium	< 2
Arsenic, Potassium	< 5
Titanium	<20
Barium	<0.5
Sodium	1
Zirconium	3

TABLE 3.6: Typical impurity content of Spicer single crystal Cr/MgO.

field as well as at the standard full field. The same powders were then reheated for 1 hr at 800°C and remeasured after cooling, and finally after 2½ hrs at 800°C. The susceptibility measurements were then calculated to see if there was any variation in susceptibility which suggested the formation of the spinel. The results are shown in Table 3.7.

The initial susceptibilities, both at full field and half field, appear to have no dependence upon the chromium doping level. All the samples had higher susceptibilities for the lower field value than at full field, i.e. the susceptibility is not linear with field and the material is not paramagnetic.

The first two heat treatments both reduce the susceptibilities for all the samples. After the first heat treatment the half field values are still greater than the full field values, but after a further hour of heating the half field susceptibilities are lower than (or equal given the resolution of the balance) to their full field equivalents. However, for the lower doping levels of chromium the values are negative, i.e. the material is diamagnetic ; here again the force is not proportional to the field.

The long heat treatment has the effect of raising the susceptibilities generally to a value a little below the initial value. The lower field values are again greater than their full field counterparts.

The detachment of these results from the chromium concentrations was considered. The crystal chippings are taken from the edge of the fused single crystal region, and, on comparison with single crystals of the same chromium concentration, were found to be darker and less even in colour. An X-ray diffraction spectrum of the unheated/MgO (9,500 ppm Cr) crystal chippings was taken to assess the purity of the as-received

Cr/MgO sample (ppm Cr)	hrs heat treatment	Measurements with 7.0 A supplied to magnet				Measurements with 3.5A to electromagnet			
		0	$\frac{1}{2}$	$1\frac{1}{2}$	4	0	$\frac{1}{2}$	$1\frac{1}{2}$	4
9,500		31	22	11.4	24.3	47.8	35.6	0	37.1
7,400		31	0	-7.9	-4.5	18.6	20.8	0	0
5,000		58.2	-4.8	0	28.4	68.1	9.8	0	34.0
3,000		17.1	0	-12.8	-8.2	17.5	9.4	-26.2	-20.2
1,300		-4.1	-12.3	-16.7	-4.0	16.8	8.4	-25.6	15.8
760		35.7	0	-8.3	35.7	73.0	18.0	-17	64.2

TABLE 3.7: Susceptibility data for Cr/MgO crystal chippings
($J T^{-2} m^{-3}$)

material. The results are shown in Fig 3.6 and are summarised in Table 3.8.

As the susceptibility results suggest, the magnetic properties are not dominated by the dopant chromium, but by impurities. Of the three main impurities, magnesioferrite is most likely to be dominating the magnetic properties of the sample, as it is a ferrimagnetic, whereas the other substances making up the sample are either paramagnetic or diamagnetic. The ferrimagnetic $MgFe_2O_4$ would not produce a linear relation between force and field, and would indeed tend to saturate at higher fields producing a lower gradient at higher applied field values.

The apparent reduction in magnesioferrite after $\frac{1}{2}$ hr and $1\frac{1}{2}$ hrs of heat treatment is of interest, since the commercial powders were found to contain magnesioferrite, (see Chapter 2) and the electrical properties (see intro) show it to be lossy. However, with no guide to the proportions of magnesioferrite present in the samples, little can be concluded from the present results.

3.6 Results from Iron Doped Magnesia and Magnesioferrite/MgO Mixtures

Previous electron spin resonance studies of iron-doped magnesia (Fe/MgO) showed clustering (Inglis and Thorp 3.6) and magnesioferrite formation on heat treatment (Inglis, Thorp and Russell 3.7). In the latter study single crystals of MgO doped with iron in the range 100 to 12,900 p.p.m weight Fe/MgO (W & C Spicer Ltd, Cheltenham) were examined before and after heat treatment in oxygen in the temperature range 600-800°C. After heat treatment an isotropic ferrimagnetic resonance appeared on the ESR spectrum and the electron diffraction pattern revealed the appearance of a spinel pattern. In view of these results it seems likely that the concentrations of iron and magnesioferrite in the commercial powders could be influenced by the calcining and indeed subsequent use of these products.

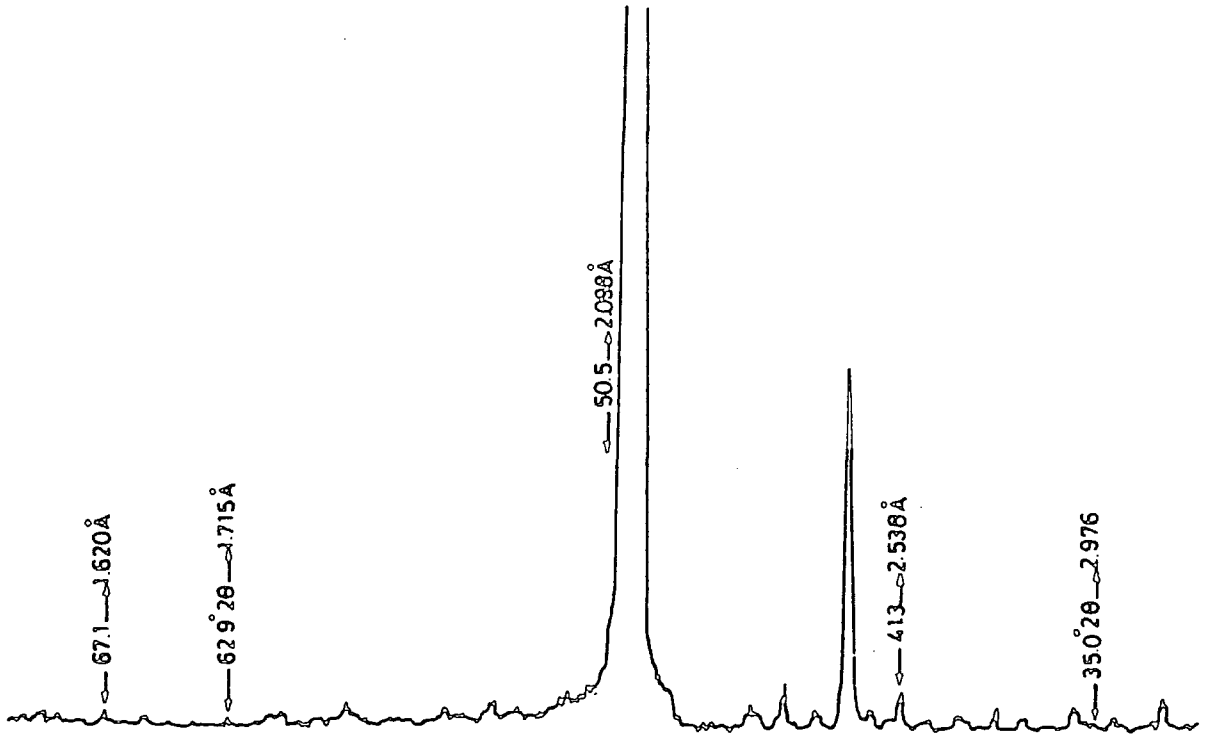


Figure 3.6(a).

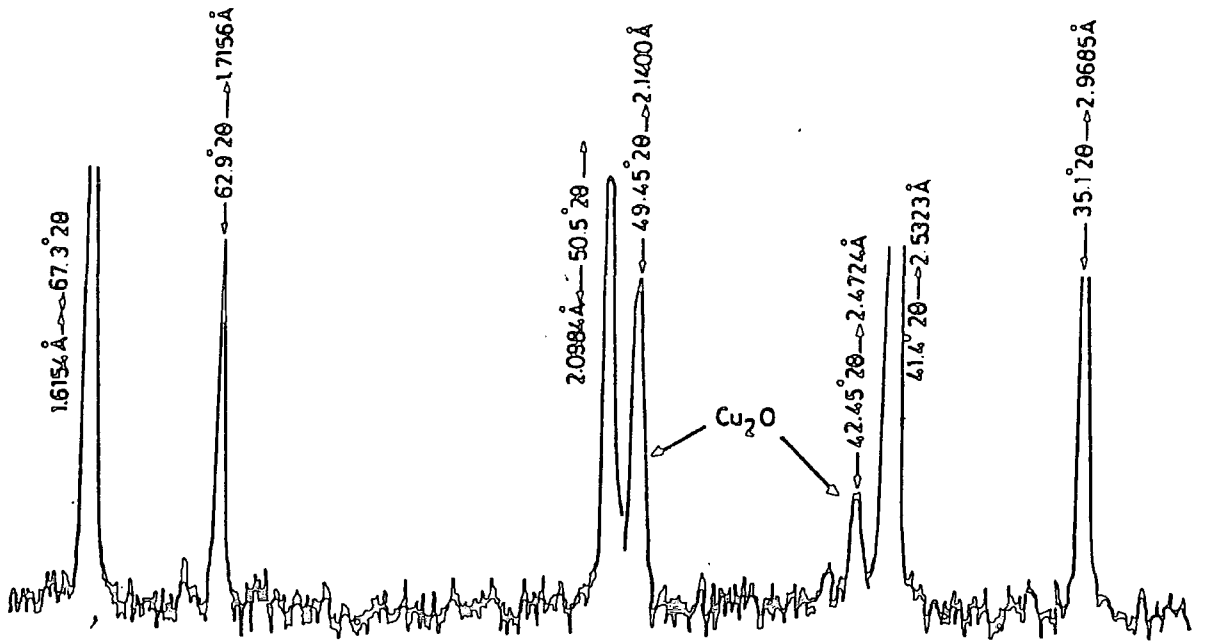


Figure 3.6(b).

Figure 3.6. Comparison of XRD spectra of (a) Cr/MgO single crystal chippings and (b) Alpha Ventron 99% pure Magnesioferrite ($MgFe_2O_4$).

Experimental d values	d values according to ASTM				
	MgO	MgO ₂	Mg ₂ O ₃	MgFe ₂ O ₄	Fe ₂ O ₃
6.09					5.95
4.89				4.89	
3.99		3.96			
3.87			3.84		
3.73			2.74		3.75
3.43			2.72		
3.14		3.14			3.42
2.96				2.96	
2.95					2.95
2.70					
2.54				2.53	2.52
2.47			2.48		
2.44	2.43	2.42 2.41		2.43	
2.33		2.32			
2.11	2.11				
1.71				2.09	2.09
1.66			1.66	1.71	1.70
1.64		1.63			
1.61				1.61	1.61
1.49	1.49				
1.48				1.48	
1.41		1.41			
1.34		1.34			
1.27	1.27				
1.22	1.22				
1.21				1.21	
1.16		1.16			

TABLE 3.8: X-ray diffraction data for Cr/MgO single crystal containing 9500 ppm Cr.

To confirm and characterise this effect, a similar study was made using the Gouy Magnetometer, for which powder was required. However, in order to preserve the benefit of having well characterised starting material, and to give a good comparison with the study of the previous work, each specimen was prepared by grinding single crystal chippings of the same composition and growth batch as the corresponding doped single crystal. The chippings (again, grown by electrofusion by W & C Spicer Ltd) had iron concentrations in the range 310 p.p.m to 12,900 p.p.m Fe/MgO as determined by X-ray fluorescent analysis. The measurements were made at room temperature using the Gouy technique as above, except that, due to an initial limit in sample availability, a shorter sample column was used.

The ageing heat-treatment consisted of heating the powdered samples in oxygen at 800°C (as for the Cr/MgO samples), this being the treatment used in the previous work to form the ferrimagnetic line. The susceptibility was measured before heat treatment and, after quenching at intervals of half an hour during ageing; ageing times up to four hours were used, there being no pronounced changes subsequently.

The initial collected results for the iron doped magnesia powders are shown in Fig 3.7, in which the susceptibility is plotted as a function of ageing time for each level of iron doping. Several points may be noted. For each specimen corresponding to a particular doping level there is a marked increase in susceptibility with time; the rate of increase is largest in the initial stages of ageing and subsequently decreases to zero so as to give a constant value of susceptibility after about 2h ageing; this plateau region extends to the maximum ageing times used (about 4h). Comparison of the behaviour of the different specimens shows that the susceptibility values in the plateau regions increase successively with increasing iron concentration although the times taken for the various specimens to reach the plateau region are approximately

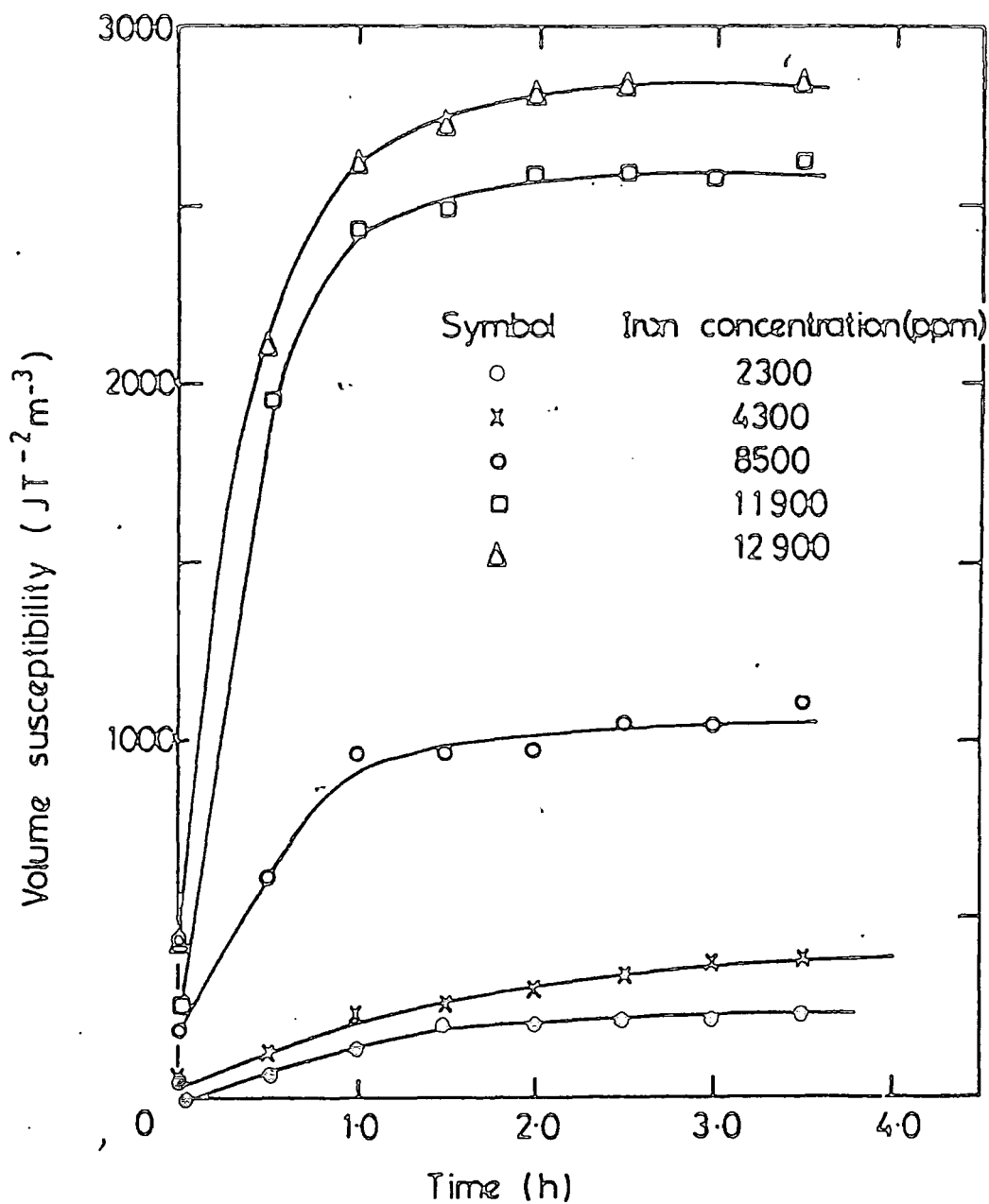


Figure 3.7. Variation of volume susceptibility with length of heat treatment for Fe/MgO samples.

constant. The data given in Fig 3.7 provides direct evidence for the formation of a high-susceptibility magnetic phase after heat treatment and the occurrence of a plateau in each instance implies that all the available iron has been converted. The higher values of resultant susceptibility after ageing for the higher iron concentrations are to be expected on the grounds that more iron is available for conversion. Examination of the data for the specimens in the "as-grown" state, i.e. before ageing, also shows that whereas the susceptibility of the specimen with the lowest doping level (2300 ppm Fe) is comparable with that of pure (undoped) MgO, there is a significant increase in initial susceptibility with concentration. Although even in the extreme case of the 12,900 ppm Fe specimen this initial increase (to $0.4 \times 10^9 \text{ JT}^{-2} \text{ m}^{-3}$) is still quite small in comparison to the much greater increase (to $2.8 \times 10^9 \text{ JT}^{-2} \text{ m}^{-3}$) after 4 h ageing, this result provides confirmation of the deduction from magnetic resonance Fe^{3+} spin-count data that in the as-grown crystals not all of the iron is in the Fe^{3+} state.

The validity of a two-phase model for the system may be assessed by examining the variation of this resultant susceptibility with iron concentration in terms of the applicability of Wiedemann's law. If one postulates a two phase system consisting of the pure MgO (or MgO containing Fe^{3+} substituted as isolated ions at cubic sites) and a single magnetic phase, the magnesioferrite phase, the overall resultant susceptibility will be given by:

$$kT = ak_{\text{MgO}} + bk_{\text{Magnesioferrite}} \quad 3.16$$

where a and b are the respective volume fractions of the two phases. Here $k_{\text{MgO}} \ll k_{\text{Magnesioferrite}}$ so to a good approximation the resultant susceptibility should vary linearly with iron concentration. When the equilibrium value data from Fig 3.7 are used to show the variation of

resultant susceptibility with iron concentration the plot of Fig 3.8 is obtained. Up to concentrations of 8300 ppm Fe a reasonable fit to a linear variation is obtained but it is noticeable that the points corresponding to the two higher concentrations depart considerably from the extrapolation of the line fitting the lower concentration data. This suggests the possibility of the breakdown of the two phase model and perhaps the occurrence of an additional magnetic phase at high doping levels. It is interesting to note also that the magnetic resonance data showed that an intermediate state characterised by a strong isotropic ESR line, exists as a precursor to the formation of fully ferrimagnetic material, adding weight to this explanation. This additional magnetic phase would be very unlikely to be caused by impurities as these are present at such low concentrations compared with that of the iron (e.g. Nickel 2 ppm wt percent, Manganese 0.1 ppm at percent [Table 3.6]). The present results are not adequate further to support or reject this conjecture.

However, the departure from the straight line predicted by Wiedemann's law may be explained in other ways. From equation 3.11, the calculated susceptibility, k , depends directly on the Force measured on the balance, given that the field values were constant and the packing densities were very similar for all the susceptibilities calculated. From equations 3.5 and 3.6 it is found that the force measured on the balance is given by:-

$$F_z = V M_x \frac{\partial B_x}{\partial z} \quad 3.17$$

The magnetic properties of the samples in question will be dominated by the ferrimagnetic properties, even though more than 98% of the sample is MgO. Thus the force measured (e.g. 3.13) is approximately equal to the

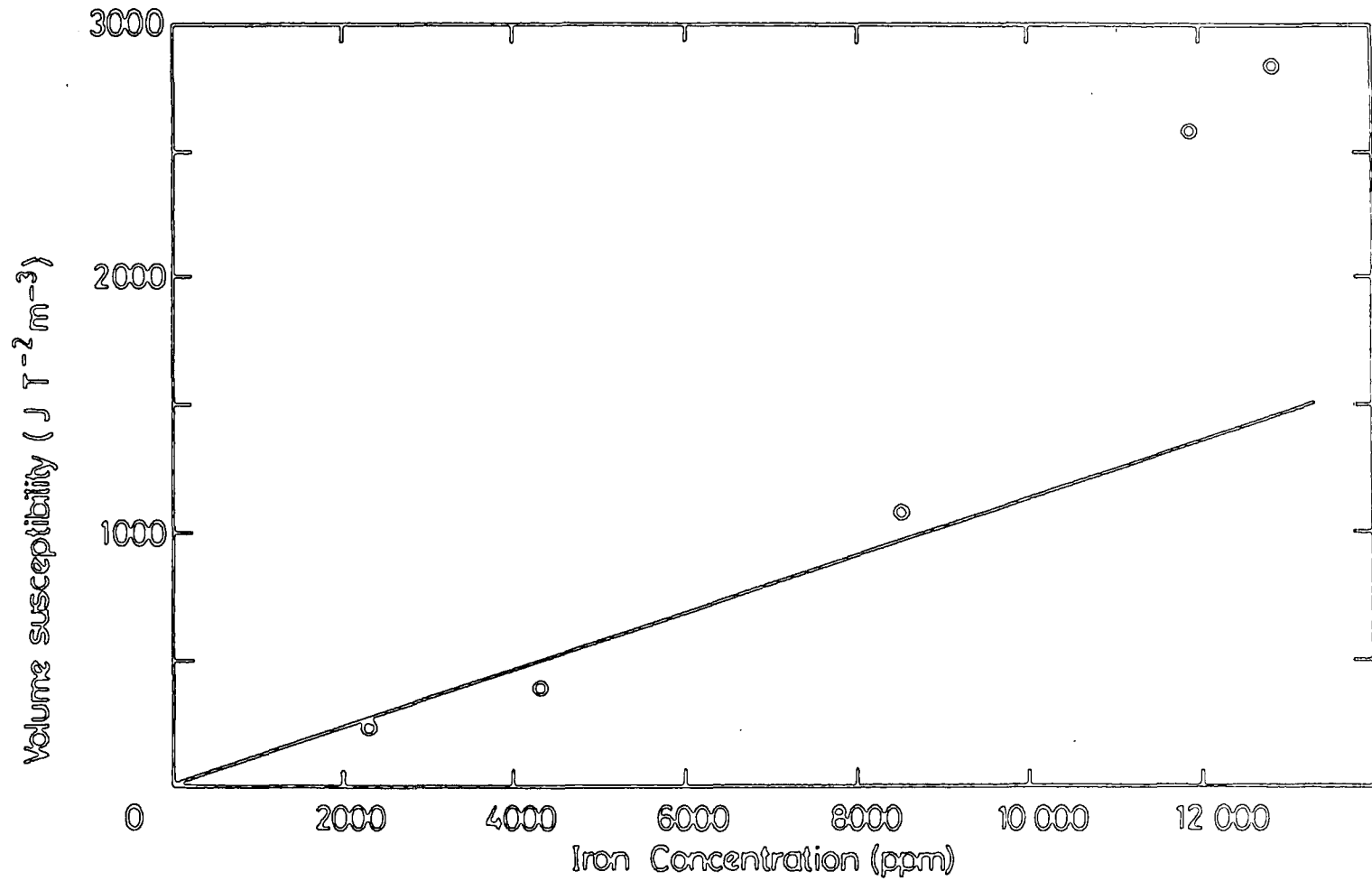


Figure 3.8. Variation of volume susceptibility with iron concentration.

product of the volume of ferrite, the magnetisation per unit volume of ferrite and the constant quantity $\frac{\partial B_x}{\partial z}$.

$\frac{\partial z}{\partial z}$

The volume of ferrite may increase with increasing iron concentration, as, at higher concentrations, the average distance between iron ions is lower and clustering is thus more likely. This would imply that, at saturation, a lower proportion of the iron dopant formed clusters in low concentration powders than in higher concentration powders.

If this is the case then the measured susceptibility of the sample, k_T , given by Weidemann's law as suggested at equation 3.12:-

$$k_T = a k_{MgO} + b k_{Magnesioferrite}$$

(again, assuming that the susceptibility of k_{MgO} is approximately equal to zero) can be given by:-

$$k_T \sim b k_{Magnesioferrite} \quad 3.18$$

If $k_{Magnesioferrite}$ could be established then the fractional concentration of ferrite, b , and its relationship to the initial iron concentration could be determined.

It is obviously necessary to ascertain the susceptibility of magnesioferrite. To this end Alfa-Ventron 99.998% pure magnesioferrite ($MgFe_2O_4$) was diluted with Aldrich Chemicals pure magnesia in order to measure the 'susceptibility' of the former which is far too magnetic to be measured undiluted; (the transverse forces are not negligible and the sample is attracted to one of the magnet pole faces). Four samples were prepared at about 0.25, 0.67, 3.7; and 6.3% magnesioferrite by volume; the last was too magnetic to yield accurate measurement. The results are given in Table 3.9. The measurements were made in

accordance with the standard set by previous data, i.e. they were made at room temperature (20° C) when 7 amps were supplied to the electromagnet inducing a field of 360 mT between the poles and the column height was 138 mm. From these results the susceptibility of MgFe_2O_4 was determined using Wiedemann's law of equation 3.13; these results are also shown in Table 3.9. An average of $872000 \text{ J T}^{-2} \text{ m}^{-3}$ is calculated from the lower percentage mixtures, an enhancing effect being apparent for the highest concentration, probably caused by the attraction of the sample to the magnet poles. The samples are, of course, non-paramagnetic and hence this value is only of use in comparison with other measurements made on the same apparatus, at the same field and with samples of the same column height.

The procedure on the Fe/MgO powdered chippings was therefore repeated using the standard column height, and new stock (see Fig 3.9 and 3.10). The results implying the presence of a strongly magnetic phase, even before heat-treatment, and again reinforcing the findings of Thorp et al [3.6] suggesting clustering in as-received crystals even at low concentrations. It is difficult to understand how the susceptibility of the 12,900 ppm Fe/MgO powder could be half that of the 8,000 ppm Fe/MgO powder. The ESR data on these samples (see Chapter 4) also suggested a marked departure from the pattern of lines and linear widths of the lower iron-concentrations, so discussion is primarily based on powders of 8500 ppm Fe or fewer ppm Fe/MgO, although the results on 12,900 ppm Fe/MgO are not totally discounted. It is noted that the iron concentrations quoted are for single crystals of the centre of the melt, where good homogeneity can be achieved. However, the present samples are taken from the edge of the melt which is less liable to be homogeneous and being less crystalline is prone to being less pure.

Volume % of Magnesioferrite in Aldrich pure magnesia	Total volume 'susceptibility' at 7 amps ($J T^{-2} m^{-3}$) \pm 5%	Ferrite volume 'susceptibility' at 7 amps ($J T^{-2} m^{-3}$) \pm 5%
0	0	-
0.25	2,174	866,100
0.67	5,771	864,400
3.71	32,840	886,200
6.32	59,300	939,000

TABLE 3.9: Susceptibility Data for Magnesioferrite/Magnesia Mixtures.

Concentration of Fe in MgO (ppm)	Total volume 'susceptibility' at 7 amps ($J T^{-2} m^{-3}$) \pm 5%	Total volume 'susceptibility' at 3.5 amps ($J T^{-2} m^{-3}$) \pm 5%
310	- 4.28	0.0
2,300	-25.4	34.8
4,300	128.8	157.9
8,500	552.2	934.2
12,900	273.2	491.2

TABLE 3.10: Susceptibility data for as-received Fe/MgO powdered chippings.

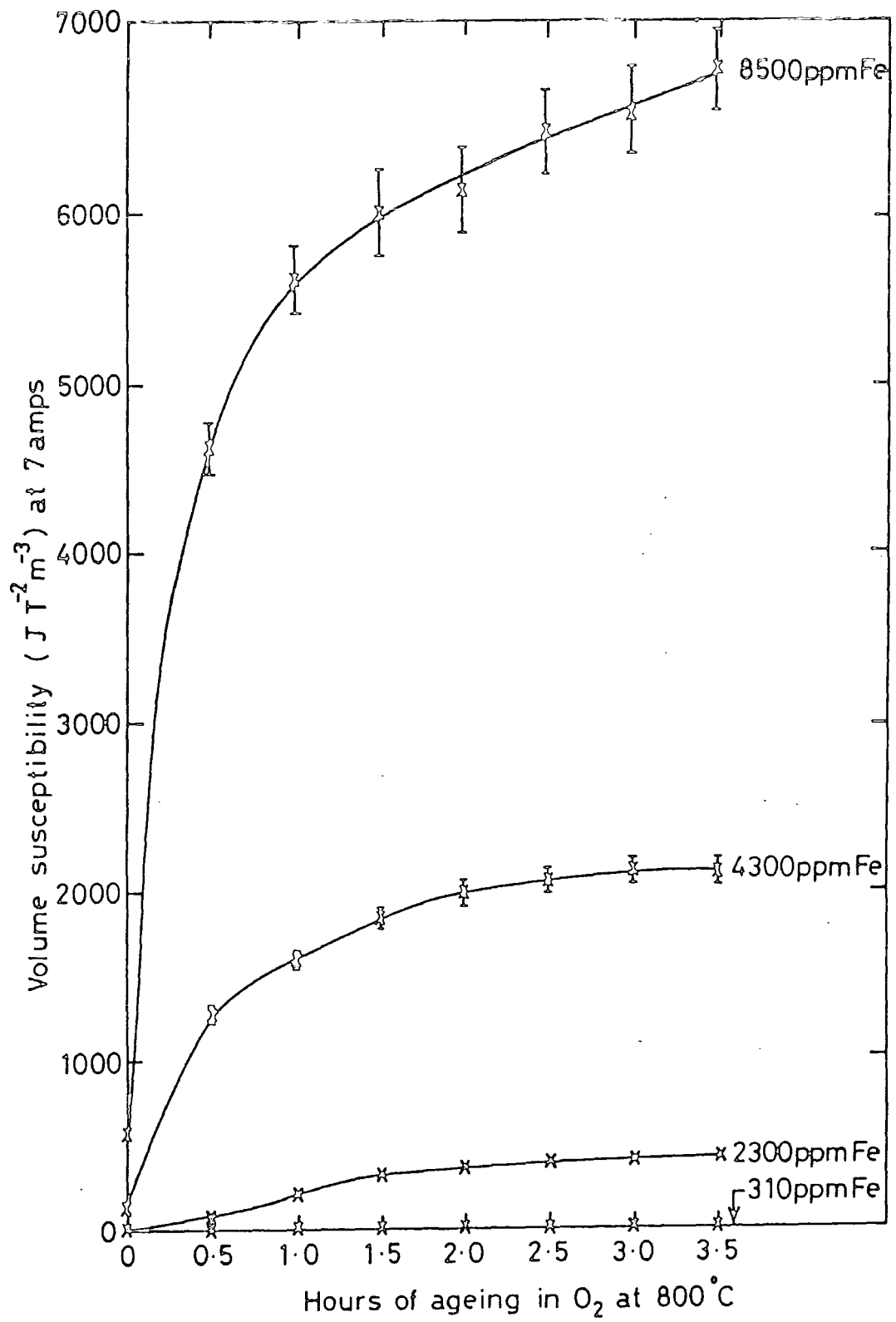


Figure 3.9. Variation of volume susceptibility with duration of heat treatment.

The values of 'b' the fractional concentration of magnesioferrite, calculated using equation 3.14 are shown in Table 3.11. As b is here assumed to be proportional to k_T the graph of b against hours of heat treatment for the various initial iron concentrations will be of the form of that for k_T against ageing time (see Fig 3.9) and the graph of fractional concentration at saturation against initial iron concentration will be of the form of Figure 3.10.

Referring now to Table 3.11, the greatest value of b calculated was 0.803% for the MgO + 8,500 ppm Fe sample after 3½ hours heating. The equivalent value for the 4,300 ppm Fe sample was 0.241%. However it is generally of more use to compare the values of b with the weight fraction of iron in the as received samples, (see Table 3.12). For the 8,500 ppm iron sample after 2½ hours of heat treatment, the ratio is greater than one. This could be explained by the addition of Magnesium and Oxygen atoms to the iron to form ferrite, but little more can be conjectured from these results.

3.7 Further Studies using the Gouy Magnetometer

The results discussed above revealed surprisingly detailed features of the non-paramagnetic systems investigated, especially given that the Gouy Magnetometer allows absolute measurement of the susceptibility only of pure paramagnets that are completely free from ferromagnetic impurity. Indeed, it is generally held [Crangle 6.1; Bates 6.2] that the method is inaccurate and misleading for any sample where the apparent susceptibility depends to some extent on the applied field, because different parts of the specimen are situated in different and undefined fields.

However, the Gouy Magnetometer actually measures the force exerted on a balance by a sample in a variable magnetic field, and the form of the relation between the force and field reveals greatly more about the non-paramagnetic sample than the calculated susceptibility values.

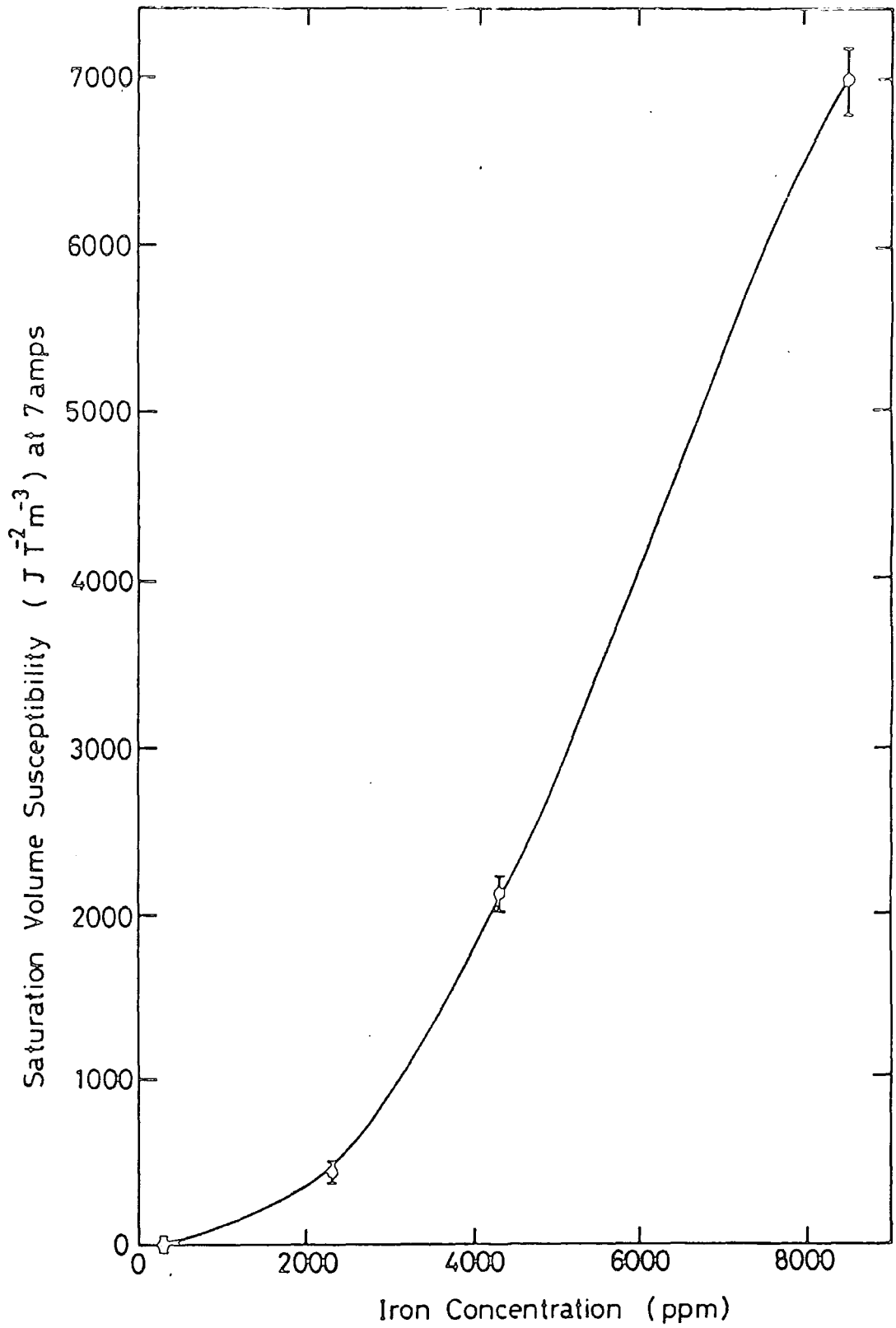


Figure 3.10. Dependence of saturation susceptibility on iron concentration.

heat-time (hrs)	Fe/MgO Samples				
	310 ppm	2,300 ppm	4,300 ppm	8,500 ppm	12,900 ppm
0	-0.0005	-0.0003	0.015	0.063	0.031
½	0.001	0.009	0.145	0.530	0.258
1	0.0009	0.029	0.183	0.645	-
1½	0.0009	0.037	0.206	0.691	0.258
2	0.0007	0.043	0.229	0.708	0.2687
2½	0.0007	0.046	0.238	0.745	0.767
3	0.0001	0.046	0.244	0.756	0.298
3½	0.0001	0.052	0.241	0.803	0.298

TABLE 3.11: Calculated values of fractional concentrations, b , of magnesioferrite in aged samples in % volume

hours of heating	Fe/MgO Sample				
	310 ppm	2,300 ppm	4,300 ppm	8,500 ppm	12,900 ppm
0	-0.020	-0.001	0.044	0.093	0.051
½	0.004	0.049	0.430	0.789	-
1	0.037	0.159	0.538	0.959	0.421
1½	0.037	0.204	0.605	1.028	0.421
2	0.029	0.236	0.674	1.053	0.435
2½	0.029	0.253	0.699	1.107	0.435
3	0.004	0.253	0.717	1.124	0.485
3½	0.004	0.286	0.708	1.195	0.485

TABLE 3.12: Calculated ratios of fractional concentration of magnesioferrite to initial fractional weight concentration of dopant iron.

Comparison of the electron spin resonance results (Chapter 5) with the susceptibility results for the Fe/MgO system (Chapter 3, section 3.6) suggests that magnetic properties are dominated by the formation of a ferrimagnetic phase whose concentration increases with increased iron concentration and on heat treatment in oxygen. Furthermore, the broad line, which is obscured thus to increase in intensity in the series of ESR spectra; is very similar to the broad line observed in the commercial products investigated. Therefore the force against field relation of the Fe/MgO system was investigated with the Gouy Magnetometer in order further to characterise its magnetic properties.

A previous study of similar systems [Wirtz and Fine 6.3] which was made using a vibrating sample magnetometer and single crystals, attributed the susceptibility enhancement caused by heat treatment in an oxidising atmosphere to the formation of a superparamagnetic precipitate of the ferrimagnetic magnesium ferrite. It is possible that the same would occur in a powdered sample, and that it could be detected using a Gouy Magnetometer measuring the variation of force with field.

Magnetic particles that are smaller than single domain particles, i.e. particles that contain only a few thousand atoms, still have intrinsic magnetisation and Curie temperature that are essentially independent of particle size. However, the magnetic anisotropy energy of such a particle is proportional to its volume, and hence, at these very small volumes the magnetic energy of the particle approaches its thermal energy, kT . This causes the magnetisation vector to fluctuate in a thermally activated manner.

An assembly of such particles will therefore have no magnetisation even after a field has been applied (and removed), although significant relaxation time τ may occur on approach to the superparamagnetic region, decreasing rapidly as the magnetic energy approaches kT (see Table 3.13).

$\frac{\mu B_0}{kT}$	τ (s)
50	5×10^{12}
25	10^2
18	10^{-1}
10	2×10^{-5}
1	3×10^{-9}

TABLE 3.13: Relaxation times of single-domain particles

In an applied field, B , an assembly of n such particles per unit volume, each of volume, V , and saturation magnetisation, M_s , at absolute temperature, will have an apparent magnetisation, M_A , given by:-

$$M_A = n M_s V \coth \frac{M_s V B}{kT} = \frac{kT}{M_s V B} \quad (3.19)$$

For such a sample suspended in a Gouy magnetometer, the force, δF , acting on an element of column length, δz , and cross-section, a , in the transverse field, B_x , is:

$$\delta F_z = M_A \frac{\delta B_x}{\delta z} a \delta z \quad (3.20)$$

Combining equations 3.19 and 3.20 and integrating with respect to B between the top and the bottom of the sample column, the force acting on the balance has been derived [Williams, Hoon and Thorp 3.10]

$$F = a n k T \ln \frac{B_B \sinh(M_s V B_A)}{B_A \sinh(M_s V B_B)} \quad (3.21)$$

When the field at the top of the sample, B_B , is much smaller than that at the bottom of the sample column, B_A , then:-

$$F \sim a n k T \ln \frac{kT \sinh \frac{M_s V B_A}{kT}}{M_s V B_A} \quad (3.22)$$

If $\frac{M_s V B_A}{kT} \gg 1$ then:-

$$F \sim a n M_s V B_A - \frac{kT}{M_s V} \ln \frac{M_s V B_A}{kT} \quad (3.23)$$

and if $\frac{M_s V B_A}{kT} \ll 1$ then:-

$$F \sim \frac{1}{2} a B_A^2 \frac{n M_s^2 V^2}{3 k T} \quad (3.24)$$

In favourable conditions these equations may be used to gain estimates of $nM_s V$ and $M_s V$.

For pure paramagnetics, the gradient of the plot of Gouy Magnetometer force against $(B^2 - B^2)$ is constant and proportional to the

A B

susceptibility. It is known that plots for heat-treated Fe/MgO powders and also for the commercial products cannot have a constant gradient, since the susceptibilities measured at full and half field values were not the same, for each of these samples. Figure 3.11 shows the plot of force against $B^2 - B^2$ for three concentrations of Fe/MgO that had been

A B

heat treated in oxygen for $3\frac{1}{2}$ hours at 800°C . The 'susceptibility' values given in Chapter 3 are proportional to the gradients of the lines joining the highest field points to the origin.

This is clear confirmation that the samples are not paramagnetic, and also that they are not hysteretic, i.e. the values of force for increasing field are the same as those for subsequently decreasing field. This adds weight to the suggestion that a superparamagnetic precipitate is formed.

Figure 3.12 shows the form of the plot of force against field typically found for superparamagnets at low field, (b) and (c), for paramagnetics (d) and theoretically predicted as $\frac{M_s V}{kT}$ tends to infinity

[3.10].

This may be compared with the force and field plot obtained for the above three samples shown in Fig 3.13. The corresponding crossed points show the plot for the a paramagnetic of the susceptibility value given to the respective samples in Chapter 3. In view of the close agreement of the form of the experimental results plotted in Fig 3.13 with the

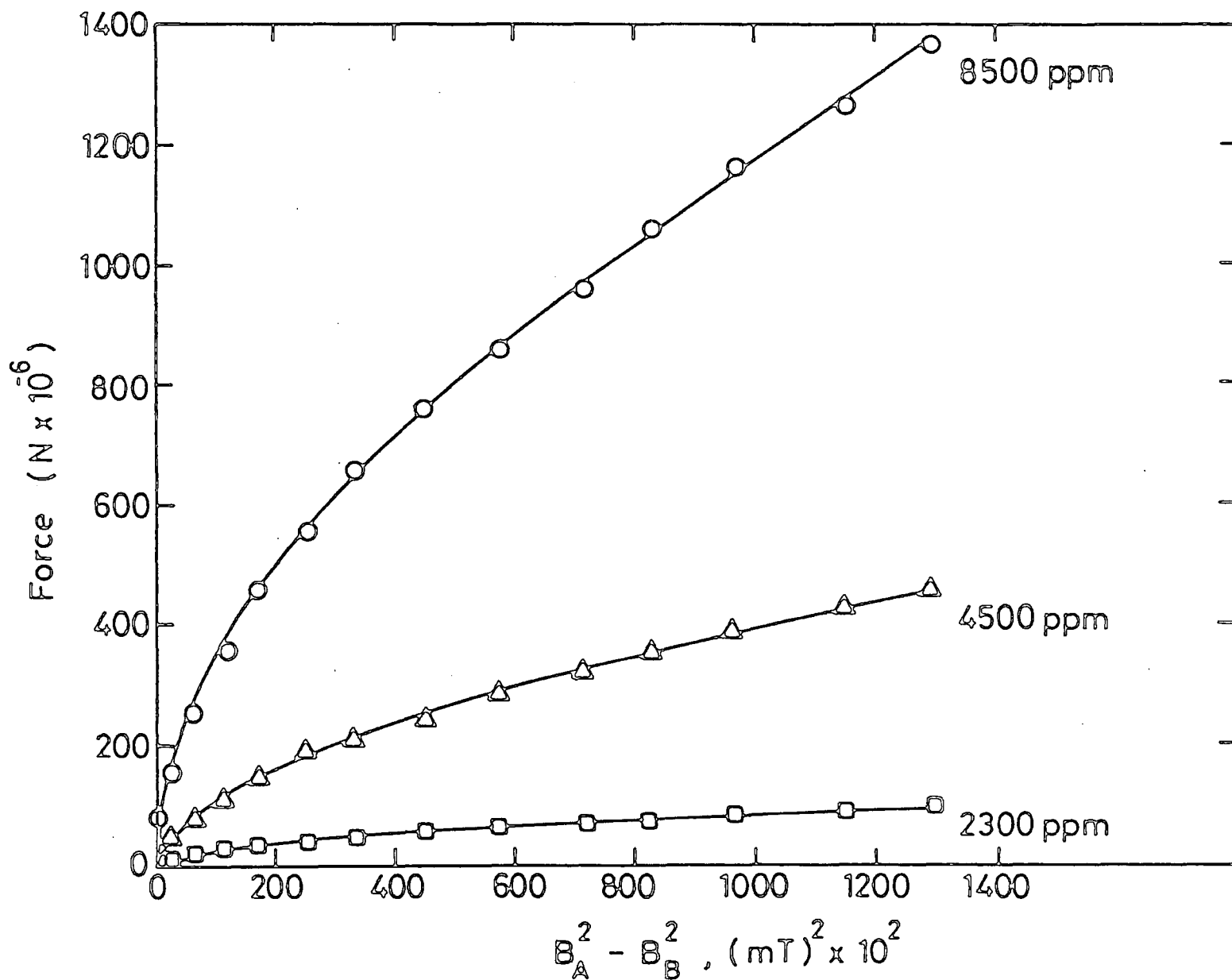
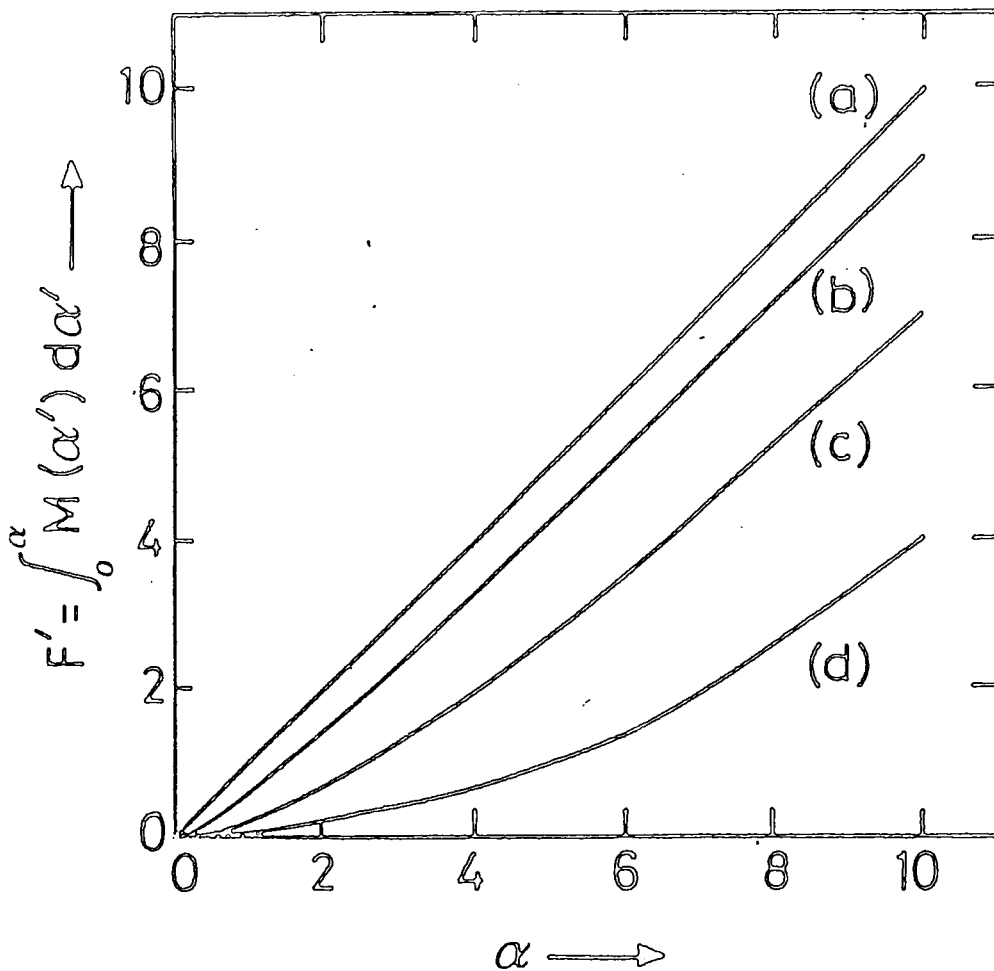


Figure 3.11. Variation of Gouy force with applied field² for Fe/MgO samples after 3½ hours heating at 800°C in Oxygen.

Figure 3.12. Form of plot of force versus field for superparamagnetics.



F' - Proportional to force, F , measured on Gouy magnetometer.

α - Proportional to field between magnet poles.

(a) - High field, low temperature limit, $\frac{M_s V}{kT} \rightarrow \infty$

(b), (c) - Typical low field superparamagnetic behaviour.

(d) - Linear paramagnetic limit.

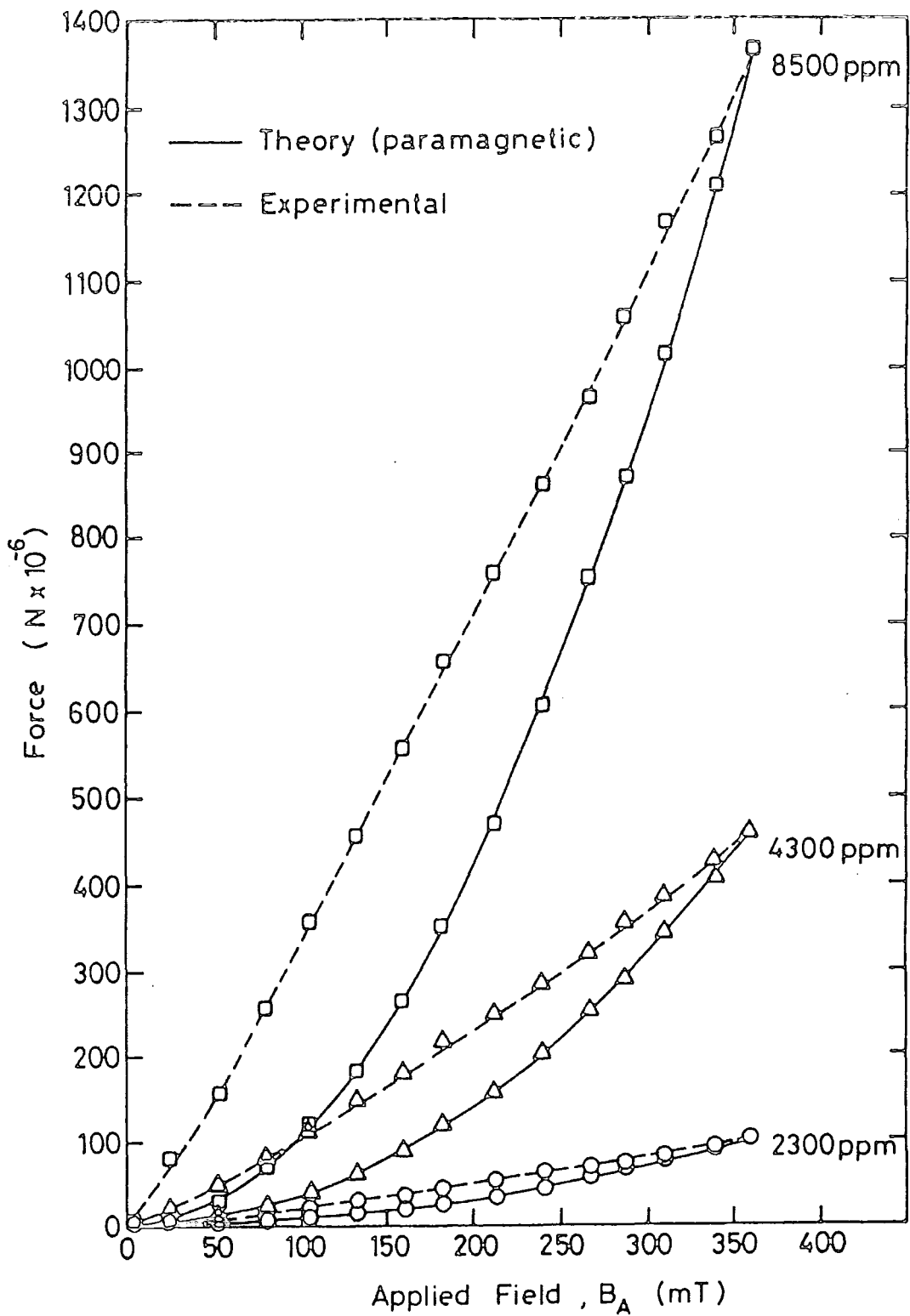


Figure 3.13. Dependence of Gouy force on applied field for heated Fe/MgO samples compared with plots for theoretical pure paramagnets.

traces shown for superparamagnetics in Fig 3.12, the heat treated Fe/MgO samples seem most likely to obtain a superparamagnetic precipitate.

Unfortunately the Gouy balance used is not sufficiently accurate, nor the conditions generally sufficiently favourable to allow a reasonable estimate of the quantities $nM_s V$ or $M_s V$.

Two commercial products were also investigated, but the variation in force with applied field was too small to yield any useful information. It should be noted that the Fe/MgO samples, after 3½ hrs heat treatment were too lossy to allow ESR spectra to be plotted, whilst the broad line of the commercial magnesias (although very similar to that of the Fe/MgO samples that was observed to increase after heat treatment) was not sufficiently intense to cause any ESR measuring difficulties. Nonetheless it seems quite possible that this lossy precipitate is present in the heat-treated commercial magnesias, and in view of the previous work [3.9] that it is indeed magnesioferrite.

CHAPTER THREEREFERENCES

- 3.1 L.G.Gouy, C.R.Acad.Sci., PARIS 109 935 (1889).
- 3.2 P.Pascal, C.R.Acad.Sci., PARIS 150 1054 (1910).
- 3.3 J.Crangle "The Magnetic Properties of Solids", Edward Arnold, London, (1977).
- 3.4 A.Skinner, Ph.D.Thesis, University of Durham, (1986).
- 3.5 A. Henderson and J.E.Wirtz, "Defects in the Alkaline Earth Oxides", Taylor & Francis Ltd, London, (1977).
- 3.6 A.D.Inglis and J.S.Thorp,
- 3.7 A.D.Inglis, J.S.Thorp, G.J.Russell,
- 3.8 L.F.Bates, "Modern Magnetism", C.U.P. (1963).
- 3.9 G.P.Wirtz, M.E.Fine, J.Appl.Phys. 38 (1967) 3729.
- 3.10 C.D.H.Williams, S.R.Hoon, J.S.Thorp, J.Mat.Sci. 5 (1986) 832.

CHAPTER 4PRINCIPLES OF ELECTRON SPIN RESONANCE4.1 General

Electron Spin Resonance (ESR) is a technique employing electromagnetic radiation to determine the separation of energy levels in atoms and ions. If energy equal to the separation energy is supplied to the atoms then their electrons absorb it and are excited from a lower to a higher level. Thus observation of the resonant frequencies at which absorption occurs yields information about the energy levels of the atoms and ions.

In ESR the energy is supplied in the form of microwave radiation of frequency often at about 9 GHz ; this does not necessarily correspond to the energy separation of neighbouring levels, but rather to the energies by which a single degenerate level may be split. The application of a strong external d.c. magnetic field, Zeeman splitting; the interactions of electrons with nuclear spin magnetic moments; and surrounding atoms exerting an electrical field, are all causes of such splitting, and hence evaluation of splitting energies may yield information about the local environment of the atom or ion.

Electrons in all materials may be considered as possessing two types of motion : motion around the nucleus of the atom giving rise to orbital angular momentum; and motion of the electron spinning about its own axis giving rise to intrinsic spin angular momentum. Since electrons have charge, both these angular momenta produce magnetic moments, so a free electron will behave like a magnetic dipole with a tendency to align with the direction of an applied field.

However, in most materials all the electrons are arranged in pairs of opposing spins so there is no net magnetic moment to interact with an applied field or with the incident electromagnetic radiation. Thus useful information can be gained only from atoms or ions where there is an unpaired electron giving rise to a residual magnetic dipole moment, i.e. from paramagnetics, (hence ESR is also referred to as electron paramagnetic resonance). In these atoms the dipole moment interacts with the magnetic component of the electromagnetic radiation absorbing energy.

There are several classes of materials in which unpaired electrons may exist : some transition metals and rare earth compounds have an unpaired electron in the incomplete d or f orbitals ; free radicals leave a bonding electron associated with only one atom ; F-centres have electrons or holes trapped at point defects ; some atoms and molecules possess an odd number of electrons, and in metals and semiconductors the conduction electrons can cause paramagnetism. In such materials the allowed energy level of the unpaired electron may be shifted and split by its interaction with electric and magnetic fields.

For paramagnetic ions (e.g. Fe^{3+} , Cr^{3+}) distributed substitutionally in a diamagnetic host lattice (e.g. MgO) the magnetic properties of the material are essentially those of the paramagnetic ions, modified from the free ion situation by the influence of the crystalline electric field arising from the host lattice and the difference (if any) in electric charge between the doping ion and the divalent magnesium at the impurity ion site. The resultant splitting, in the absence of an external magnetic field is known as "zero field splitting". However the application of a magnetic field produces Zeeman splitting of each of the Kramers doublets as shown in Fig 4.1.

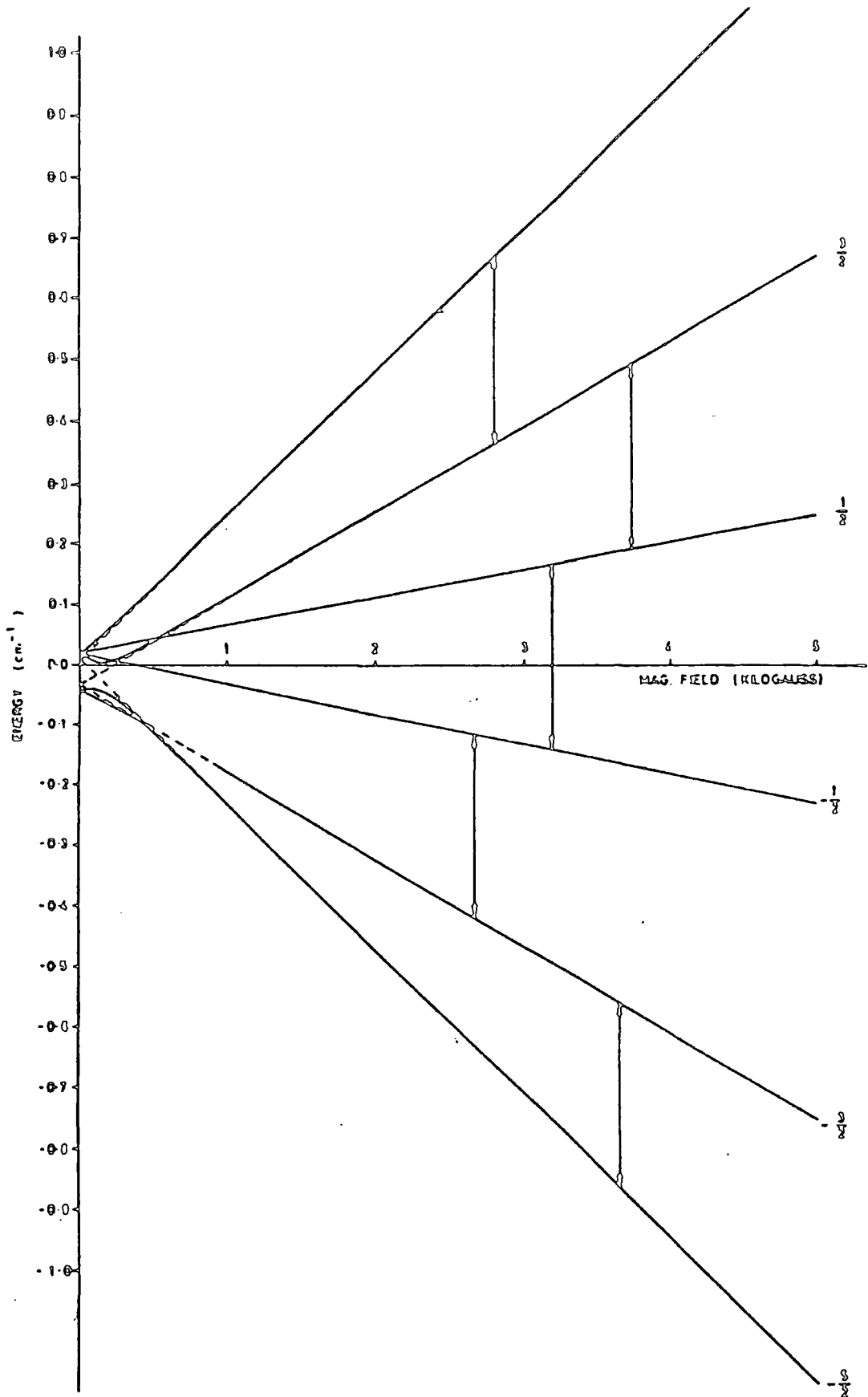


Figure 4.1. Energy levels in the Fe^{3+} ion.

(In the doped MgO system at room temperature fields of about 400 mT cause splitting by energy separations comparable to that of the microwave radiation). While many ESR spectra are observable at room temperature, some signals (e.g. Fe^{2+}) may be detected only at liquid nitrogen (270 K) or even liquid helium (~ 4 K) temperatures. The materials may be in single crystal, sintered polycrystalline or powder form, but the two latter groups require much more complex interpretation and also present difficulties in experimental handling, particularly at low temperatures.

For power absorption to occur the energy of the incident radiation must exactly match that of the energy separation of the split level, i.e., in classical terms, resonance occurs. To achieve this condition experimentally, it is more convenient to keep the microwave frequency fixed and to vary the energy level separations by variation of the external magnetic field, which is swept in the immediate vicinity of the resonance condition(s). Thus a dynamically recurring, rather than a static point-by-point event is observed.

The last mentioned splitting mechanism is caused by electron-nuclear interactions and is termed hyperfine splitting. The magnitude of this splitting is proportional to both the nuclear magnetic moment and the probability of finding the electron at the nucleus.

Thus ESR spectra may contain information about the charge state, type of binding, amount of interaction with surrounding nuclei, and the symmetry of the environment of the paramagnetic centres present in the material. Additionally comparison with theoretical free electron behaviour gives an indication of crystal field strength and degree of spin-orbit coupling. Finally, since the area under an absorption line is proportional to the number of unpaired spins, ESR can be used as a method of determining paramagnetic defect concentrations.

Overall, ESR is a powerful tool for the study of paramagnetic defects in insulators since it detects signals only from the paramagnetics, not from the insulator and thus can detect very low concentrations of impurity to resolutions sufficient to yield detailed models for the paramagnetic centres present.

4.2 Theory of the Single Free Electron

All signals detected by ESR must have an unpaired electron whose particular environment is determined by its difference from the theoretical single free electron as defined below.

Quantum Theory states that the angular momenta and hence magnetic moment of an electron may hold only certain discrete values. In the simplest case of a single free electron there can be no orbital angular momentum, and the only allowed value of spin angular momentum is given by:-

$$P_s = \frac{1}{2} \frac{h}{2\pi} \quad (4.1)$$

and the corresponding magnetic moment by:-

$$\mu_s = \frac{eh}{4\pi mc} = \beta \quad (4.2)$$

where e and m are charge and mass of the electrons and h and c are Planck's constant and the speed of light respectively. β is the Bohr magneton, the unit of magnetic moment.

If an external magnetic field, H_0 , is applied the electron experiences a torque which tries to align its magnetic moment vector, \underline{M} , with the direction of the field. However, quantisation restricts the

possible orientations of the vector to exclude that of H_0 , so the torque forces the magnetic moment to precess around the field direction at an angular frequency, ω_0 , independent of orientation and given by:-

$$\omega_0 = \gamma H_0 \quad (4.3)$$

as shown in Fig 4.2.

γ is the gyromagnetic ratio and the ratio of magnetic moment to angular momenta (17.6×10^{10} second⁻¹ T⁻¹ for a free electron).

The energy, E , of the magnetic dipole moment, μ , is dependent on orientation with respect to the applied field and is given by:-

$$E = \mu H_0 \cos \theta \quad (4.4)$$

where θ is the angle between the magnetic field and the axis of the dipole. In the case of the free electron there are only two allowed orientations of the magnetic moment corresponding to "spin-up" and "spin-down" (there being no orbital magnetic moment) and thus equation 4.4 becomes:-

$$E = M_s \beta H_0 \quad (4.5)$$

where M_s are the magnetic quantum numbers of the allowed energies, i.e. $M_s = \pm \frac{1}{2}$.

Thus the applied field has split the energy level into two levels separated by energy $2\beta H_0$, i.e. the ground state has a two-fold degeneracy lifted by H_0 .

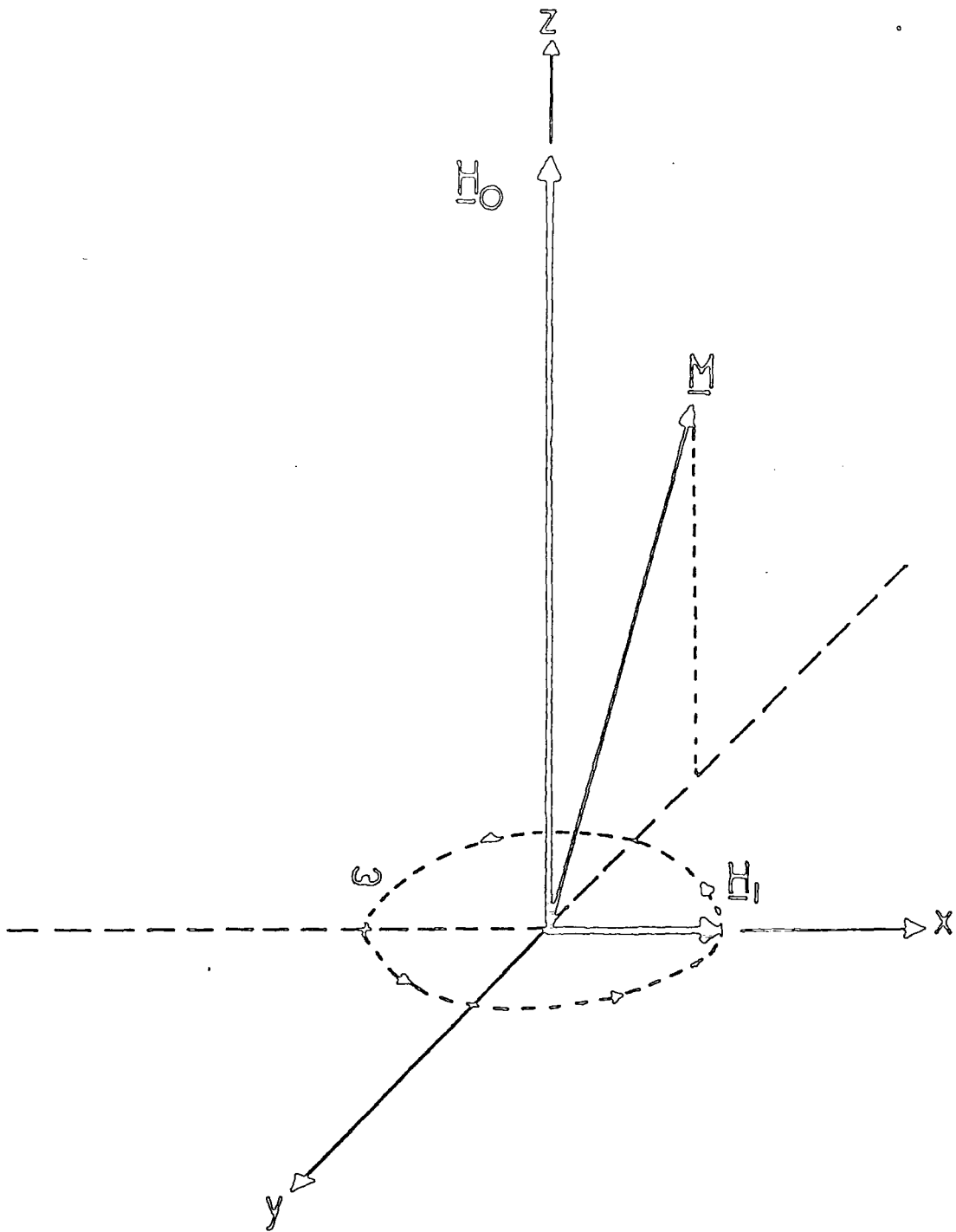


Figure 4.2. Precessing electron moment.

In general, i.e. for all systems, equation 4.5 becomes:-

$$E = g\beta H_0 \quad (4.6)$$

where g is a numerical factor determined experimentally. Making relativistic corrections to the above theory g , for a single free electron is 2.0023.

4.3 The Paramagnetic Ion in the Crystalline Environment

A free ion has spin and orbital angular momenta assigned by quantum numbers S and L respectively. The total angular momentum has a quantum number J which is the vector sum of L and S . Quantum theory states that the ground state of such an ion has degeneracy of $(2J + 1)$ in the absence of an applied magnetic field.

However, the strong crystalline electric fields may modify the quantum state by breaking the coupling between L and S , i.e. quenching ; thus causing ground state degeneracy due to S alone of $(2S + 1)$. The higher orbital states are usually far removed from the ground state by energies corresponding to quanta of optical frequency radiation.

The crystal field also causes a lifting of the degeneracy of the ground state by energies corresponding to microwave quanta (or less). This lifting is limited by Kramer's Theorem which states that an ion with an odd number of unpaired electrons must retain two-fold degeneracy of these levels.

In reality the spin-orbit coupling is not completely broken and so the degeneracy of the ground state does not correspond to the true spin quantum number of the free ion, but to an effective spin quantum number, S' , corresponding to an observed degeneracy of $(2S' + 1)$.

The application of a magnetic field causes further lifting (see Fig 4.1 and eq. 4.6):-

$$E = g \beta H_0 M \quad (4.7)$$

where M is the quantum numbers (between S and S') and g is the spectroscopic splitting factor. The deviation of this quantity from the free electron value of 2.0023 is a measure of orbit quenching (i.e. spin-orbit coupling).

Similarly, theory also declares that transitions only for spin state separations of $\Delta M = 1$ may be seen. Since the crystalline field breaks down the pure spin states, this rule may be broken and so-called "forbidden transitions" may be seen, e.g. for an ion of $S' = 3/2$ (e.g. Cr^{3+}) an energy level, $|1\rangle$, may be described with eigenvectors a_1, b_1 etc:-

$$|1\rangle = a_1 |3/2\rangle + b_1 |1/2\rangle + c_1 |^{-1/2}\rangle + d_1 |^{-3/2}\rangle \quad (4.8)$$

where the eigenvectors are normalised by:-

$$|a_1|^2 + |b_1|^2 + |c_1|^2 + |d_1|^2 = 1 \quad (4.9)$$

4.4 The Spin Hamiltonian and Energy Levels

The Hamiltonian Operator, is a convenient description of the energy of an atom containing unpaired electrons and nuclei with non-zero spins.

$$H = H_{el} + H_{CF} + H_{LS} + H_{SS} + H_{Ze} + H_{Zn} + H_{II} + H_{HF} \quad (4.10)$$

The first three terms comprise the atomic Hamiltonian and the last six form the spin Hamiltonian. The operator H_{e1} accounts for electron kinetic and potential energy and electron-electron repulsion, and is not seen in microwave spectroscopy. The crystalline field operator H_{CF} is also too great to be detected directly by microwave frequencies, but represents energies which have a strong influence on the magnitude of Spin Hamiltonian parameters. It has the general form:-

$$H_{CF} = -eV(x_i, y_i, z_i) \quad (4.11)$$

where V is the potential of the crystalline field and x_i, y_i, z_i are the co-ordinates of the i^{th} electron of the unfilled shell.

The spin-orbit operator H_{LS} is proportional to the dot-product of the spin and orbit vectors, and forms part of both the atomic and the spin Hamiltonian:-

$$H_{LS} = \lambda \underline{L} \cdot \underline{S} \quad (4.12)$$

These energies are much smaller than the H_{CF} energies, and may be seen in microwave spectroscopy. However, if the resultant angular momentum of the ion is zero (i.e. S ground state as opposed to S' ground state) then $H_{LS} = 0$.

The general spin-spin operator H_{SS} is given by:-

$$H_{SS} = -\rho(\underline{L} - \underline{S})^2 + \frac{1}{2}(\underline{L} \cdot \underline{S}) - \frac{1}{3}L(L+1)S(S+1) \quad (4.13)$$

and represents energies of magnitude similar to the electronic Zeeman

(magnetic field splitting) operator, H_{Ze} , which is given by equations 4.6 and 4.7 or:-

$$H_{Ze} = g \beta_n \underline{H} \cdot \underline{S} \quad (4.14)$$

The equivalent nuclear Zeeman term H_{Zn} is given by:-

$$H_{Zn} = -\gamma \beta_n \underline{H} \cdot \underline{I} \quad (4.15)$$

where β_n is the nuclear Bohr magneton and I the nuclear spin quantum number. The nuclear spin-spin interaction takes the same form as the spin-orbit coupling operator:-

$$H_{II} = J \underline{I} \cdot \underline{I} \quad (4.16)$$

and similarly for the hyperfine operator:-

$$H_{HF} = A \underline{S} \cdot \underline{I} \quad (4.17)$$

However the microwave spectroscopy terms can be collected together in the Spin Hamiltonian if the effect of H_{CF} (eq.4.11) is taken into account using the effective spin S' -

$$H_S = g \underline{H} \cdot \underline{S}' + D(S')^2 + S' (S' + 1) + H_{Zn} + H_{II} + H_{HF} \quad (4.18)$$

Thus, using the Spin Hamiltonian, the solutions of:-

$$H_S |i\rangle = E_i |i\rangle \quad (4.19)$$

(see eqs. 4.8, 4.9) may be derived in terms of E_i , the eigenvalues (energies) of the states $|i\rangle$. (see eqns. 4.8, 4.9 and Reference 4.1).

4.5 Microwave Power Absorption

To detect the splitting of the electron energy levels, transitions must be excited between two levels by electromagnetic radiation of frequency, ν , such that:-

$$h\nu = g\beta H_0 \quad (4.20)$$

The transition is induced by the oscillating magnetic field component exerting a torque on the electronic magnetic moment and thus altering its energy. There is an equal probability of absorption and emission of power on interaction between the microwave beam and electron; the net absorption relies on there being an excess population of electrons in the lower level. The relative populations are given by Boltzmann statistics:-

$$\frac{n_1}{n_2} = \exp - \frac{g\beta h_0}{kT} \quad (4.21)$$

where n_1 and n_2 are the populations in the upper and lower levels respectively. Power absorption is temperature sensitive and increases as temperature decreases, improving the ESR signal-to-noise ratio.

To a first approximation the population difference $n = n_2 - n_1$ between the levels may be expressed as:-

$$n = N \frac{gh_o}{2kT} \quad (4.22)$$

where N is the total population of unpaired spins. Integration of the detected absorption intensity with respect to the varying applied magnetic field gives a measure of the total net power absorbed, P , :-

$$P = \frac{2\pi^2 v^2 H_o S(S+1)Ng^2\beta}{3kT} \quad (4.23)$$

Showing the power absorbed to be proportional to the number of unpaired electrons present in the sample. In practice, then, the levels have a narrow but finite band of energies, and the excitations occur over a range of magnetic field values giving an absorption line of finite width.

4.6 Paramagnetic Relaxation

At any given temperature the linewidth of an ESR signal is determined primarily by relaxation processes, i.e. mechanisms by which the spin system attains thermal equilibrium. The main relaxation mechanisms, are spin-spin relaxation, spin-lattice relaxation and cross-relaxation.

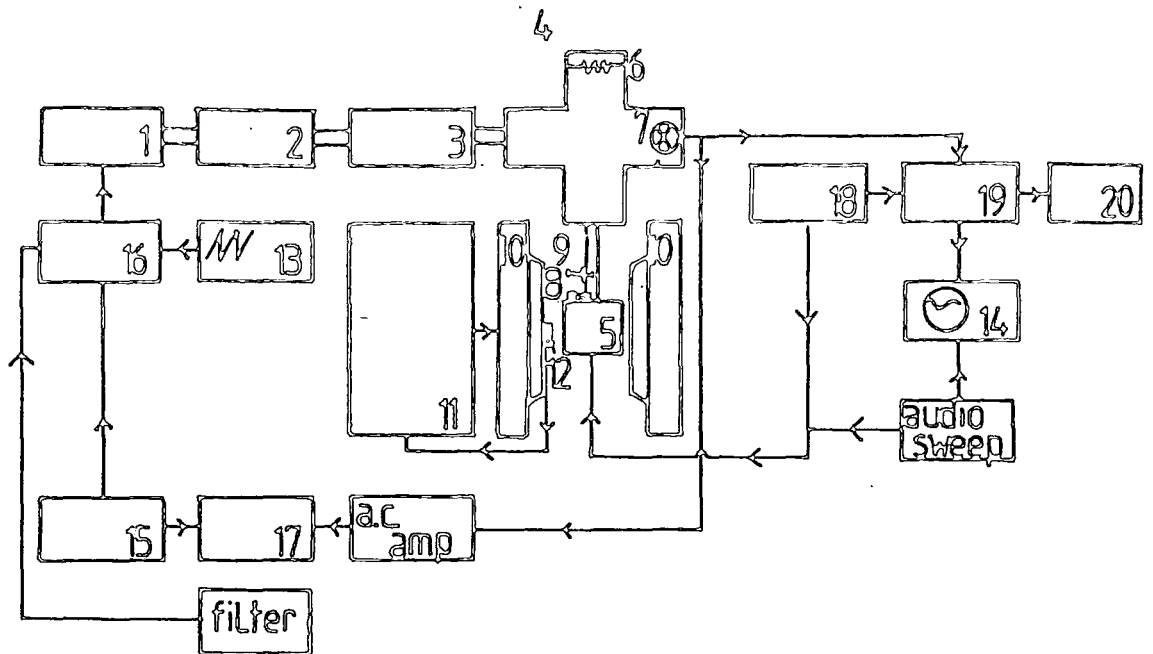
The time taken for a spin system to return from an initial perturbed state to a state in thermal equilibrium is known as the relaxation time. The spin-spin relaxation time depends upon the square root of the spin population and is inversely proportional to the cube of the interatomic spacing and thus is invariably proportional to the cube

of the interatomic spacing and hence it is invariably the shortest of the relaxation times with typical values of about 10^{-9} seconds. The spin-lattice relaxation time is much greater since it depends on the much weaker residual spin-orbit coupling : present theory proposes that the lattice vibrations (phonon) modify the crystalline field at the paramagnetic centre which in turn modifies the orbital angular momentum and, via spin-orbit coupling, the phonons are weakly coupled to the spin. The importance of this is that, as the linewidth is approximately inversely proportional to the (spin-lattice) relaxation time, the experimental conditions must be adjusted to ensure that the latter is relatively long (i.e. milliseconds) so that the energy in the absorption line is confined to a relatively narrow, and hence observable, width rather than being too spread out and undetectable above the noise level. As mentioned before, these considerations apply to $\text{Fe}^{2+}/\text{MgO}$ and also to $\text{Co}^{2+}/\text{MgO}$.

4.7 Experimental

Most ESR spectrometers operate on similar principles, and since all the measurements were made using a Varian V-4502-12 9 GHz (X-band) spectrometer (see Fig 4.3, and reference 4.1), this model can be used to illustrate the general features of spectrometer design and operation.

The microwave source, an X-band Klystron (1), can be tuned to produce an output frequency in the range 9-10 GHz. The r.f. power applied to the sample is controlled by the variable attenuator (2), and an isolator (3) protects the Klystron from damage by radiation reflected from the hybrid tee (4). The hybrid tee or microwave bridge is a device which will not permit microwave power to pass directly from one arm to the opposite arm. Power entering from arm 1 (see figure 4.3) is divided equally between arms 2 and 3. Arm 3 is terminated by the microwave cavity (5) and arm 2 is terminated by a matched load (6). The



- | | |
|--------------------------|---|
| 1 Klystron | 12 Hall probe |
| 2 Attenuator | 13 Sawtooth modulation |
| 3 Isolator | 14 Oscilloscope |
| 4 Hybrid tee | 15 10 KHz sweep generator |
| 5 Cavity | 16 Klystron reflector voltage |
| 6 Load | 17 Phase-sensitive detector |
| 7 Detector | 18 100 KHz sweep oscillator |
| 8 Coupling | 19 Lock-in amplifier and phase-sensitive detector |
| 9 Tuner | 20 Chart recorder |
| 10 Magnet | |
| 11 Supply and sweep unit | |

Figure 4.3. E.S.R. Spectrometer.

crystal detector (7), located in arm 4, receives power only when the bridge is unbalanced by absorption in the cavity. In fact a small amount of power is needed to bias the detection, so after adjusting a nylon coupling screw (8) to balance the bridge and give a null reading at the detector, the slide screw tuner (9) is inserted to unbalance the bridge slightly, yielding the bias power.

The cavity is located between the poles of a V3605 12" electromagnet (10) controlled by a VFR5203 field regulated power supply and linear sweep field unit (11). A Hall Effect field sensor (12) measures the d.c. field, the output voltage being fed to the power supply and sweep unit for comparison with a reference voltage proportional to the required field. If these are not equal an error signal is generated and applied to the supply current to correct the field. This ensures that the field is set with long term stability (1 part in 10^5 repeatability) and linearity of sweep (field resolution 0.002 mT).

The microwave cavity consists of a gold-plated section of waveguide which stores energy by building up standing waves of high electric and magnetic fields. A V4531 cavity operating in the TE_{102} mode is used, i.e. the sample is placed in the centre of the cavity which is a region free of electric field but having a high r.f. magnetic field (see Fig.4.5). Absorption of power at resonance changes the impedance of the cavity thus unbalancing the microwave bridge.

The Klystron frequency is adjusted to match the resonant frequency of the cavity with sample and sample holder by variation of the Klystron reflector voltage. A sawtooth modulation (13) is applied to this voltage to ease the matching process and the output of the crystal detector is displayed on an oscilloscope (14). When the frequency is swept through the resonant condition the bridge is unbalanced and a dip

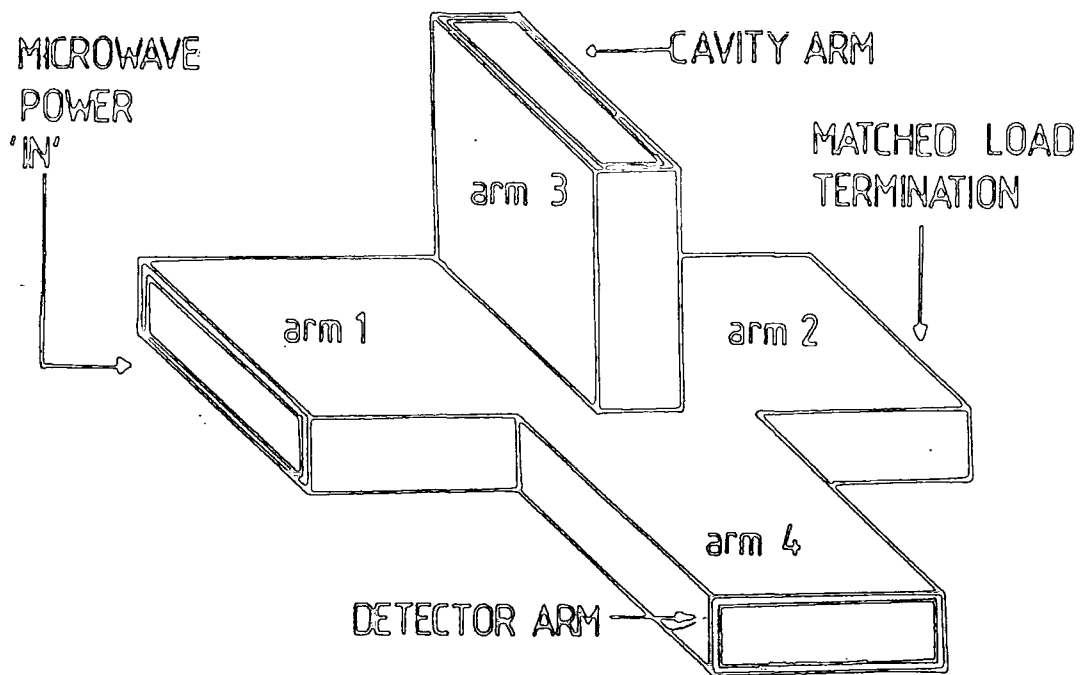


Figure 4.4. Microwave bridge (showing Varian numbering).

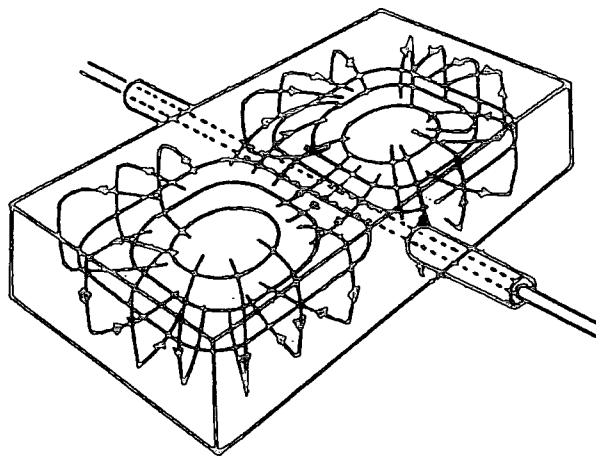


Figure 4.5. Fields and currents in the TE_{102} mode.

is seen in the display. When the frequencies are matched the modulation is switched off.

To maintain this condition for the duration of the experiment the spectrometer incorporates an automatic frequency control (A.F.C) system. A low amplitude 10 kHz modulation (15) is applied to the Klystron reflector voltage (16), modulating frequency and hence power output. The modulated output is fed to a phase-sensitive detector (17) together with the reference 10 kHz signal. When the Klystron frequency is identical to the cavity resonant frequency the reflected modulation frequency is double the original frequency, i.e. 20 kHz, but under other conditions the 10 kHz component can be detected. This component is then filtered generating the appropriate D.C. correction to the Klystron reflector voltage.

The noise generated by the crystal detector is inversely proportional to frequency, so high frequency modulation of the E.S.R. signal is introduced to increase the signal-to-noise ratio. A pair of field modulation coils are built into the walls of the cavity and a low amplitude (0.01 => 0.1 mT) 100 kHz Signal (18) is superimposed on the large swept D.C. field. At resonance the D.C. power level is detected with the 100 kHz modulation, the phase and amplitude of which are determined by the slope of the resonance line. Then by use of a lock-in amplifier (19) and phase sensitive detector (19) with 100 kHz reference signal a D.C. output approximating to the first derivative of the absorption line is produced and displayed on a chart recorder (20).

4.8 Reference Spectra

4.8.1 E.S.R. Spectra of Fe/MgO

At relatively low concentrations (i.e. less than a few thousand ppm) magnesium oxide can be doped with iron which enters the lattice as Fe^{3+} ions occupying magnesium sites substitutionally. To achieve charge compensation in Fe/MgO (since the trivalent Fe^{3+} substitutes for the

divalent Mg^{2+}) one extra vacancy is introduced per two iron ions. The Fe^{3+} ion has a $3d^5$ electronic configuration and application of Hund's Rules shows that the ground state is ${}^6S_{5/2}$. Theory (4.1,4.2) and experiment (e.g. 4.3, 4.4) agree in confirming that the single crystal spectrum, shown in Fig 4.6a contains a strong central ($+\frac{1}{2}$ to $-\frac{1}{2}$) transition, A, flanked by the weaker ($3/2$ to $5/2$) and ($\frac{3}{2}$ to $3/2$) transitions marked B and C respectively; line A, which is almost isotropic, is centred at $g = 2.0033$ while the hyperfine lines B and C are anisotropic. The material used for recording the spectrum shown in Fig 4.6a was a W.C.Spicer (Cheltenham) single crystal grown by electrofusion using 4N grade MgO starting material; the absence of lines due to other trace impurities is noticeable, even though fairly high gain was used to render lines B observable. This spectrum can be seen at room temperature.

The corresponding powder spectrum is shown in Fig 4.6b. This was obtained by using ground up single crystal Fe/MgO and thus comparison of Fig 4.6a and Fig 4.6b shows the differences produced by the presence of a large number of randomly oriented small crystallites each having the same chemical composition as the original large single crystal. The most important of those differences are:-

(a) Whereas the spectra of single crystals are formed as first derivatives, symmetrical about the centre and having positive and negative parts of equal magnitude, the features in the powder spectrum do not necessarily appear in this form. The powder features may not be symmetrical and may not have equal magnitude positive and negative parts; their exact lineshapes are determined in a complex manner by the way in which components that form anisotropic lines stack up or cancel at particular values of magnetic field. Powder lineshapes can be found either by experimental observation using reference specimens of known

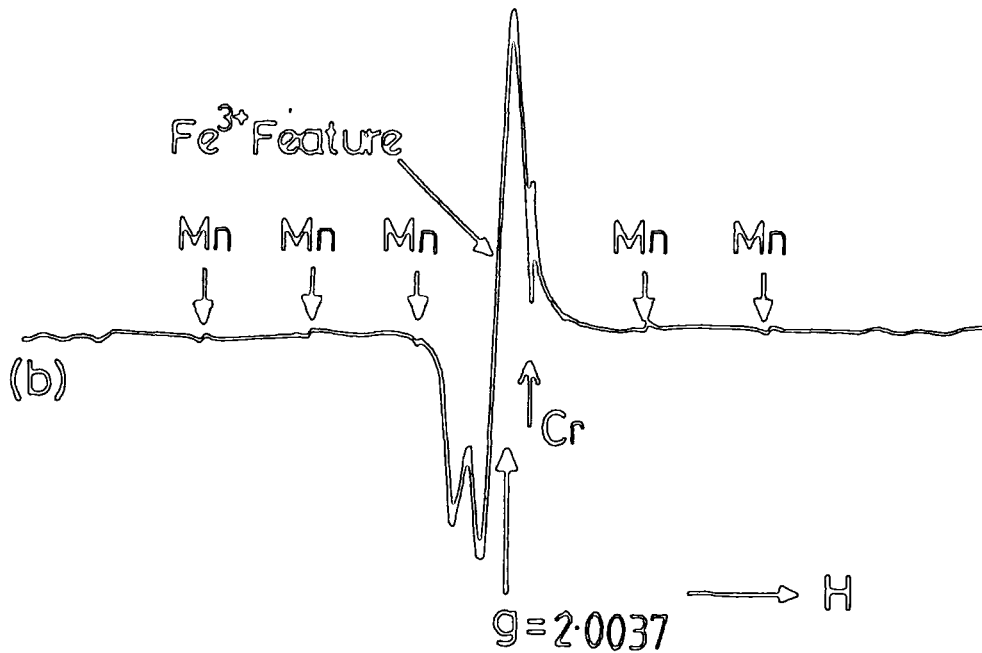
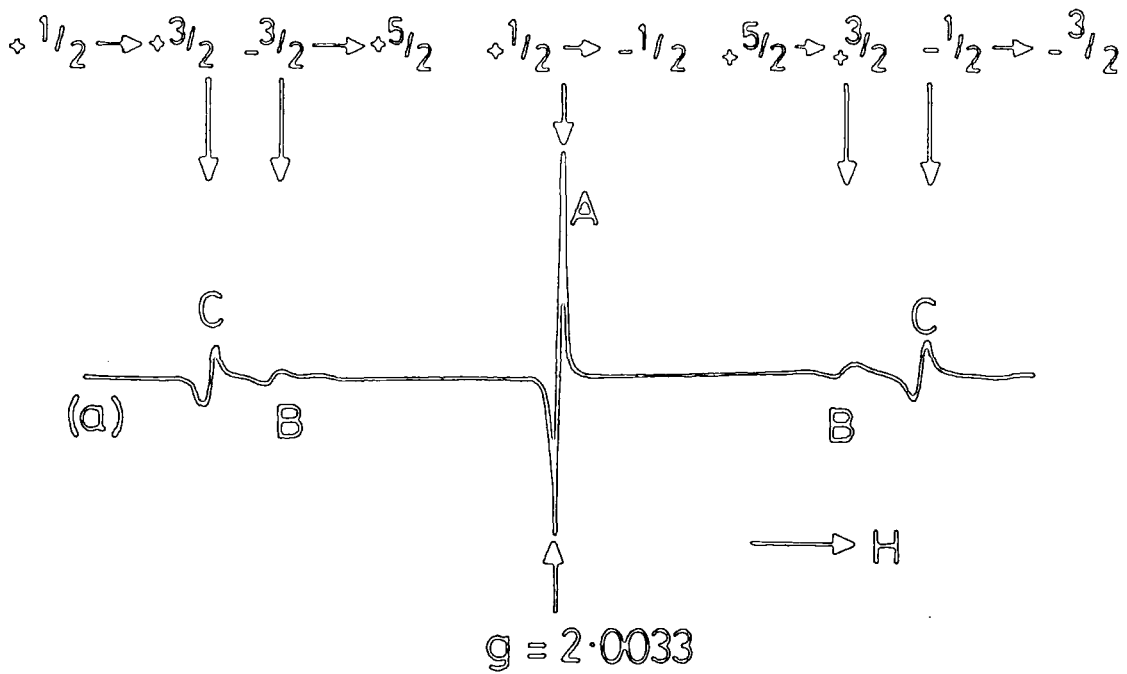


Figure 4.6. ESR spectra of Fe/MgO samples; (a) 310 ppm Fe single crystal, $H//[100]$, (b) 310 ppm Fe powdered crystal. (9.20 GHz, 291 K).

composition or by employing computer simulation techniques based on knowledge of the single crystal spectrum, (including details of the linewidths), and the crystalline electric field properties of the host lattice. A review of computer modelling of ESR powder spectra and a comparison of predicted and observed powder spectra for some transition group ions in MgO has recently been made by A.R. Skinner (University of Durham, Department of Applied Physics and Electronics) to whom we are indebted for permission to reproduce Figures 4.6b, 4.7, 4.8 and 4.9.

(b) Isotropic lines in the single crystal spectrum produce enhanced features in the powder spectrum at nearly the same g-value.

(c) The g-value of the main powder feature is close to that of the corresponding isotropic line in the single crystal spectrum.

(d) In some situations ions present at trace level that are unobservable in the single crystal spectrum give noticeable features in the powder spectrum of the same material. Here, for example, features due to Cr^{3+} and Mn^{2+} are clearly visible in the powder spectrum although their lines were not present with the same intensity relative to Fe^{3+} in the single crystal spectrum.

Thus, as regards powdered Fe/MgO the ESR spectrum is characterised by a single feature centred near $g = 2.003$ which has approximately equal positive and negative parts, is a little broader than the main single crystal line and (as seen on a first derivative plot) has a distinctive double peak on the low field side of the absorption. The Fe^{3+} spectrum is observable at room temperature.

As regards other possible valency states of isolated iron ion in MgO, Henderson and Wirtz [4.18] report that the Fe^{2+} line occurs in the low field region - at approximately $g = 8.6$ - but, since the

Fe^{2+} ion is characterised by being a very fast relaxer, the line is observable only at low temperatures, usually below about 10 K.

4.8.2 E.S.R. Spectra of Cr/MgO

There is a considerable amount of information available in the literature on the Spin Hamiltonian for the isolated ion Cr^{3+} spectrum in single crystals (Low 4.6), linewidth-concentration studies (Thorp, Hossain and Bluck 4.7), line broadening (Thorp and Hossain 4.8) and magnetic interaction mechanisms (Cordischi, Gazzole and Valigi 4.9).

At low concentrations most of the chromium enters the MgO lattice substitutionally as Cr^{3+} . The ground state of the Cr^{3+} ion (${}^4\text{F}_{3/2}$) is split by the octahedral crystalline field into an orbital singlet, which is lowest in energy and two orbital triplets. Figure 4.7a shows in detail the type of spectrum observed. The chromium isotopes without nuclear spin produce a one-line spectrum with a g-value of $g = 1.9800$ (Low 6); the isotopes give rise to the hyperfine structure but since the Cr^{53} isotope is only 9.5% abundant the intensities of the hyperfine lines are only about 1/42 of that of the central $M_s = \frac{1}{2} \Rightarrow \frac{1}{2}$ transition. All five lines of the spectrum are isotropic and can be observed at room temperature.

In powdered single crystal $\text{Cr}^{3+}/\text{MgO}$ the ESR powder spectrum is very similar, Figure 4.7b. It may be noted in particular that

(a) the g-value of the main powder feature is $g = 1.979$, almost exactly the same as the single crystal g-value for this transition.

(b) for the same chromium concentration the peak-to-peak $M_s = -\frac{1}{2} \Rightarrow +\frac{1}{2}$ linewidths are almost the same in both the single crystal and powder spectra.

(c) the hyperfine transitions are observable at about the same level in either spectrum.

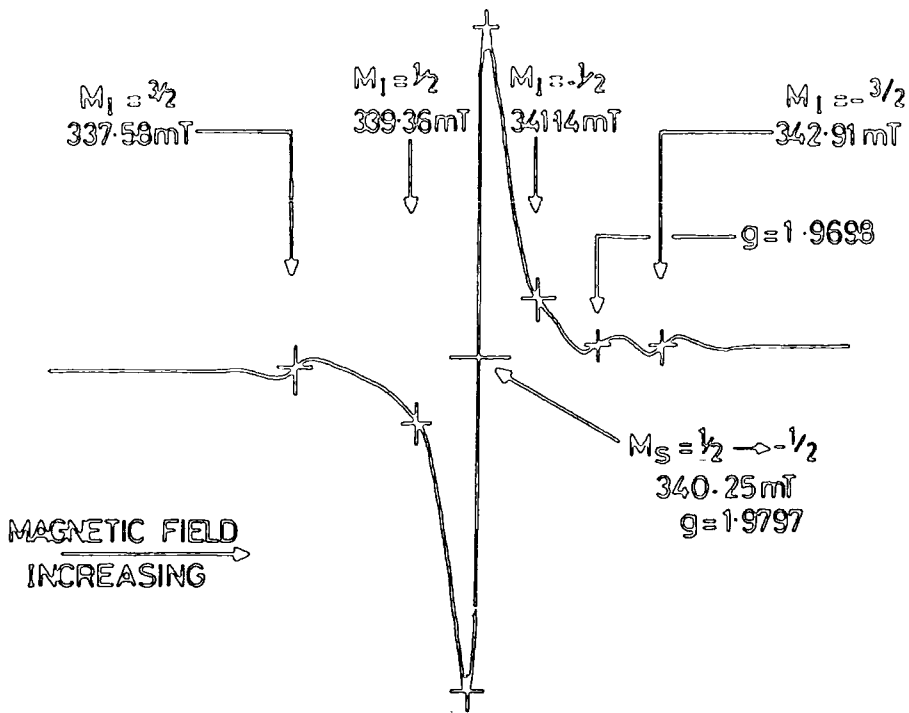


Figure 4.7(a). Detail of ESR spectrum of single crystal Cr/MgO; 800 ppm Cr, 293 K, $H//[100]$, 9.4275 GHz.

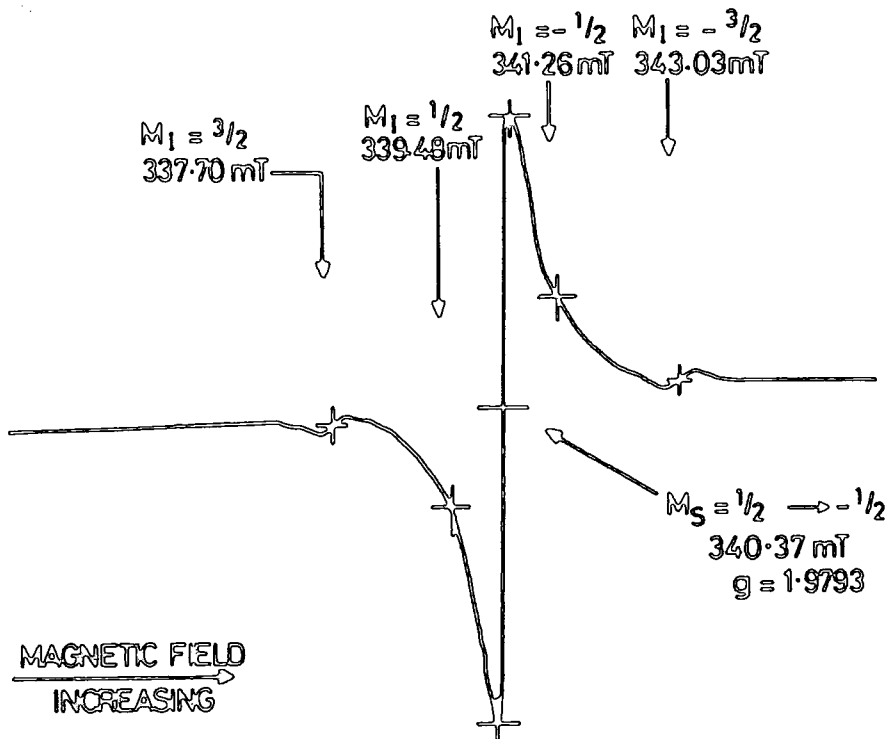


Figure 4.7(b). Detail of ESR spectrum of powdered Cr/MgO single crystal; 800 ppm Cr, 293 K, 9.429 GHz.

4.8.3 E.S.R. Spectrum of Mn/MgO

Manganese enters the MgO lattice substitutionally as Mn^{2+} . This ion is isoelectronic with Fe^{3+} since both have a $3d^5$ electronic configuration giving a ${}^6\text{S}$ ground state. As with Fe^{3+} , the ground state of Mn^{2+} is unaffected by the octahedral field in MgO. Manganese contains a naturally occurring isotope, Mn^{55} , which has a nuclear spin, I , of $I = 5/2$, and the spectrum should form a pattern of six hyperfine groups of lines with five fine structure lines in each hyperfine group, (Low, 6,10: Materisse and Kikuchi 11).

This complex spectrum, which can be seen at room temperature, is illustrated by Fig 4.8a which refers to single crystal $\text{Mn}^{2+}/\text{MgO}$ containing 840 ppm Mn; many of the hyperfine lines are anisotropic and overlap at the polar angle of $\theta = 32^\circ$ to give the rather simpler spectrum of six evenly spaced main lines. The corresponding powder spectrum is shown in Figure 4.8b and here the main characteristic is the occurrence of the easily recognisable six-line spectrum; the identification as Mn^{2+} can of course be made by measurement of g -values and calculation of the Hamiltonian parameters from the observed magnetic field spacing between the individual components of the spectrum. The effect of increasing the manganese concentration is shown by Figures 4.9a and 4.9b which refer to 2900 ppm Mn. The line broadening caused by the increased manganese concentration is sufficient to mask much of the detail of the fine structure lines but, particularly in the powder spectrum, the characteristic "six-line" spectrum remains. The values of the parameters characterising the powder spectrum are slightly concentration dependent but may be taken as close to $g = 2.0008$ with A (the hyperfine structure constant) as $A = -81 \times 10^{-4} \text{ cm}^{-1}$.

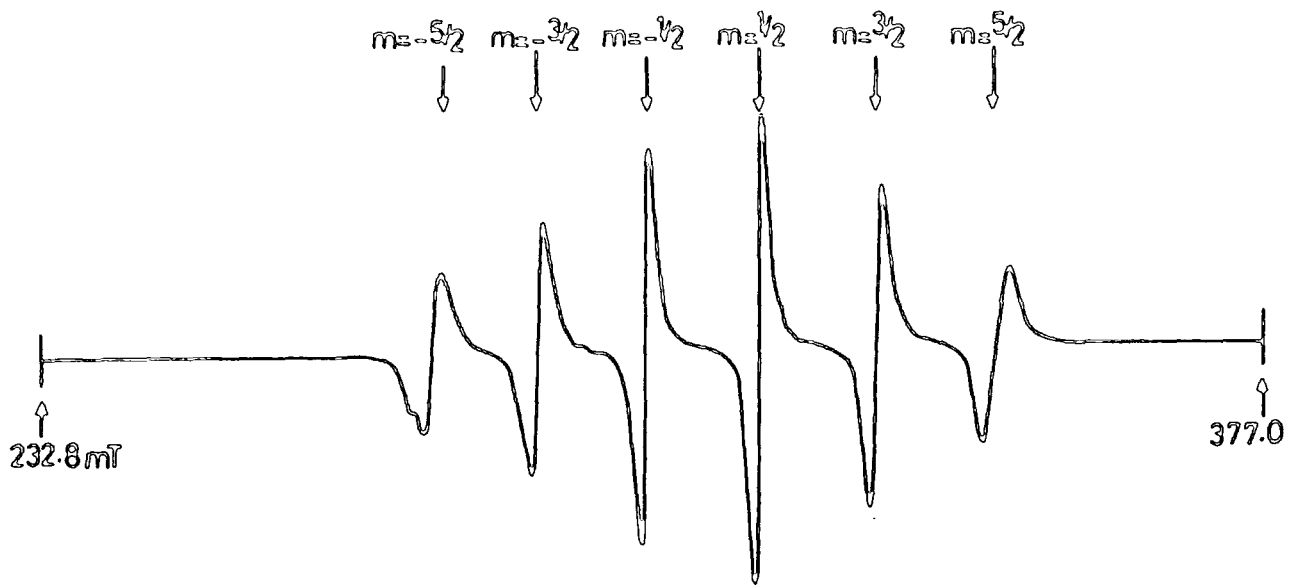


Figure 4.8(a). ESR spectrum of single crystal Mn/MgO at $\theta=32^\circ$; 840 ppm Mn, 9.331 GHz, 293 K.

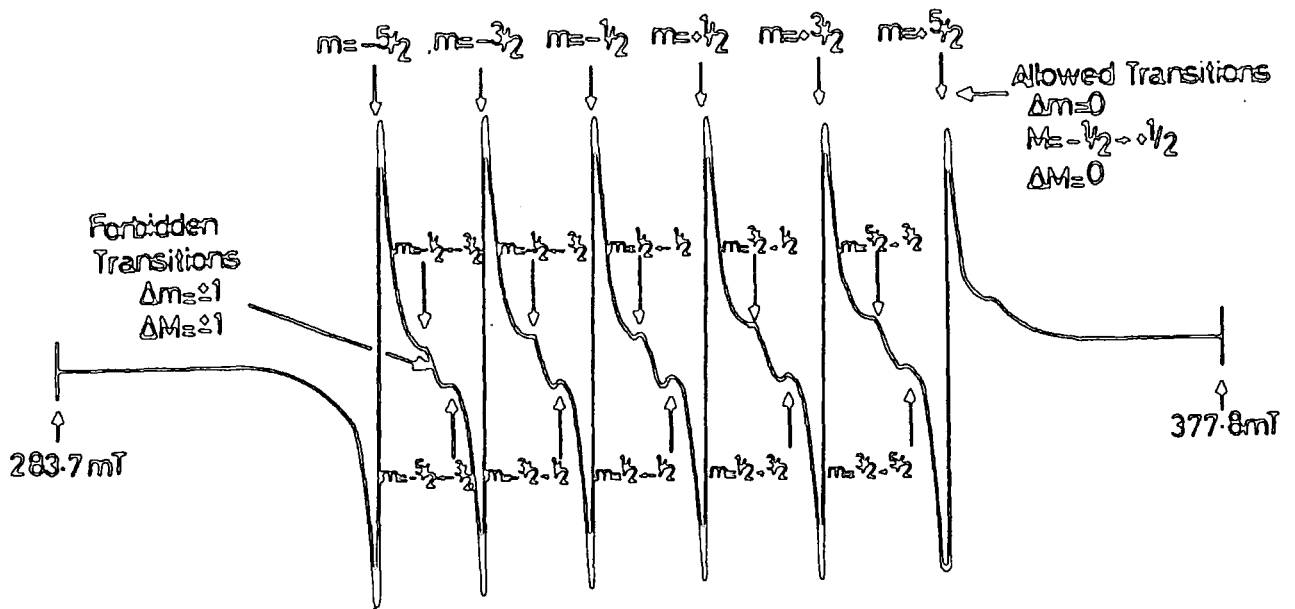


Figure 4.8(b). ESR spectrum of powdered Mn/MgO; 840 ppm Mn, 9.375 GHz, 293 K.

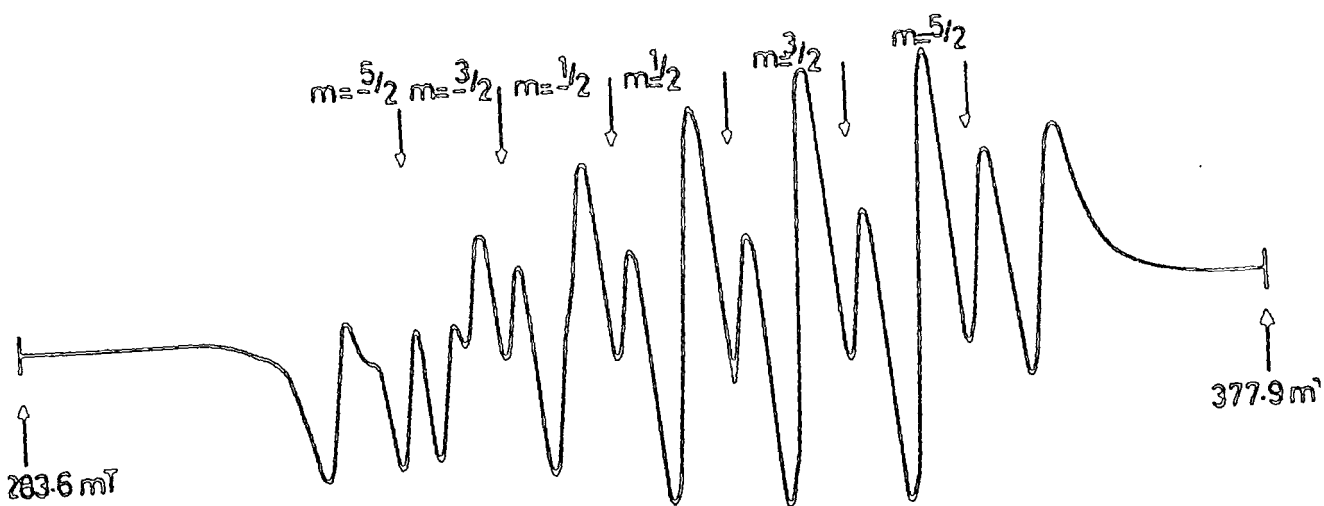


Figure 4.9(a). ESR spectrum of single crystal Mn/MgO;
 2900 ppm Mn, $H//[100]$, 9382 GHz, 293 K.

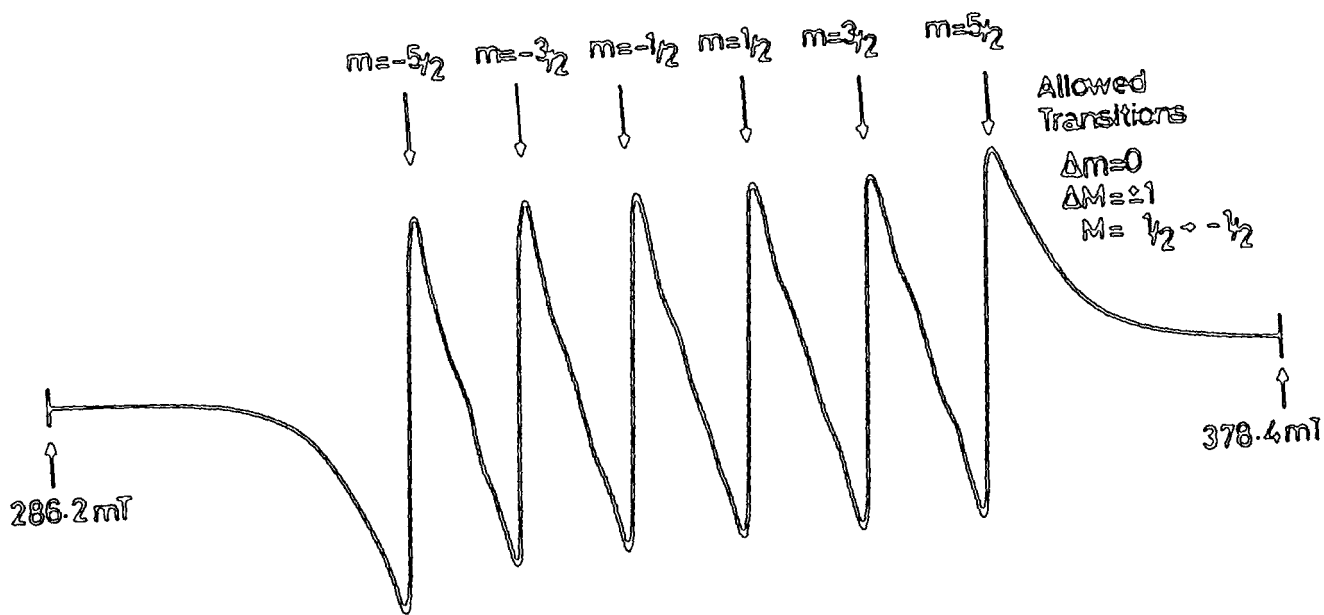


Figure 4.9(b). ESR spectrum of powdered Mn/MgO; 2900 ppm
 Mn, 9.380 GHz, 293 K.

4.8.4 E.S.R. Spectra of Ni/MgO

The ESR spectrum of $\text{Ni}^{2+}/\text{MgO}$ has been reported by several authors (e.g. Low 12, Orton 13, Thorp and Hossain 14). It is generally accepted that nickel enters substitutionally occupying magnesium sites. In single crystal material the spectrum consists of a line centred near $g = 2.215$ which is the superposition of the transition $-1 \rangle \langle \Rightarrow 0 \rangle$ and $+1 \rangle \langle \Rightarrow 0 \rangle$ together with a central dip with the same g -value due to the double quantum transition $-1 \rangle \langle \Rightarrow +1 \rangle$. The line is nearly isotropic with a width of about 6 mT for 1400 ppm Ni. The spectrum can be observed at and below room temperature and Walsh (15), using a powdered sample of $\text{Ni}^{2+}/\text{MgO}$, reported that the linewidth was temperature independent at low temperatures.

4.8.5 E.S.R. Spectrum of Co/MgO

The divalent ion of cobalt has an electronic configuration $3d^7$ giving rise to a ground state of ${}^4F_{9/2}$. In the MgO lattice the 4F level splits into three levels; these are further split by spin-orbit interaction (Low 16) so that the lowest level is a Kramers doublet. Since the only natural isotope of cobalt is Co^{59} which has a nuclear spin of $I = 7/2$, considerable hyperfine interaction is expected. The Co^{2+} ion enters the MgO lattice in the octahedral sites and the spectrum, (which is observable only at low temperatures and has recently been examined in detail by Thorp, Hossain, Bluck and Bushell (17)), is isotropic and shows a total of eight hyperfine lines with a g -value of about $g = 4.278$ and a hyperfine constant of $A = 98 \times 10^{-4} \text{ cm}^{-1}$.

4.9 Conclusions

This chapter summarizes the known features of the electron spin resonance spectra of some transition group ions in MgO, results being

specifically given for Fe^{3+} , Cr^{3+} , Mn^{2+} , Co^{2+} and Ni^{2+} . Attention is drawn to the differences which may appear between the single crystal and powder spectra of a given material. The listed spectra provide "magnetic fingerprints" by which, through observation of its ESR spectrum, the paramagnetic impurities present in an unknown magnesia powder could be identified. The reference spectra also show that with a good but conventional ESR spectrometer (e.g. a Varian 9 GHz ESR spectrometer) sufficient sensitivity is available to suggest that, at the impurity levels expected from direct chemical analysis, spectra should be observable from commercial magnesia powders.

It should perhaps be noted that of the selection given in Section 4.3 only "isolated ion" spectra have been considered, i.e. the spectra correspond to situations where the dopant enters the lattice as separate well-spaced individual ions. Some of the transition ions, notably Fe^{3+} and Cr^{3+} are known to form clusters and spinel-phase compounds under certain conditions of heat-treatment. The iron-spinel and chromium spinel structures give rise to ESR spectra which possess characteristics significantly different from those of the corresponding "isolated ion" spectra. These structures are likely to be relevant since there is direct evidence from X-ray Diffraction measurements (Chapter 2) that spinel phases are present in MgO powders taken from some stages of the manufacturing production process.

CHAPTER FOURREFERENCES

- 4.1 N.M.R. and E.S.R. Spectroscopy, (Varian Associates)
Pergamon Press, London, 1964.
- 4.2 A.Abragam and B. Bleaney,
Electron Paramagnetic Resonance of Transition Ions,
Clarendon Press, Oxford, (1970).
- 4.3 W. Low,
Paramagnetic Resonance in Solids, Solid State Physics
Supplement 2; Academic Press, New York, (1960).
- 4.4 J.S.Thorp, R.A.Vasquez, C. Adcock and W.Hutton,
J.Materials Sci.11, (1976), 89.
- 4.5 A.D.Inglis and J.S.Thorp,
J.Materials Sci, 16 (1981), 1887.
- 4.6 W.Low,
Phys.Rev.,105, (1957), 801.
- 4.7 J.S.Thorp, M.D.Hossain and L.J.C.Bluck,
J.Mater.Sci.14, (1979), 2853.
- 4.8 J.S.Thorp and M.D.Hossain
J.Mater.Sci.15, (1980), 3041.
- 4.9 D.Cordishi, D.Gazzoli and M. Valigi,
J.Sol.State Chemistry 24, 1978, 371.

- 4.10 W.Low, Ann.N.Y.Acad.Sci. 72, (1958) 69.
- 4.11 L.M.Matarrese and C.Kikuchi,
J.Phys.Chem.Solids 1, (1956), 117.
- 4.12 W.Low,
Phys.Rev.109 (1958) 247.
- 4.13 J.W.Orton, P.Auzius, J.H.E.Griffiths and J.E.Wirtz,
Proc.Phys.Soc. Lond.78, (1961), 584.
- 4.14 J.S.Thorp and M.D.Hossain,
Jour.Mag. and Magn.Materials 22, (1981), 311.
- 4.15 M.M.Walsh,
Phys.Rev.122, (1961), 762.
- 4.16 W.Low, Phys.Rev.109 (1958), 256.
- 4.17 J.S.Thorp, M.D.Hossain, L.J.C.Bluck and T.G.Bushell
J.Mater.Sci., 15, (1980), 903.
- 4.18 A.Henderson and J.E.Wirtz, "Defects in the Alkaline
Earth Oxides", Taylor and Francis Ltd., London, (1977).

CHAPTER FIVEELECTRON SPIN RESONANCE - RESULTS AND DISCUSSION

The principles underlying electron spin resonance techniques have been outlined and reference spectra given for a selection of paramagnetic ions in MgO. This chapter is concerned with the experimental data obtained from various commercial magnesias, referring to measurements made at room temperature with a Varian V4502-15 9 GHz ESR spectrometer.

5.1 Method of Identifying Impurities

It must first be borne in mind that pure MgO (i.e. spectroscopically pure grade MgO) is diamagnetic and consequently - as proved to be the case - it will generate no signals when examined in the Varian spectrometer. Hence any signal actually observed must be due to some paramagnetic (or possibly ferromagnetic or ferrimagnetic) impurities.

An example of the general approach adopted in identifying impurities is illustrated by Figure 5.1. Here the centre trace (b) refers to the experimental spectrum recorded for a particular commercial sample, in this case powdered green polycrystalline material taken from a fused melt near the boundary between green and brown material. This shows a large amplitude central line having some five structures in its wings together with a series of five smaller lines which by their equal amplitude and spacing suggest a common origin. All the lines are quite narrow suggesting immediately that the spectrum corresponds to two paramagnetic species present at levels of about 100 to 1000 ppm; there are also indications of some other lines present at much lower intensities. The g-value of the central line suggests Cr^{3+} as a

possibility and close comparison with Fig 5.1a (the upper trace), which gives the reference spectrum for $\text{Cr}^{3+}/\text{MgO}$, shows the exactness of the fit as regards g-value, lineshape and number and positions of the fine structure lines, confirming the identification as Cr^{3+} . Similarly, comparison of the group of five equi-spaced lines with the lower reference spectrum, Fig 5.1c, confirms the presence of Mn^{2+} , (The sixth line overlapping with the central Cr^{3+} transition).

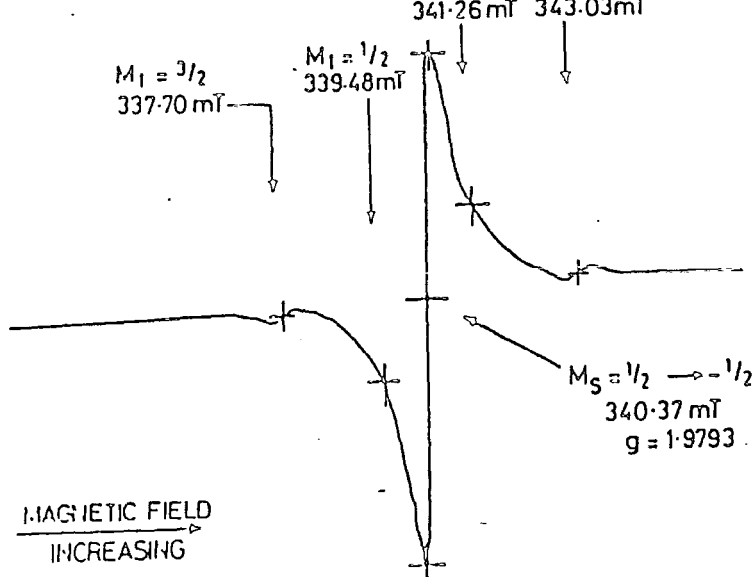
The experimental esr spectrum (Fig 5.1b) may also be used in the reverse sense in that lines due to some species which might have been expected were not revealed. Here there is no evidence for any Fe^{3+} spectrum, although the chemical analysis suggests that iron is a major impurity, present at as much as about 0.1%. This is surprising and indicates that any iron present must be in a form other than substitutional isolated-ion Fe^{3+} . It will be seen later that a possible explanation is that the iron is present as a magnesio-ferrite.

5.2 Results from Commercial Magnesia Powders

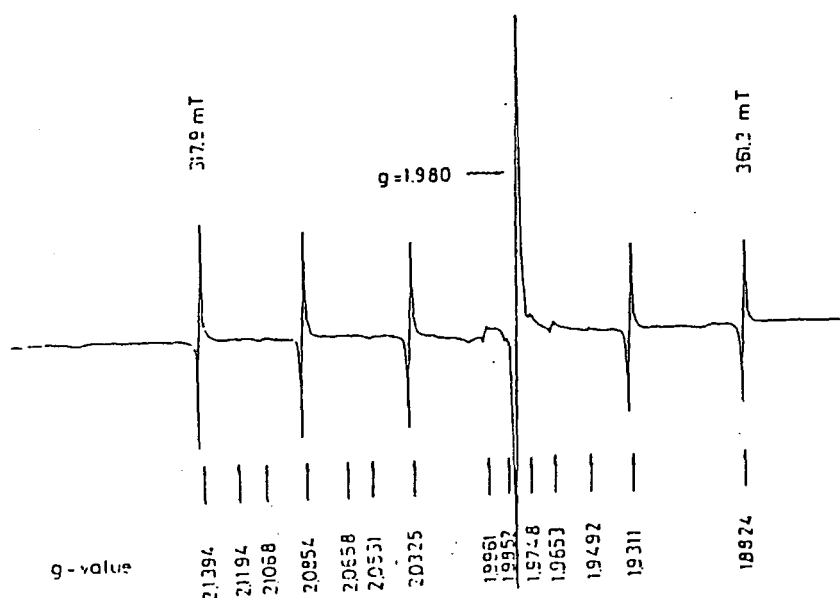
The range of samples examined with the ESR technique included those tested with X-ray diffraction and the Gouy magnetometer. It was known from the chemical analysis that the major paramagnetic impurities were likely to be iron, chromium, manganese, nickel, and cobalt, all of which are amenable to study by ESR methods as may be seen from the following results.

(a) E.S.R. Spectrum of Magnesite.

The starting material for the fusion process - magnesite - was examined briefly because it is likely that impurities present in it may be carried through to subsequent, and even the final, stages of the preparation of the product. The esr spectrum is shown in Figure 5.2b. There is a strong signal, manifest as a wide line with evidence of unresolved structure, which is centred near $g = 2.00$. Brief examination with an expanded field scale revealed that the broad line, whose



(a) Detail of ESR spectrum of powdered Cr/MgO single crystal; 800 ppm Cr, 293K, 9.429 GHz.



(b) Unknown powder spectrum.

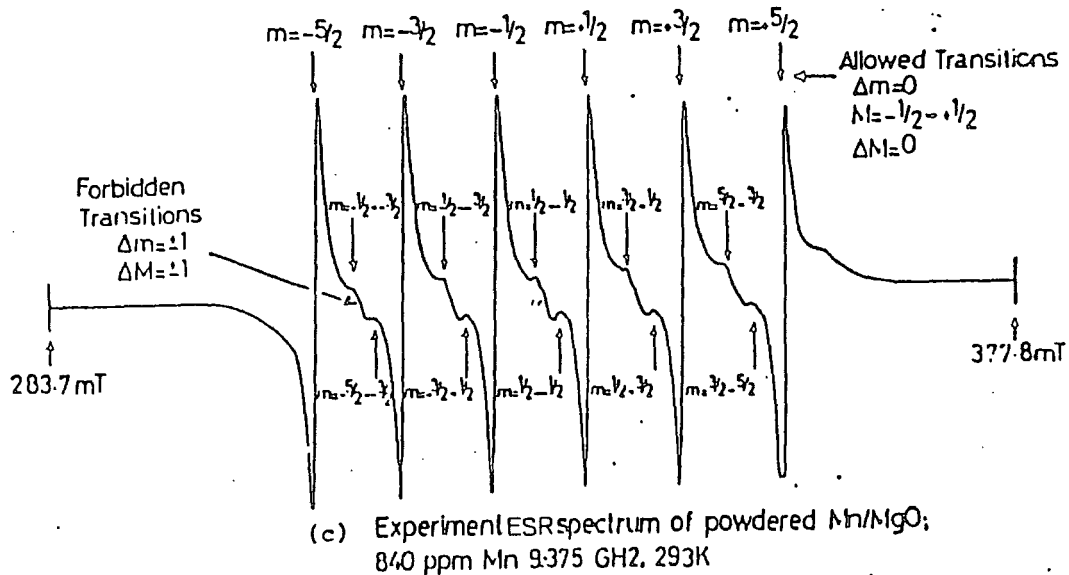


Figure 5.1. Analysis of an unknown powder spectrum.

peak-to-peak linewidth is about 80 mT, is asymmetric and that narrow width (~ 5 mT) transitions are present as well ; this supports the view that the main broad line feature is probably ferrimagnetic rather than paramagnetic in origin. Comparison should here be made with the spectrum of pure MgO powder, Fig 5.2a, which even at very high sensitivity, gives no lines ; the spectrometer gain used to record Fig 5.2a was some 500 times greater than for Fig 5.2b.

(b) E.S.R. Spectra of Material from the Centre of the Fusion.

Figure 5.3a shows the spectrum of ground material from the centre of the fusion. The central (highest intensity) line is due to Cr^{3+} and the smaller amplitude group all to Mn^{2+} ; the baseline is fairly flat, though there is a possible indication of a broad line underlying the Cr^{3+} transition. After heat treatment, this material shows the same Cr^{3+} and Mn^{2+} lines (Fig 5.3b) but now there is in addition a very broad line, centred near $g = 1.99$, whose linewidth suggests that it is unlikely to be paramagnetic in origin. Figures 5.3a and 5.3b were recorded at the same spectrometer gain and (as might be expected) show little difference in the intensities of the Cr^{3+} and Mn^{2+} spectra before and after heat treatment.

(c) E.S.R. Spectra of Material from the Outer Region of the Fusion.

The corresponding spectra for outer material are shown in Figures 5.4a and 5.4b. The spectrum of unheated material from the fusion (Fig 5.4a) exhibits the Cr^{3+} and Mn^{2+} lines but also shows a pronounced broad-line feature which appears to show some asymmetry having a longer tail on the high field side. After heat-treatment, (Fig 5.4b) the spectrum shows Cr^{3+} and Mn^{2+} much as before, but the broad-line spectrum is stronger with some change in lineshape - becoming slightly more asymmetrical - although centred at the same g-value.

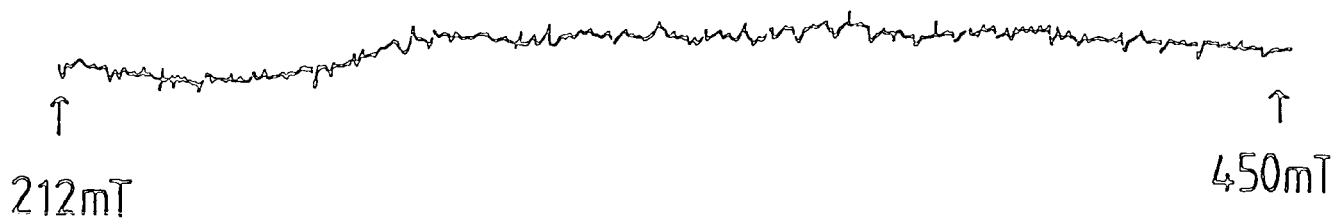


Figure 5.2 (a).

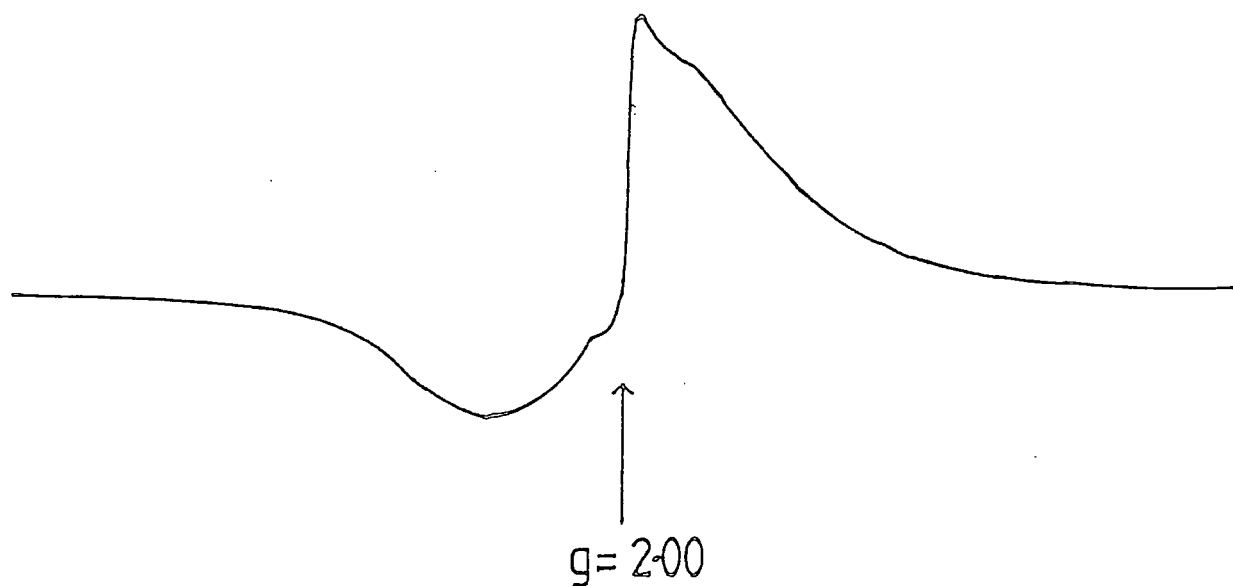


Figure 5.2 (b).

Figure 5.2. Comparison of the ESR spectra of (a) Koch-Light 99.998% pure MgO and (b) magnesite.

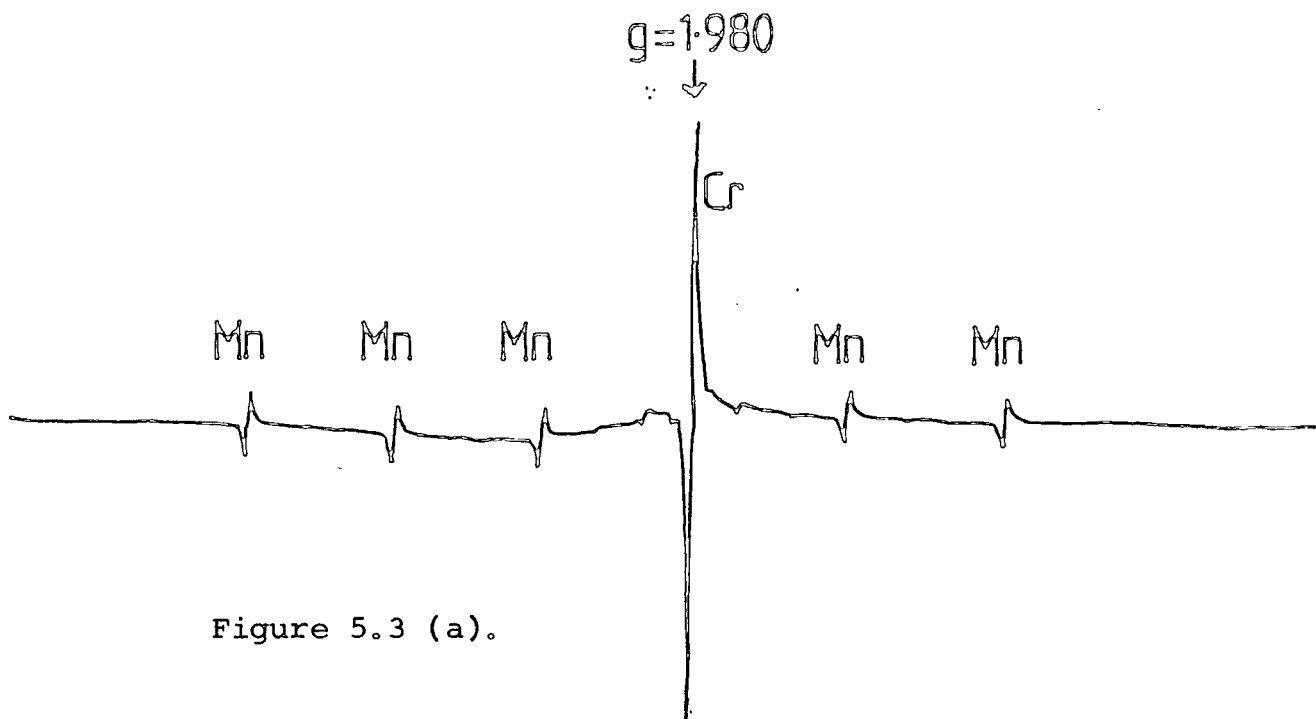


Figure 5.3 (a).

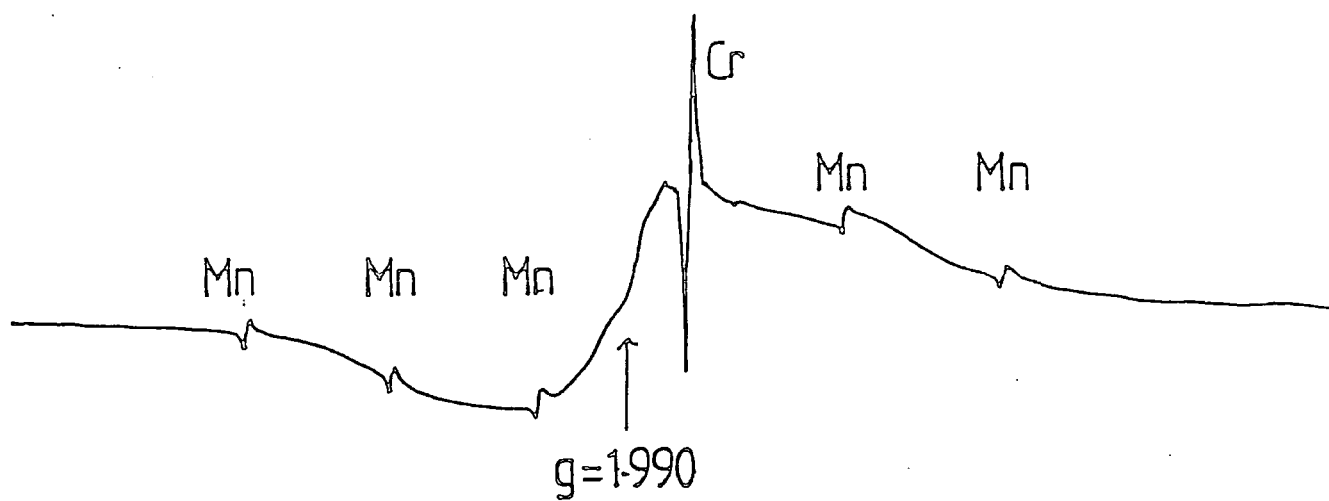


Figure 5.3 (b).

Figure 5.3. E.S.R. spectra of samples from the centre of the fusion (a) before and (b) after annealing heat treatment.

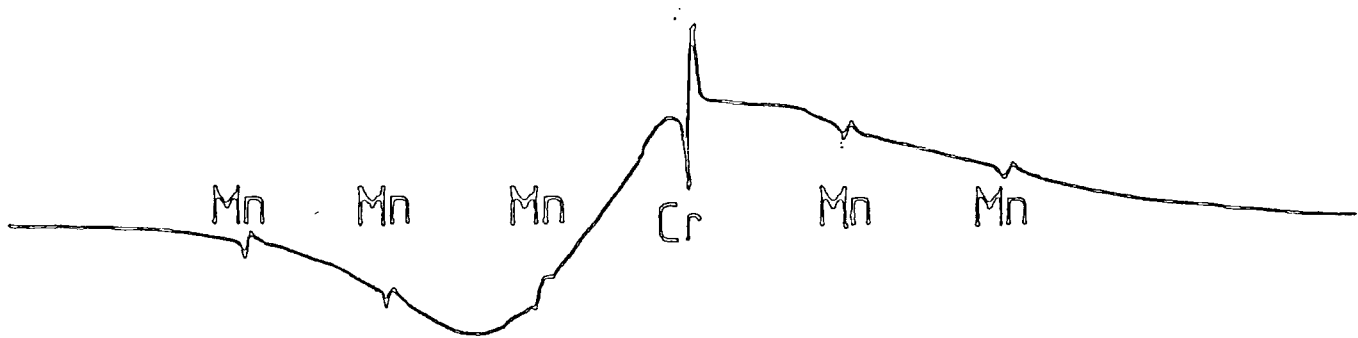


Figure 5.4 (a).

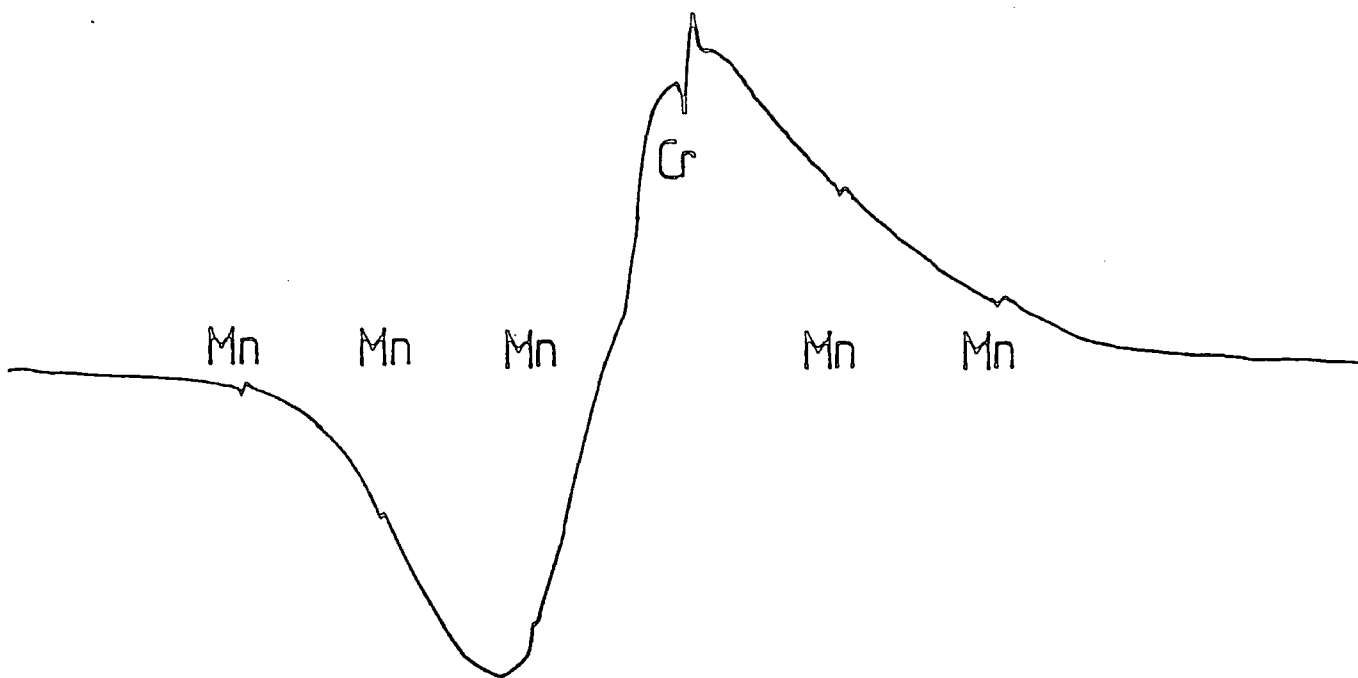


Figure 5.4 (b).

Figure 5.4. E.S.R. spectra of samples from the outer region of the fusion (a) before and (b) after the annealing heat treatment.

(d) ESR Spectra of Quenched Powders.

Two samples of commercial magnesia powders that had been quench cooled after heat treatment were examined. These results are shown in Fig 5.5. The upper trace, Fig 5.5a refers to material originating from the centre of the fusion and the lower to material from the outer fused material. Each spectrum shows the paramagnetic species Cr^{3+} and Mn^{2+} and, in addition, some broadline signal which is much less evident in the inner material than in the outer material. Comparison with the powders that had been annealed after heat treatment (Figures 5.3 and 5.4) shows that the quench cooled product contains noticeably less broadline impurity than the corresponding annealed product.

In summary, the ESR study has identified, unambiguously, the presence of chromium and manganese in all the commercial powders examined, both those entering the MgO lattice substitutionally, as Cr^{3+} and Mn^{2+} respectively, probably at levels of a few hundred ppm. Further there is conclusive evidence for an additional impurity (which gives rise to a broad linewidth signal) which is present to varying degrees in all the samples examined, though to a lesser degree in material from the inner region of the fusion than in outer material, and is very markedly less intense in quench cooled than in annealed magnesia. No signal due to Fe^{3+} has been found in any commercial powder studied.

In the context of the role of impurities in determining the dielectric loss characteristics of the magnesia powder it appears from previous work on doped MgO single crystals that neither chromium or manganese (at the levels present here) would give any significant change in either permittivity or dielectric loss, [Thorp and Rad 5.1; Thorp, Kulesza, Rad and Kenmuir 5.2; Thorp, Hossain and Kenmuir 5.3].

Some importance attaches to the observation of the broad linewidth feature; the measurements made so far suggest that it is of ferri-magnetic origin possibly arising from the presence of a magnesioferrite, [Inglis and Thorp 5.4; Inglis, Russell and Thorp 5.5; Thorp, Johnson and

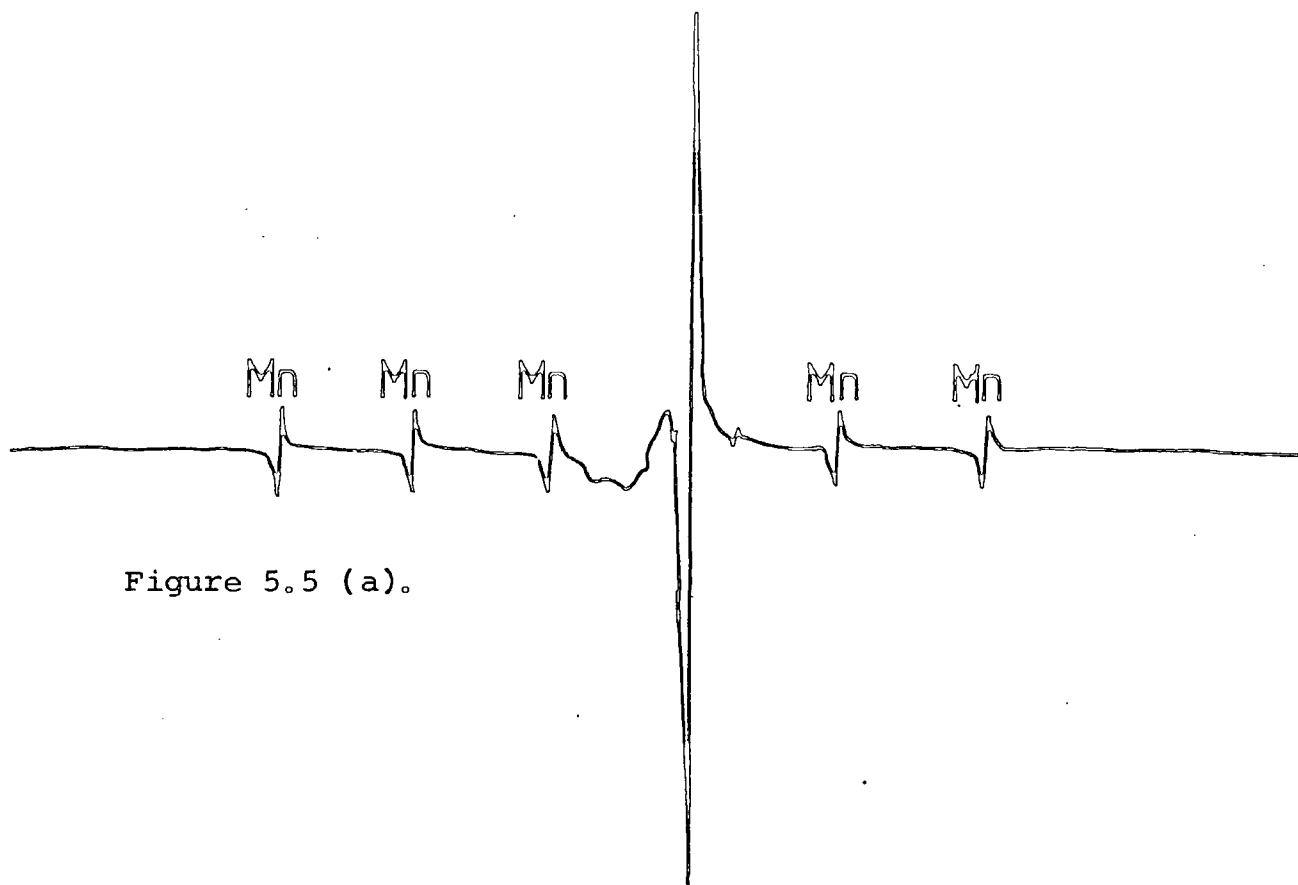


Figure 5.5 (a).

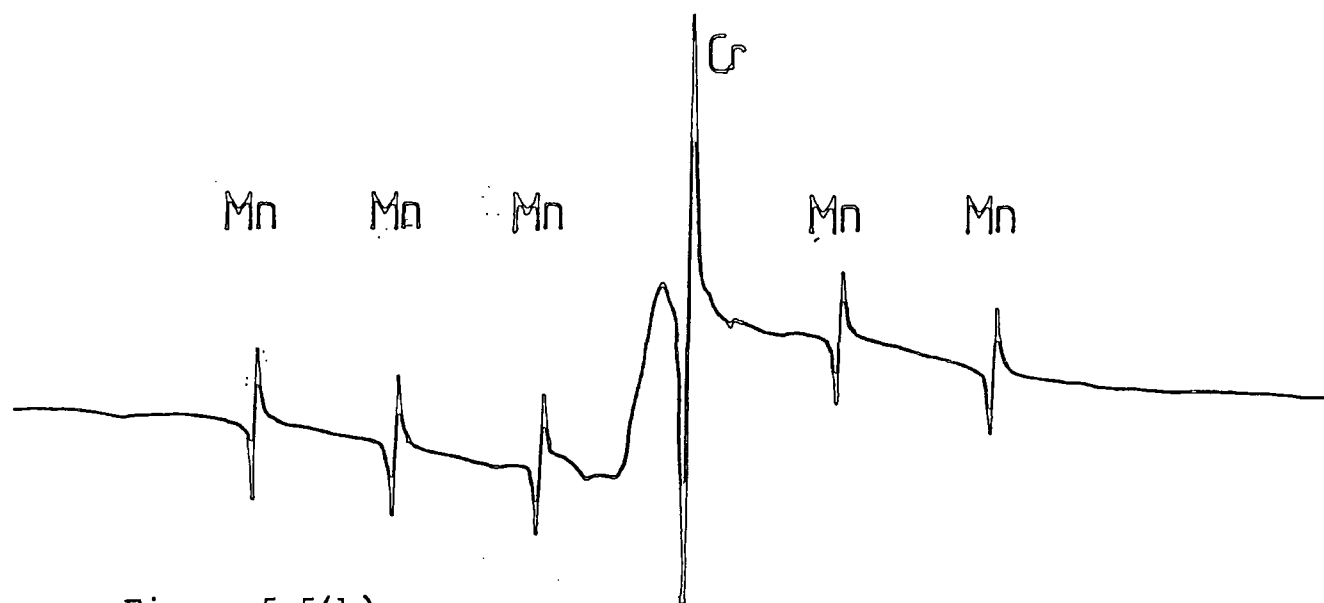


Figure 5.5(b).

Figure 5.5. E.S.R. spectra of samples after quenching heat-treatment; (a) material from the centre of the fusion and (b) material from the outer region of the fusion.

Savage 5.6] or a magnesiochromite phase. Preliminary dielectric measurements show that each of these is very lossy compared with pure MgO, the iron-magnesium ferrite being worst. If this model is correct, the practical implication is that the removal of this phase - which might be achieved by enhancing the magnetic separation stages of manufacture - would be advantageous ; on the scientific side there is a need to verify the dielectric loss behaviour of iron and chromium ferrites.

5.3 Results from Chromium Doped MgO and Magnesium Chromite

A sample of 99% pure magnesium chromite powder was obtained from Alfa Chemicals Ltd. and was then examined in the Varian spectrometer. The resulting spectra showed a broad line (~ 300 mT wide) centred at $g = 1.978$. Thus the g value of the centre of this line is indistinguishable from that of the Cr^{3+} line seen in the commercial powders. However the broad line of the commercial powders is centred at about $g = 2.00$, i.e. at distinctly lower field value. Therefore the broad line of the commercial powders could be attributed solely to magnesium chromite. Nonetheless the possibility that an asymmetric broad line, seen in some commercial samples, cannot be caused in part by magnesium chromite cannot be ruled out.

The effect of the heat treatment on the chromium impurity in the commercial powders will be assessed by simulating the heat treatment on pure magnesia samples deliberately doped with chromium. To this end, single crystal chippings containing chromium in the range 760 ppm to 9,500 ppm Cr/MgO were obtained from W & C Spicer Ltd. (Cheltenham) and were then ground to powder. They were then treated in oxygen at 800°C and were quench cooled (to freeze in high temperature effects) after $\frac{1}{2}$ hr, $1\frac{1}{2}$ hrs and 4 hrs of total heating time; ESR spectra were obtained at each stage.

Two points emerge from the resulting spectra : first, that the heat-treatment has no effect on Cr/MgO that is measurable with electron spin resonance; second, as the concentration of the dopant increases the width of the Cr^{3+} line increases (see figure 5.6).

Thus it seems most likely that the broad line feature in the commercial powders is in no way related to their chromium impurity. Further, comparison of the linewidths of the spectra Cr^{3+} line in Fig 5.6 with those of the commercial powders suggests that the latter contain less than 760 ppm Cr/MgO. This is in agreement with the findings of the chemical analysis.

5.4 Results from Iron Doped MgO

The susceptibility study on Iron doped magnesium oxide (Chapter 3, section 6) revealed the growth of a magnetic phase on heat treatment of the samples. To characterise the phase, ESR spectra were made before and after each successive stage of the heat treatment.

The spectrum of the lowest dopant concentration, (310 ppm Fe/MgO) tested before heat treatment, showed an asymmetric double paramagnetic line corresponding to Fe^{3+} superimposed on another line, most probably Cr^{3+} . The six lines due to Mn^{2+} were also visible (see Fig 5.7).

The spectra of the higher concentrations before heat treatment were similar, but the Fe^{3+} , Cr^{3+} , Mn^{2+} lines were superimposed on a broad line whose intensity increased with increasing dopant concentration. The broad line is centred at about $g = 2.003$ and is about 300 mT wide, suggesting that a ferrimagnetic, rather than a ferro- or para-magnetic impurity, is present even in as-received iron doped crystals.

On heat treating at 800°C in oxygen the intensity of the broad line grew dramatically ; for higher concentration the spectrum became unrecordable after 1 hr of heat treatment, whereas, for the lower concentrations the broad line could still be recorded after $3\frac{1}{2}$ hrs heating time (see Figs. 5.7 and 5.8).

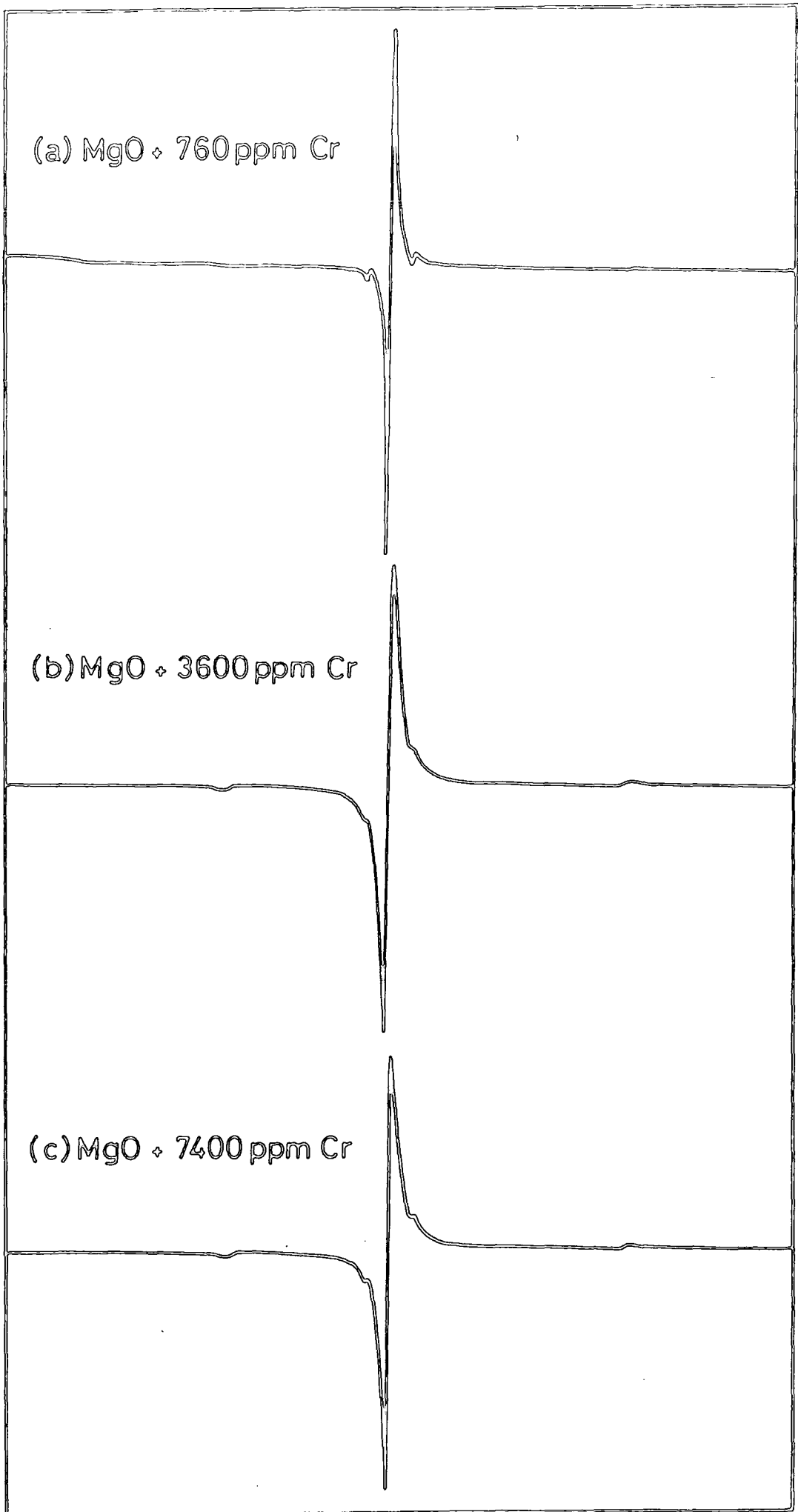


Figure 5.6. Line broadening in MgO/Cr powders.

(a) MgO + 310 ppm Fe
before heat treatment

(b) MgO + 310 ppm Fe
after 1.5 hours
heat treatment

(c) MgO + 310 ppm Fe
after 3.5 hours
heat treatment

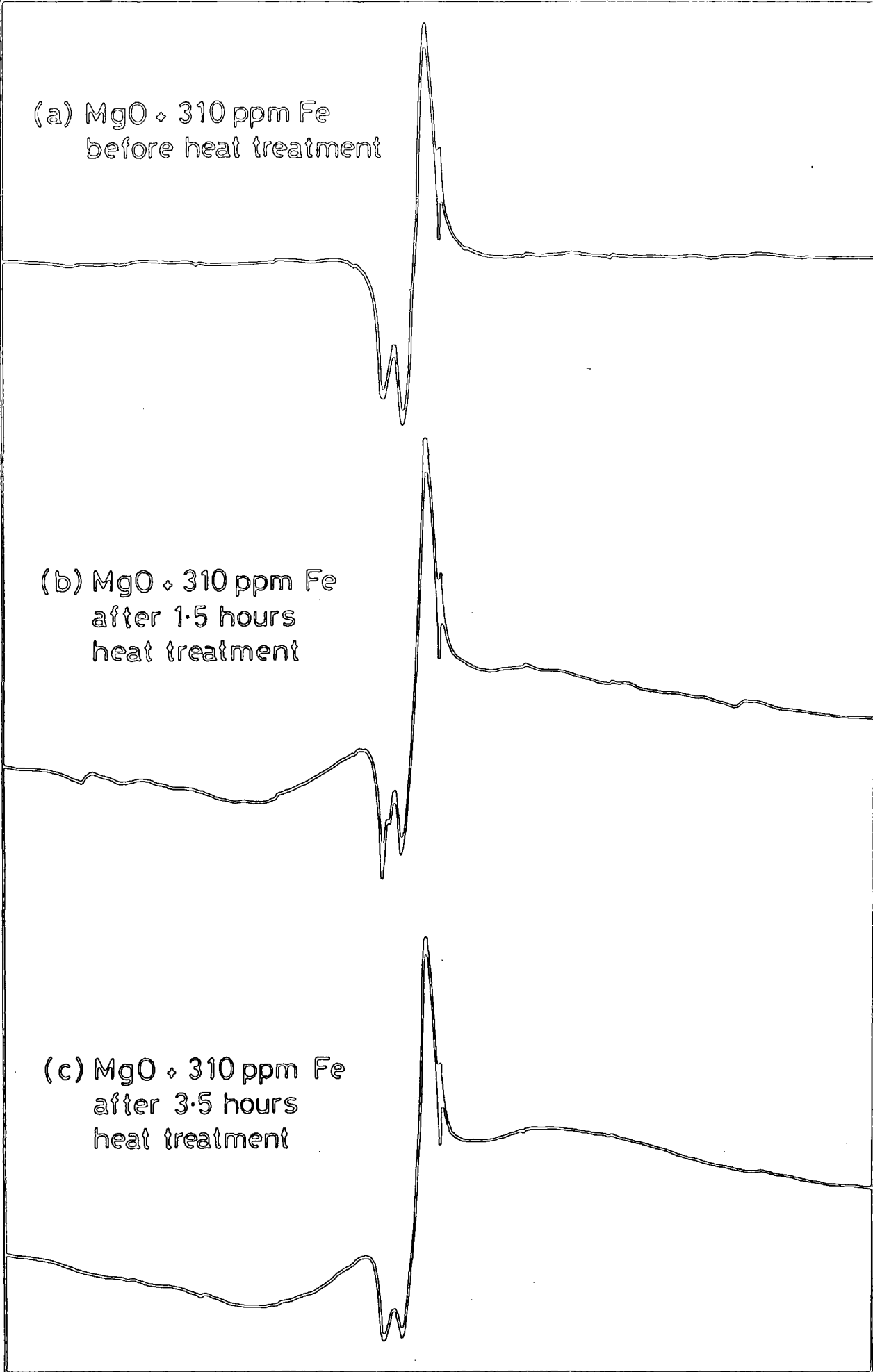


Figure 5.7. Samples of Fe/MgO before and after heating at 800° C in Oxygen.

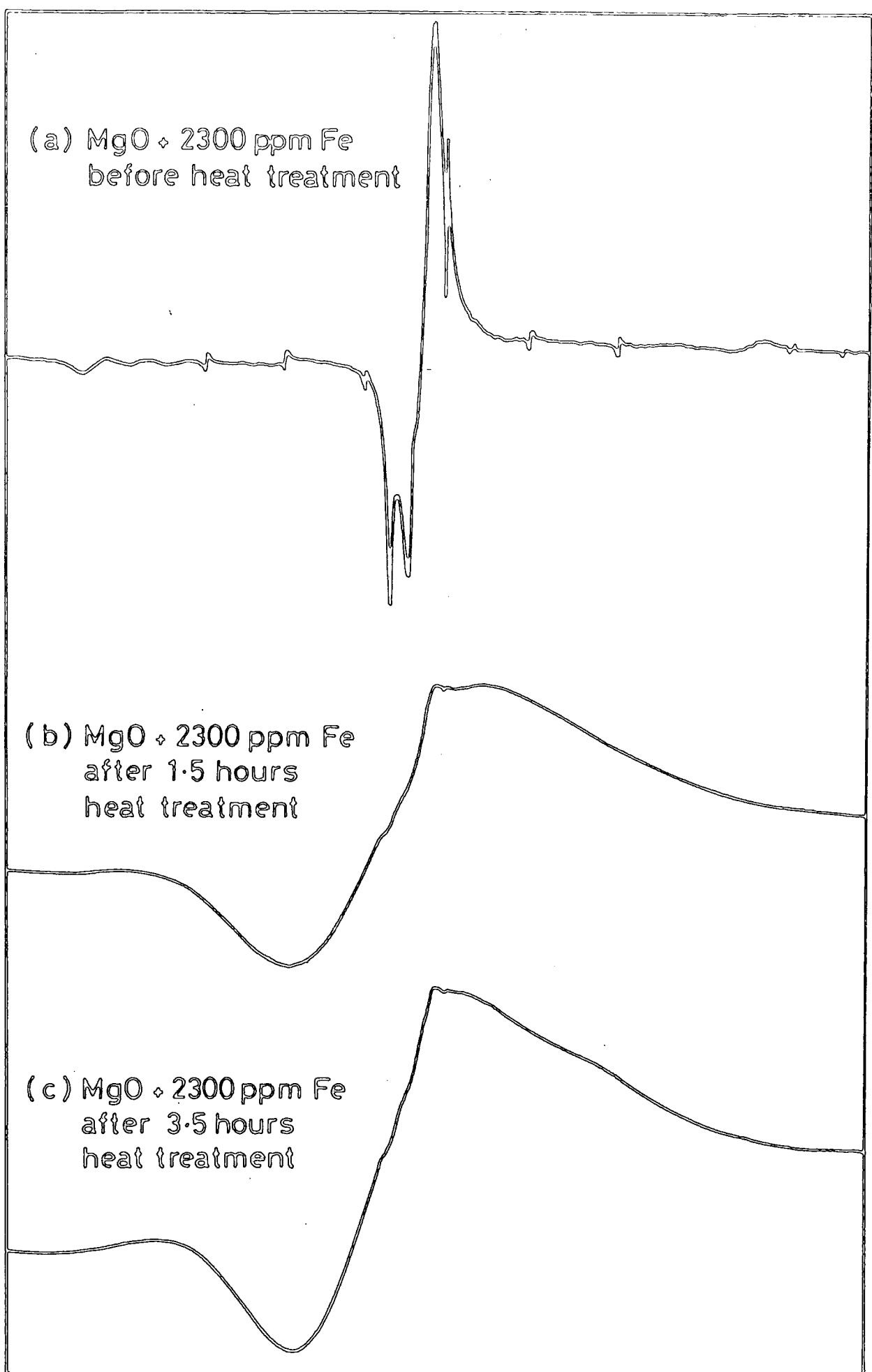


Figure 5.8. Samples of Fe/MgO before and after heating at 800°C in Oxygen.

Several points emerge : the appearance and growth of the broad line centred at $g = 2.003$ coincides with the growth in susceptibility values reported in Chapter 3 ; this line is very similar to that seen in the spectra of the commercial powders; its width is typical of a ferrimagnetic, and for higher concentrations, after even short heating times, the signal becomes too lossy to measure.

In view of previous work (Inglis, Russell and Thorp, 5.5; Thorp, Johnson and Savage, 5.6; Wirtz and Fine, 5.7) the present results support the view that magnesio-ferrite is formed on the heat treatment of iron doped MgO. That the broad line formed in these Fe/MgO powders is so similar to that observed in the commercial powders (see figure 5.9) is perhaps not so surprising when the chemical analysis has suggested that the commercial powders do indeed contain iron (up to 0.16%). Indeed, what is perhaps more surprising is that the intensity of the broad line in the commercial powder spectra is not greater. Nonetheless, that at higher iron concentrations after heat treatment, the sample becomes too lossy to measure suggests that the impurity would have deleterious effects on the use of the MgO as an electrical insulator.

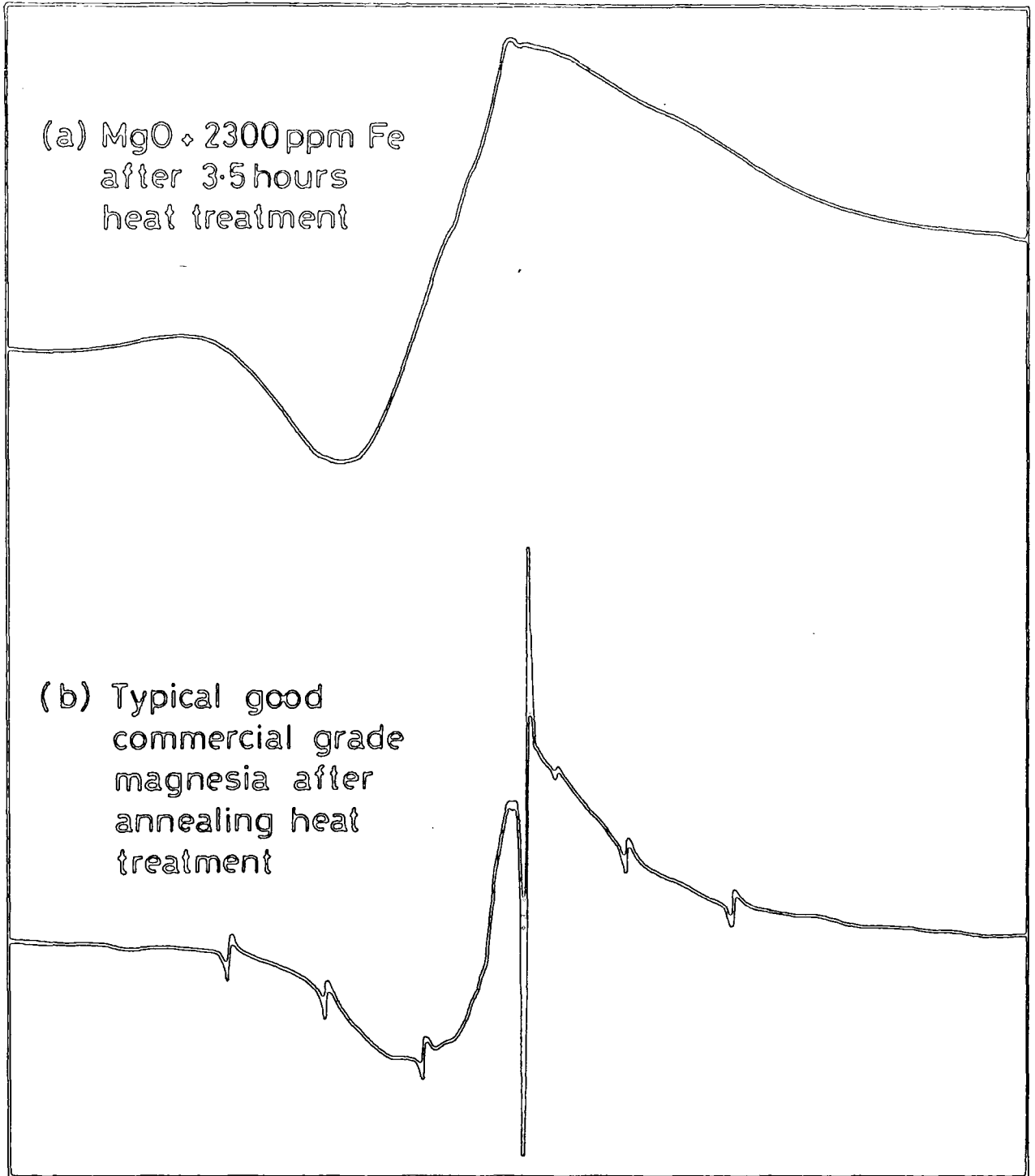


Figure 5.9. Comparison of (a) deliberately doped Fe/MgO after 3½ hours at 800°C in oxygen with (b) good commercial magnesia after annealing heat treatment.

CHAPTER 5REFERENCES

- 5.1 The Dielectric Behaviour of Single Crystal MgO, Fe/MgO and Cr/MgO,
J.S.Thorp and N. Enayati Rad,
J.Mater.Sci.16, (1981), 255.
- 5.2 High Frequency Dielectric Properties of MgO, Fe/MgO and Cr/MgO,
J.S.Thorp, B.L.J.Kulesza, N.E.Rad, S.V.J.Kenmuir,
J.Mater.Sci.16, (1981), 1052.
- 5.3 Dielectric Properties of Single Crystal Co/MgO,
J.S.Thorp, M.D.Hossain and S.V.J.Kenmuir,
Solid State Comm. 58, (1981), 455.
- 5.4 Clustering and Electron Spin Resonance Linewidths in Fe/MgO,
A.D.Inglis and J.S.Thorp,
J.Mater.Sci.16, (1981), 1887.
- 5.5 Magnesio-ferrite Formation in Fe/MgO Single Crystals
A.D.Inglis, G.J.Russell and J.S.Thorp
J.Mater.Sci.17, (1982), 2939.
- 5.6 Magnesio-ferrite Formation in Heat-Treated Fe/MgO Powders
J.S.Thorp, A.P.Johnson and C.Savage,
J.Mater.Sci.Lett.4, (1985), 221.
- 5.7 G.P.Wirtz, M.E.Fine,
J.Appl.Phys. 38, (1967) 3729.

CHAPTER SIXDISCUSSION AND CONCLUSIONS6.1 Magnetic Properties of MgO

Previous work on single crystals of MgO substitutionally doped with iron suggested that, on heat-treatment at temperatures around 800°C in oxygen, the iron ions migrate to form clusters of magnesio-ferrite [6.0], or a super-paramagnetic precipitate of magnesio-ferrite [6.2]. That clustering effect was traced in powdered single crystal chippings using only a Gouy magnetometer. The susceptibility, or saturation magnetisation of the precipitate being very much greater than that of the paramagnetic iron doped MgO allowed the latter to be neglected to the first approximation; the initial, dramatic, rise in susceptibility levelling to an approximately constant value after several hours of heat-treatment being attributed to precipitate growth. However, as the susceptibility increase was traced for several different concentrations of dopant iron, the 'saturation susceptibility', i.e. the constant value reached after several hours of heating, was plotted for the different initial iron concentrations. Contrary to expectations, this plot did not produce a straight line, which would have implied that a constant fraction of the variant initial iron concentration formed clusters, but instead the saturation value was enhanced at higher initial iron concentrations.

The experiment was repeated but the Gouy balance was used to measure the variation in force at the balance with increasing applied field for each sample at each stage, and ESR measurements were made where possible. Careful analysis and interpretation of the results showed that a superparamagnetic precipitate had formed, presumably of

magnesioferrite, (with a view of reference 6.2 and employing the ESR traces) and that a larger proportion of the dopant iron had formed the precipitate in the samples having higher initial iron content. It was also obvious from the results of this study that apparent values of susceptibility could be somewhat misleading for samples containing non-paramagnetic, that is to say non-linear, impurity.

The chemical and X-ray diffraction analysis of magnesite (the starting material of the commercial process) both revealed the presence of iron as a major impurity, (0.1%) and as both the fusion and heat treatment stages of the manufacturing process involve temperatures in the region of 800°C, it seemed possible that a similar process could take place in the commercial powders leaving the magnetic precipitate in the final products. Magnetic phases in commercial MgO generally are of interest, not only because they tend to be electrically conducting compared with the magnesia, but also because, potentially at least, they are extractable from the non-magnetic MgO. If however, the iron or other impurity disperses through the magnesia as a less magnetic precipitate, then it would be expected that the impurity would be less readily removable. Thus samples of commercial powders taken from before and after the fusion, heat-treatment, and magnetic separation stages of the manufacturing process were analysed using the Gouy magnetometer, X-ray diffraction and E.S.R. techniques. A hand magnet was also used to separate magnetic material from the samples for close inspection, but no sufficiently large amount of material was extracted by this method to allow the above analysis to be made on the resulting samples.

The combination of the results from these studies show that iron, but not magnesio-ferrite, is present in the starting material, whereas after fusion magnesio-ferrite may be detected in all the samples investigated, but iron only in the sample taken from the very impure block region towards the centre of the melt. Further, the broad line found in these

samples containing magnesio-ferrite was very similar to that seen in the iron doped MgO sample. Clearly, magnesio-ferrite has been grown, and close inspection of the results for these materials both before and after grinding suggests that:

- (a) the black region of the fusion is the least pure and contains the most magnetic material;
- (b) the outer material of the fusion is more magnetic than that of the inner region, but is very inhomogeneous;
- (c) the magnetic impurity in the outer material of the fusion is more extractable using the hand magnet than that of the inner material; and
- (d) the inner material of the fusion is much more homogenous than the outer material of the fusion.

The most surprising of these conclusions, perhaps is (b); that the outer material of the fusion is more magnetic than the inner material; even though its value of susceptibility before grinding is negative (whereas that of the inner fused material is about $50 \text{ J T}^{-2} \text{ m}^{-3}$) after grinding, the outer material has the higher susceptibility value, suggesting that the magnetic material was present at the fusion stage, but remained undetected, presumably because it was sufficiently isolated to avoid inclusion in the samples. That feature was not apparent in the samples from the centre of the melt, the region being cooled very slowly compared to the outer region, and which therefore spends long periods (probably a number of hours) at about 800°C , the temperature at which iron is known to form a precipitate of magnesio-ferrite dispersed throughout the solid MgO. It is not then so surprising that more magnetic material can be readily extracted from the outer material than from the inner fused material.

All the results from the combination of X-ray, Gouy and E.S.R. techniques for samples taken before and after the magnetic separation

and the two heat treatment stages of the manufacturing process together suggest that:

- (a) the annealing type heat-treatment encourages growth of the magnetic impurity;
- (b) the quenching type heat-treatment discourages the growth of the magnetic impurity; and
- (c) the quench cooled material yields more easily extractable magnetic impurity at the magnetic separation stage.

Again, the annealing type heat-treatment holds the material at temperatures near 800°C for longer periods than the quench cooling treatment with the result seen also after fusion, that the magnetic impurity is less extractable. The more surprising feature is that the quench cooling appears actually to reduce the amount of magnetic impurity present as well as leaving it in a more extractable form. As the evidence from ESR studies suggests that the magnetic material is very lossy, it is proposed that, to improve the insulating properties of the commercial magnesia, the conditions that encourage the growth of the magnetic impurity should be avoided, i.e. the annealing heat-treatment and the slow cooling of the inner region of the fusion. Whilst an alternative to the annealing type heat-treatment exists in the quenching type treatment, it is less clear how the centre of the fusing melt might be cooled through 800°C more rapidly. It is possible that the use of smaller melts might increase the relative volumes of outer quenched material to inner annealed material. Certainly it is felt that where the magnetic impurity is more extractable, e.g. after grinding, further magnetic separation stages could be usefully added.

6.2 Electrical Properties of MgO

6.2.1 Conductivity Mechanisms in Single Crystals

The mechanism of conductivity in magnesium oxide has been studied by many workers [6.6,6.4]. In some early studies Mitoff [6.4] obtained

experimental evidence for electronic conduction. He has pointed out that the number of charge carriers is controlled by the number of lattice vacancies, which in turn, are governed mostly by impurities or by defects which are caused by the presence of these impurities; thus the conductivity is dominated by impurities. Yamaka and Swamoto [6.3] have also shown that the charge carriers in the conduction mechanism in MgO are electrons which originate from impurity levels.

Later work by Pollak and Geballe [6.5] first suggested hopping as a conductivity mechanism. They measured the complex conductivity of n-type silicon containing various kinds of impurities and attributed their results to polarization caused by hopping processes. Jonscher [6.6] interpreted the conductivity behaviour of over sixteen different materials in terms of the proposed hopping mechanism. He has shown that the hopping mechanism (similar to ionic and electronic conduction) leads to a characteristic frequency dependence [6.6]. Further, the dielectric responses of quite a wide range of materials show that the behaviour obtained departs from the Debye response and follows a "Universal Law" in which the dielectric constant, ϵ' and loss factor, ϵ'' can be written as

$$(\epsilon' - \epsilon_{\infty}) \propto \omega^{(n-1)} \quad (6.1)$$

$$\epsilon'' \propto \omega^{(n-1)}, \quad (6.2)$$

respectively, where ϵ_{∞} is the limiting permittivity of the material. The frequency dependence of the real part of the conductivity follows a relationship

$$\sigma(\omega) \propto \omega^n, \quad (6.3)$$

where the exponent, n , may lie in the range $0 < n < 1$ but is usually close to unity [6.6, 6.7]. One of the characteristics of this universal relationship is that the ratio of the imaginary part to the real part of the permittivity is independent of frequency:

$$\frac{\epsilon''(\omega)}{\epsilon'(\omega) - \epsilon_{\infty}} = \cot \frac{n\pi}{2} \quad (6.4)$$

This relationship is known as the Kramers-Krönig equation. The "Universal Law" has been extensively discussed by Jonscher [6.7] who pointed out that n is temperature dependent and by Austin and Mott [6.8].

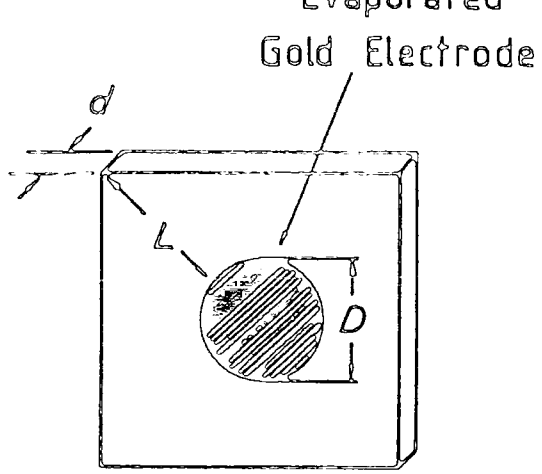
A recent systematic study has been made by Thorp and Rad [6.9]. The specimens which were measured in their experiments were pure MgO, Fe/MgO and Cr/MgO and were grown by electro-fusion from powders supplied by W & C Spicer Ltd, Cheltenham. All the specimens were single crystals and their compositions are tabulated in Table 6.1. For the measurements, the specimens were made in the form of square plates with dimensions 10 mm x 10 mm x 0.3 mm (Fig 6.1a) and the large parallel faces were polished to a 0.25 μm finish. Circular gold electrodes were evaporated onto the opposite polished surfaces of each specimen to ensure good electrical contact over a well-defined area between the crystal and the electrodes. To minimize the contribution to the conductance due to surface leakage over the edge of the sample [6.10] the diameter of the gold electrode was chosen to allow the crystal to project as much as possible beyond the electrodes.

The measurements of dielectric constant, ϵ' , and loss tangent, $\tan \delta$, (and consequently of a.c. conductivity) were made using a Wayne-Kerr bridge (Type B224), over the frequency range 500 Hz to 50 kHz.

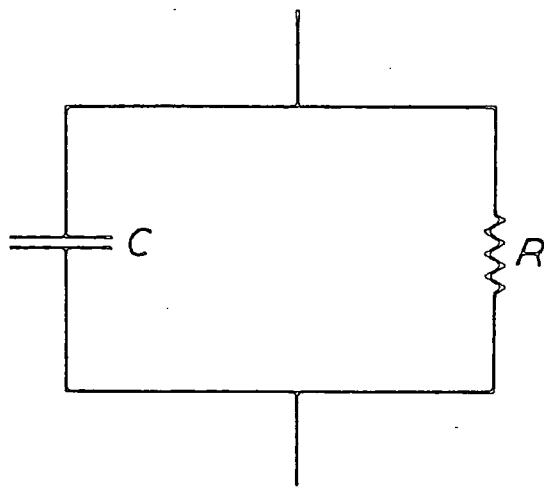
In this technique the capacitance and conductance of the specimen were measured directly. The components of the complex dielectric

Sample number	Nominal sample composition
1	MgO (pure)
2	MgO + 310 ppm Fe
3	MgO + 2300 ppm Fe
4	MgO + 4300 ppm Fe
5	MgO + 12800 ppm Fe
6	MgO + 800 ppm Cr
7	MgO + 1300 ppm Cr
8	MgO + 3600 ppm Cr

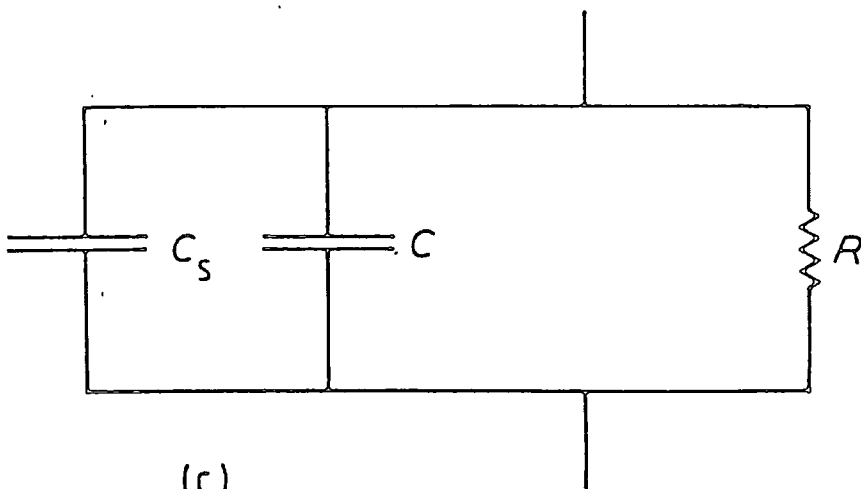
TABLE 6.1: Compositions of specimens investigated



(a) $d \ll D < L$



(b)



(c)

Figure 6.1. (a) General form of sample and (b) and (c) its equivalent circuits.

constant, ϵ'' , the loss tangent, $\tan \delta$, and the conductivity, σ , were derived from the equations:

$$\epsilon' = \frac{C}{C_0} ; \quad (6.5)$$

$$\tan \delta = \frac{\epsilon''}{\epsilon'} ; \quad (6.6)$$

$$\sigma(\omega) = \frac{dG}{A} ; \quad (6.7)$$

$$C_0 = \epsilon_0 \frac{A}{d} ; \quad (6.8)$$

where C is the measured capacitance with specimen, C_0 is the capacitance at the same spacing without specimen, G is the conductance of specimen, d is the specimen thickness, A is the area of electrode.

Since the changes in dielectric behaviour to be examined were small, the maximum precision in measurement was required and two correction factors, for surface leakage and stray capacitance, were necessary.

A correction term is required because of the edge effect resulting from the extension of the crystal beyond the electrodes [6.11]. The correction for the edge effect, C_e , ($\times 10^{-12}$ F) (with circular electrodes of the same diameter) is given by [6.12]

$$C_e = \frac{1.113 D}{8} \ln \left(\frac{8\pi D}{d} - 3 \right) \quad (6.9)$$

where D is the diameter of each electrode, and L is the distance shown in Fig.1a. Equation (6.5), then becomes

$$\epsilon' = \frac{C}{C_0 + C_e} \quad (6.10)$$

The formula assumes that the thickness of the gold electrode is negligible compared with the thickness of the specimen, d , a condition which was easily met.

A specimen can be represented by the equivalent circuit [6.13] shown in Fig 6.1b. In the capacitance measurement any stray capacitance due to the electrodes is included in the total quantity measured and so another correction factor is required before the actual capacitance of the specimen, C can be evaluated. The stray capacitance associated with the electrodes and connecting cables, C_s , is shown in Fig 6.1c. At low frequencies the inductance effect is not significant. It is assumed that the leakage admittance is eliminated by the use of the edge effect correction factor. The total capacitance, C_t , measured by the bridge when the specimen is placed between the electrodes is given by

$$C_t = C + C_s. \quad (6.11)$$

When the sample is removed from between the electrodes, the capacitance due to air and stray capacitance, C_A is measured, it is given by

$$C_A = C_o + C_s, \quad (6.12)$$

where C_o is the theoretical capacitance for air. By substitution for C_s from Equations (6.11) and (6.12) the capacitance of the sample is then given by

$$C = C_t - C_A + C_o. \quad (6.13)$$

For measurements on the type of material used in this work these corrections are significant and amount to about 8% of the total capacitance measured.

The variation of ϵ'' with frequency was first measured and it is shown in Fig 6.2. The plots are linear, following a relationship

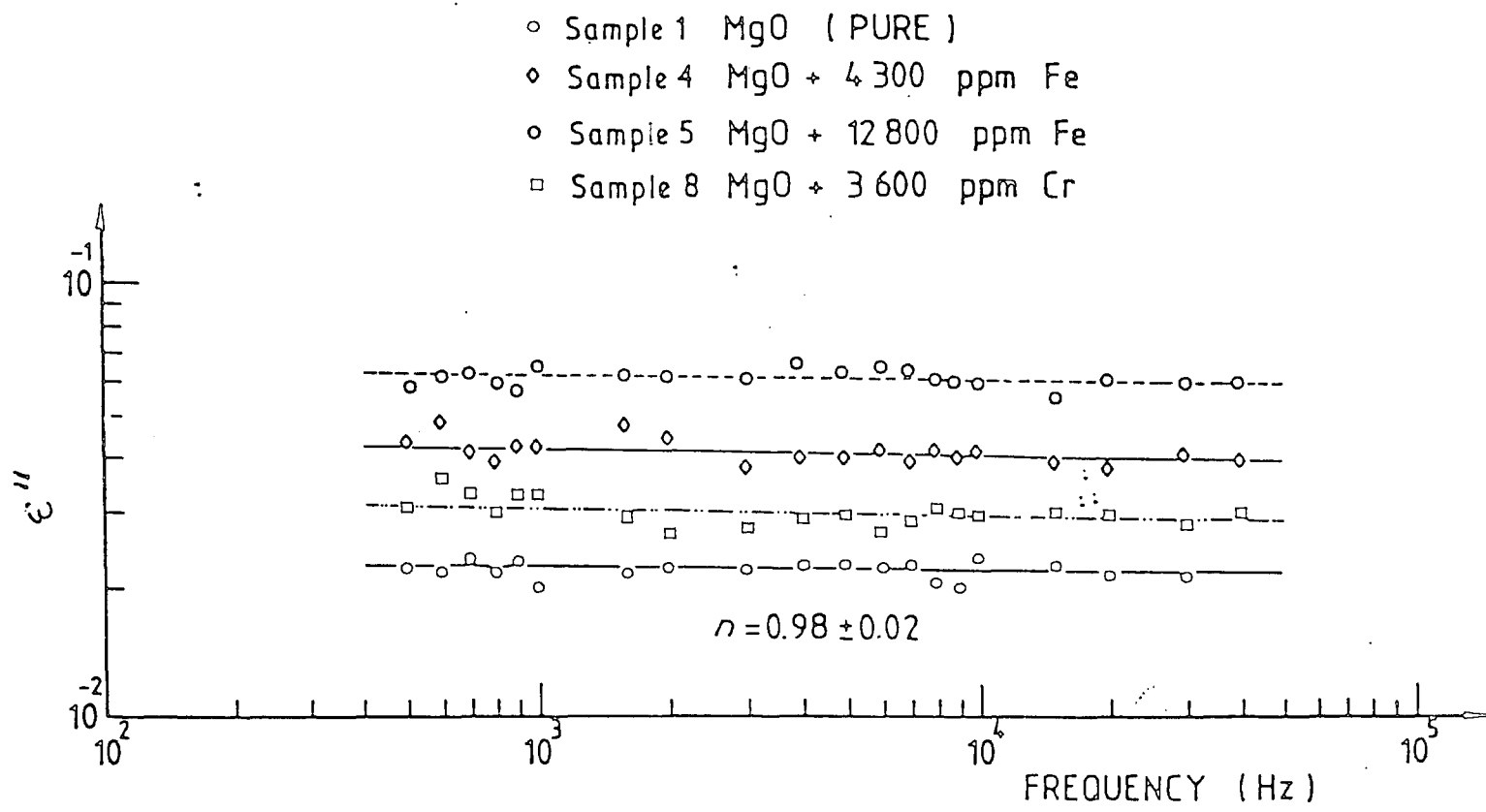


Figure 6.2. Variation of ϵ'' with frequency.

$$\epsilon''(\omega) \propto \omega^{(n-1)} \quad (6.14)$$

with $n = 9.98 \pm 0.02$; it should be noticed that the magnitude of n is the same for all the specimens. The loss factor, ϵ'' , at a particular frequency is higher for the doped specimens than for the pure MgO, giving corresponding increases in conductivity. Adding an equivalent concentration of chromium does not increase ϵ'' by as much as does the addition of iron.

The variation of $\log(\epsilon' - \epsilon_\infty)$ with $\log \omega$ was also plotted for the same specimens (Fig 6.3). In deriving this variation, ϵ_∞ , the limiting value of dielectric constant at high frequencies, was taken to be the value obtained in microwave dielectric constant measurements at 9.3 GHz. Once again all the plots of this variation for the doped specimens showed the same characteristic shape; all the characteristics are linear with the same slope, and all again fit the relation

$$\epsilon'(\omega) \propto \omega^{(n-1)} \quad (6.15)$$

with $n = 0.98 \pm 0.02$.

In order to clarify the effect of impurity concentration on permittivity and conductivity, plots of ϵ' against Fe-concentration and also of σ against concentration are shown in Fig 6.4a and b, respectively. It is seen that the variations of both ϵ' and σ are linear over the concentration range examined. There is inverse proportionality between ϵ' and concentration while σ is directly proportional to the concentration of Fe. A data list for some pure and doped crystals is given in Table 6.2.

6.2.2 Measurements on MgO Powders

When the material whose dielectric properties are to be examined is available only in powder form, adaptations have to be made to both the

- Sample 1 MgO (PURE)
- × Sample 4 MgO + 4300 ppm Fe
- Sample 5 MgO + 12800 ppm Fe
- Sample 8 MgO + 3600 ppm Cr

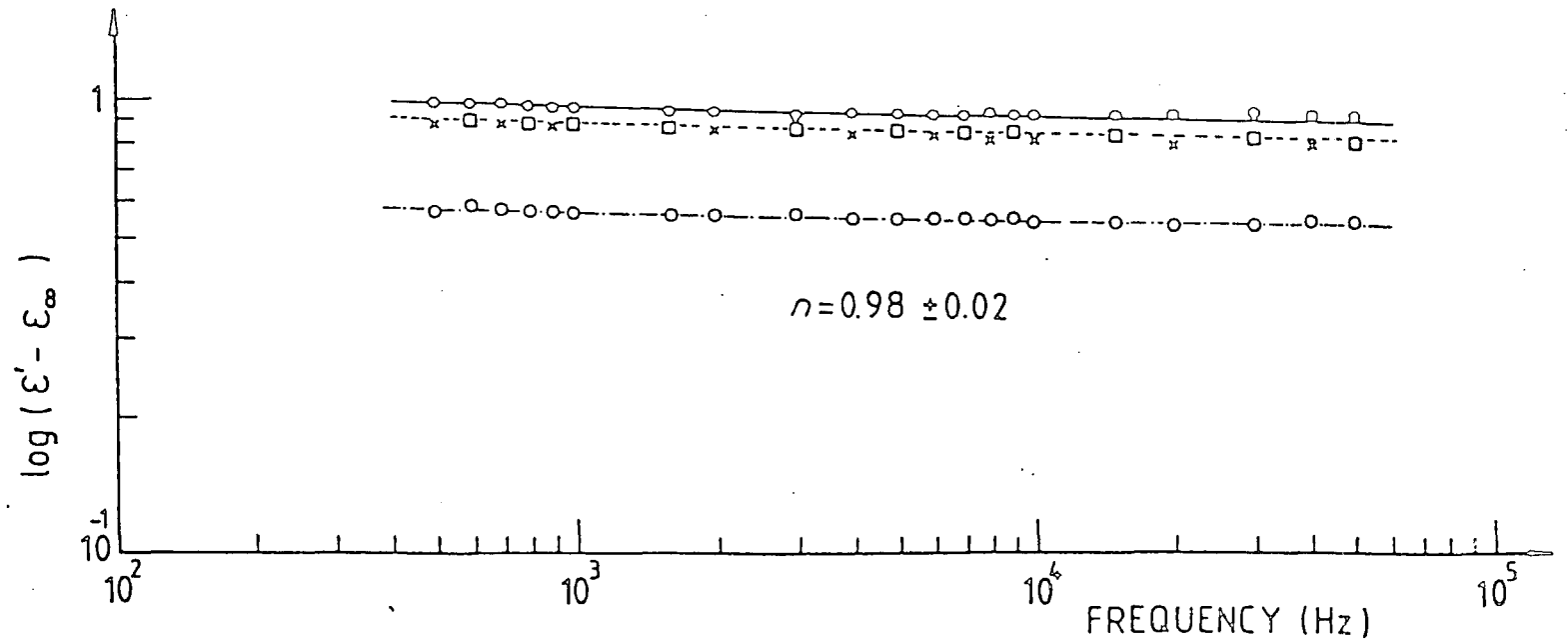


Figure 6.3. Variation of $\log(\epsilon' - \epsilon_{\infty})$ with log frequency.

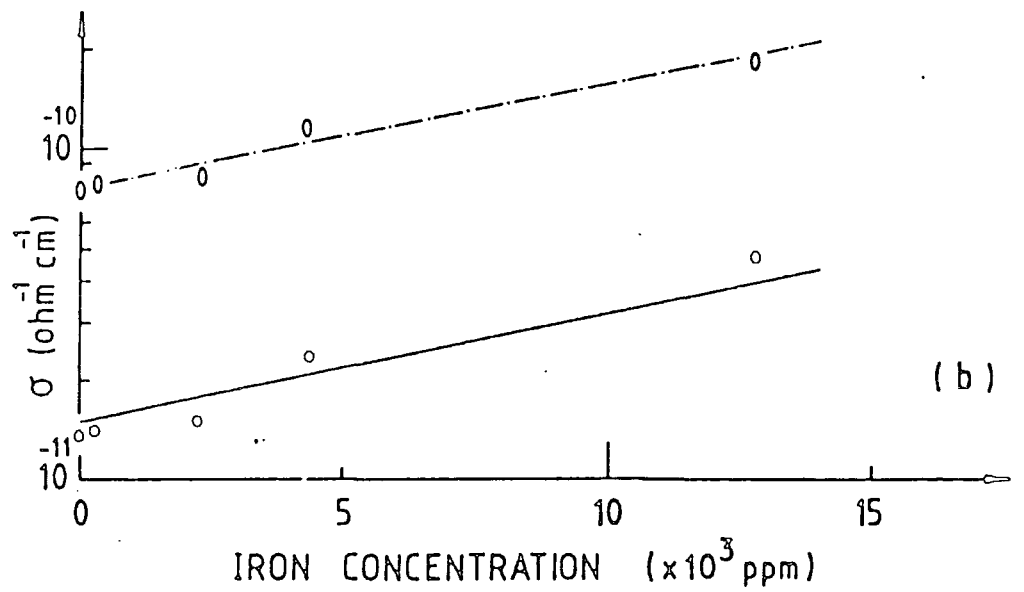
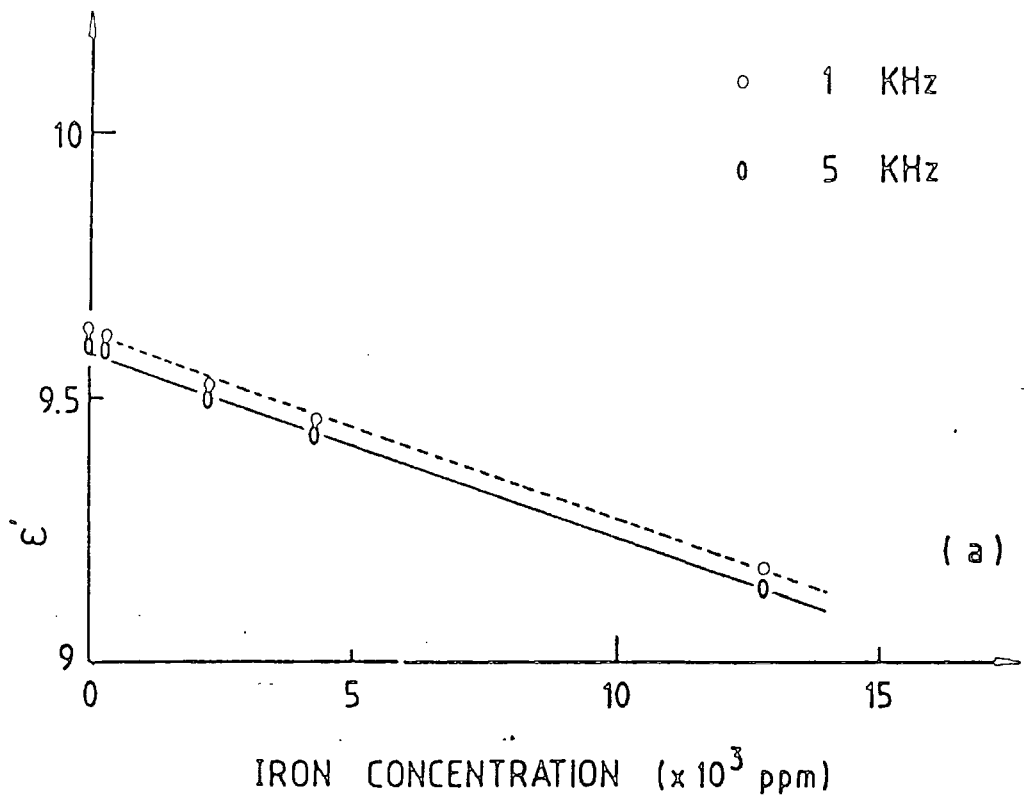


Figure 6.4. The dependence of (a) ϵ^0 and (b) σ on Fe concentration.

Specimen No	Nominal sample composition	ϵ'	$\tan\delta$ ($\times 10^3$)	Frequency, ω (Hz)
1	MgO Pure	9.62	2.16	1×10^9
2	MgO + 310 ppm Fe	9.62	2.49	1×10^9
3	MgO + 2300 ppm Fe	9.52	2.87	1×10^9
4	MgO + 4300 ppm Fe	9.46	3.91	1×10^9
5	MgO + 12800 ppm Fe	9.40	7.47	1×10^9
6	MgO + 800 ppm Cr	9.60	2.44	1×10^9
7	MgO + 1300 ppm Cr	9.28	3.15	1×10^9
8	MgO + 3600 ppm Cr	9.43	3.15	1×10^9

TABLE 6.2: Dielectric data for investigated samples at room temperature

experimental techniques and to the analysis of data. Those adaptations concern primarily the specimen holder arrangements and the corrections that must be applied to take account of the porosity of the powder sample in the measured state. A brief illustration of the methods generally employed is given in this section. As regards specimen holders, two widely used options are open. The first of those is to replace the solid sample cut from a bulk solid by a powder filled box (itself constructed from insulating material) for which due allowance is made; the second is to use some form of coaxial capacitor in which the powder to be examined acts as the dielectric between the inner and outer metallic conductors. It is convenient to use a geometry very similar to that actually employed in heating elements, (Figure 6.5) and this approach has been used here, (in collaboration with Dr.N.E.Rad) for making some preliminary electrical measurements on commercial magnesia powders.

Several steps have to be considered when deducing the dielectric properties of the powders from the measurable parameters. In the arrangement, some stray capacitance due to the connections to the element is included in the measured values, and a correction must be made to obtain the true capacitance and conductance of the element. When an element is connected to the bridge, the total capacitance, C_t , measured by the bridge is given by:

$$C_t = C + C_s \quad (6.16)$$

where C and C_s are true capacitance and stray capacitance respectively. It is necessary to find the capacitance C_a of an axially identical co-axial structure unfilled with powder. This is given by:

$$C_a = C_o + C_s \quad (6.17)$$

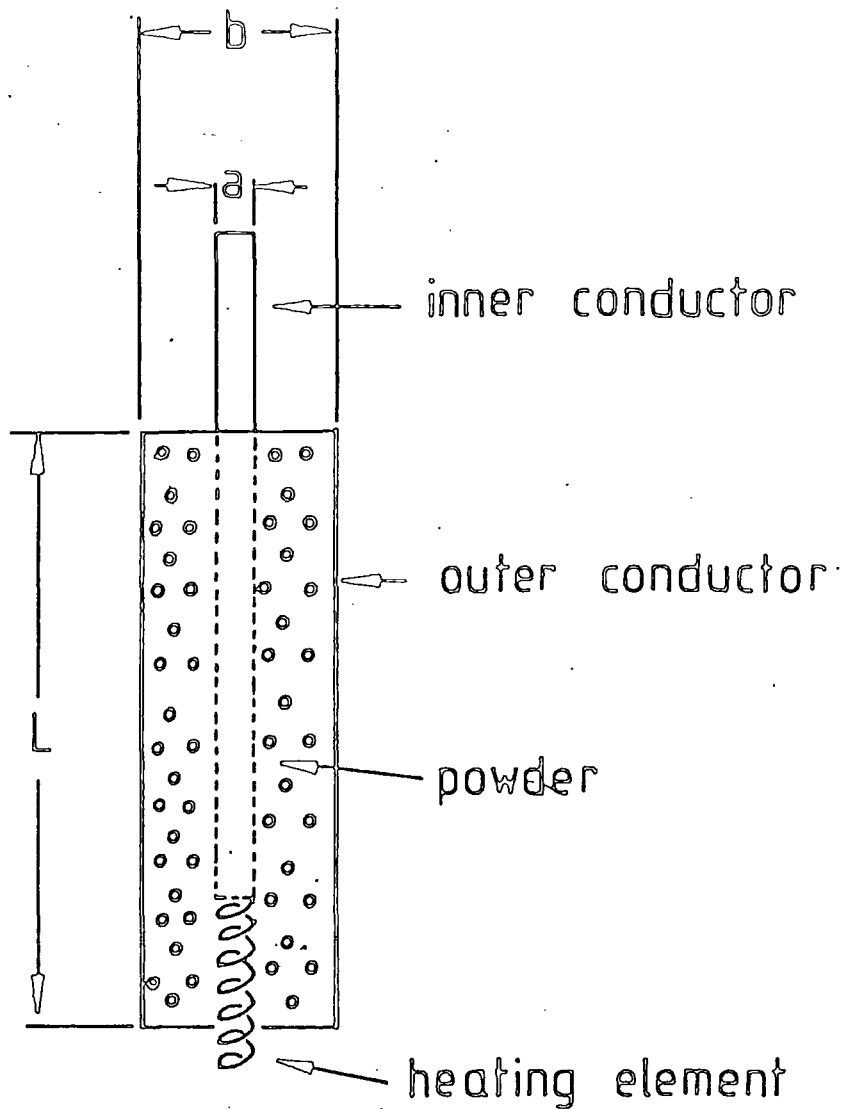


Figure 6.5. Schematic diagram of a section of a heating element (not to scale).

where C_o is the theoretical capacitance of the co-axial structure. For cylindrical geometry, the numerical value of C_o can be calculated using the relation:

$$C_o = \frac{2\pi\epsilon_o L}{\ln \frac{b}{a}} \quad (6.18)$$

where: L = length of the element;

b = inner diameter of the outer conductor;

a = diameter of the inner conductor;

ϵ_o = electric constant $(8.865 \times 10^{-12} \text{ Fm}^{-1})$.

With the unfilled element the two conductors can be kept in their relative coaxial positions using two very thin dielectric sheets for which it is reasonable to assume that the capacitance and conductance values are negligible by comparison with the totals for the whole element. Using equations 6.1 and 6.2, the true capacitance of the element with a powder in it is given by:-

$$C = C_t - C_a + C_o \quad (6.19)$$

In this method, C_t and C_a are the experimentally measured quantities, and C_o is found by calculation, so the net conductance of the element, G , can be derived using the relation:-

$$G = G_t - G_a \quad (6.20)$$

where: G_t = measured conductance of an element;

G_a = measured air conductance of equivalent geometric shape.

The components of the complex dielectric constant of the powder filling of the element, ϵ'_p and ϵ''_p can then be deduced from the equations:-

$$\epsilon'_p = \frac{C}{\epsilon_0} ; \quad (6.21)$$

and

$$\tan \delta = \frac{G}{\omega C} = \frac{\epsilon''_p}{\epsilon'_p} \quad (6.22)$$

where: C = net capacitance of the element;

G = conductance of the element;

ω = angular frequency = $2\pi f$.

The actual measurement of C_c and C_a can be made by a.c. bridge and Q-meter methods similar to those described in section 6.2.1.

The form of the results is shown in Figures 6.6 and 6.7. Considering first the permittivity data, (Fig.6.6) several features emerge, some of which are in startling contrast to the corresponding behaviour of single crystal material. Of those, the most evident is a very pronounced frequency dependence, the indication being that the frequency independent behaviour characteristic of single crystal material may apply only at frequencies greater than 10 Hz. Second, it is apparent that the technique is sensitive enough to show differences due to differing heat treatments of the same starting powder, annealing type heat-treatment increases ϵ'_p and quench cooled treatment decrease ϵ'_p with respect to the values for powders before heat-treatment. (It should be noted that ϵ'_p is the permittivity of the powder as packed in the co-axial test capacitor; direct comparison of the magnitude of ϵ'_p with ϵ' for single crystal material is not appropriate because information is not available here for the respective packing densities of the powders which, though constant, are unknown).

The dielectric loss data is shown in Fig.6.7. Here again the frequency dependence of ϵ''_p is very marked. The other important feature is the very high values of loss; these correspond to $\tan \delta \approx 1.2$ at 100 Hz falling to $\tan \delta \approx 5 \times 10^{-2}$ at 10^4 Hz which indicate losses in the

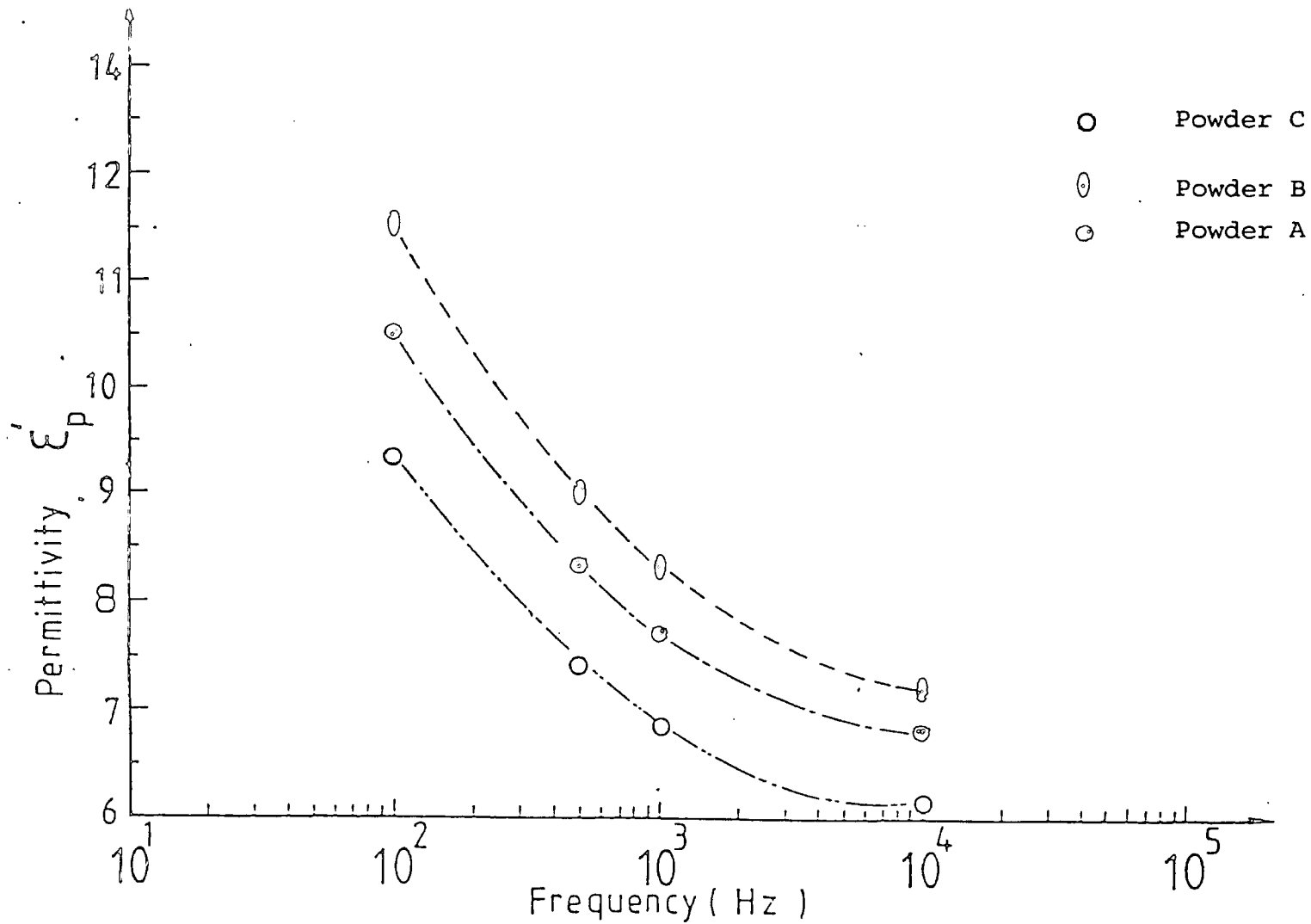


Figure 6.6. Permittivity - frequency variations for commercial MgO powders taken from the central region of a fused melt. Powder A, not heated; Powder B, with annealing heat treatment; Powder C, heat treated and quench cooled.

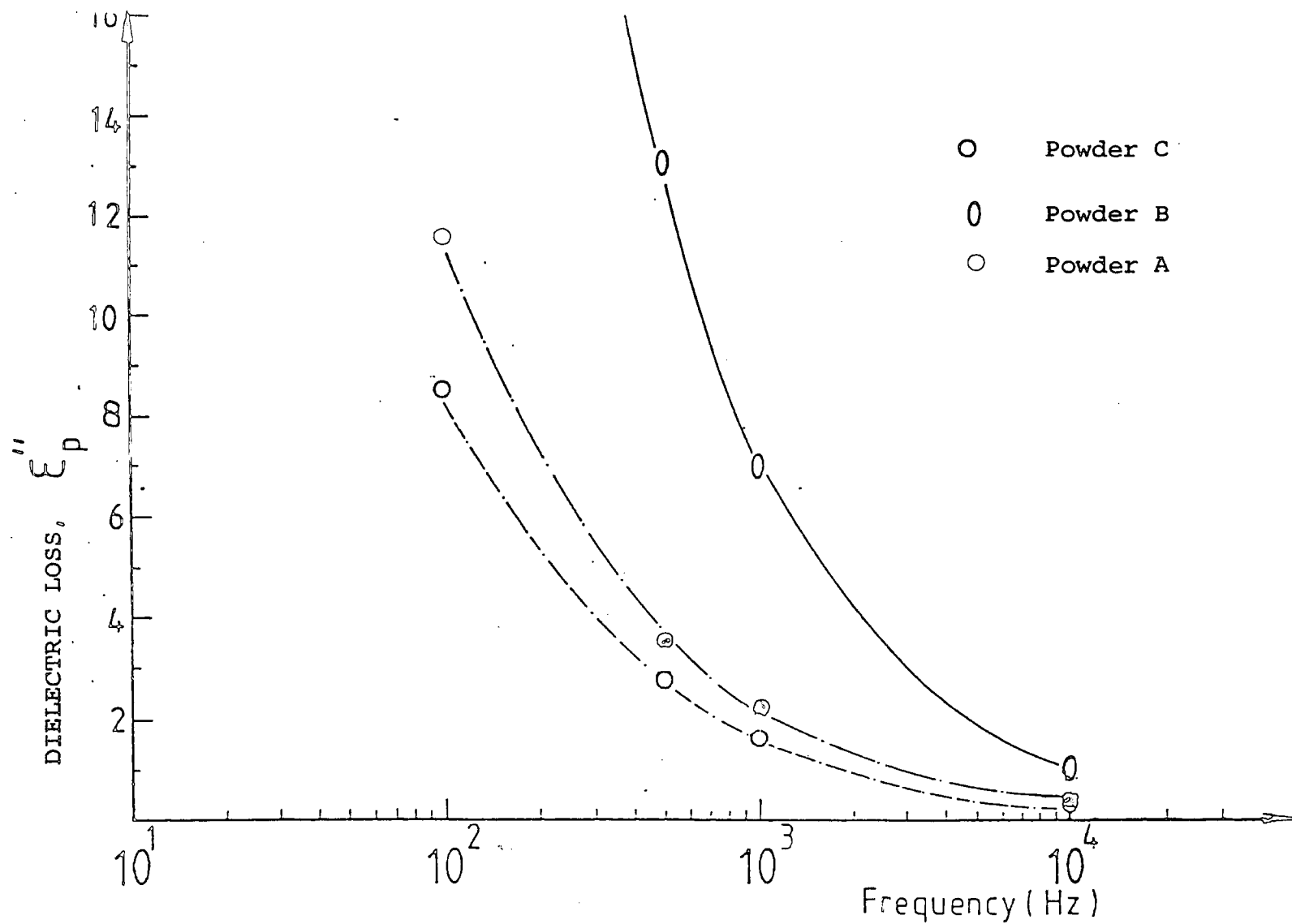


Figure 6.7. Dielectric loss - frequency variation for commercial MgO powders taken from the centre of a fused melt. Powder A, unheated; Powder B, annealing heat treatment; Powder C, heat treated and quench cooled.

powder material some two or three orders of magnitude greater than those obtained in single crystals, ($\tan \delta \sim 2 \times 10^{-3}$ at 10 kHz). The extent to which these differences can be attributed to inter-granular and surface-state effects remains to be elucidated.

6.2.3 The Dielectric Properties of Magnesio-Ferrite

It was shown that one of the impurity phases of the commercial powders, which could be positively identified by the magnetic and analytical studies described earlier, was magnesio-ferrite, $\text{Mg Fe}_2\text{O}_4$. This material can be obtained in pure powder form from chemical suppliers, and an attempt was made, in collaboration with Mr.M.Akhtarazzaman, to determine the dielectric properties of magnesio-ferrite directly. The material is extremely lossy and hence a dielectric dilution technique was used, in which increasing amounts of pure powder were added to major quantities of pure MgO powder. Each well-mixed powder was placed in turn in a cylindrical disc-shaped insulating holder to form a "parallel-plate" capacitor whose properties could then be found using conventional a.c. bridge techniques. A range of mixed powders containing from 1% $\text{Mg Fe}_2\text{O}_4$ in MgO to 60% $\text{Mg Fe}_2\text{O}_4$ in MgO were examined. The effect of increasing the magnesioferrite concentration on the permittivity is shown in Figure 6.8, from which it appears that even small percentages of ferrite increase the permittivity vary considerably compared with that of the pure MgO. The corresponding dielectric loss data is given in Figure 6.9, where the high values of ϵ''_p are to be noted. A tentative comparison can be made with the available data for pure MgO quoted in earlier sections. For pure MgO we may take ϵ' to be about 10 and ϵ'' about 2×10^{-2} giving $\tan \delta \sim 2 \times 10^{-3}$ at 1 KHz. Thus it appears that the addition of quite small quantities of magnesioferrite to magnesia can increase the loss by as much as two orders of magnitude. It is also of note (Fig.6.10) that with the mixed

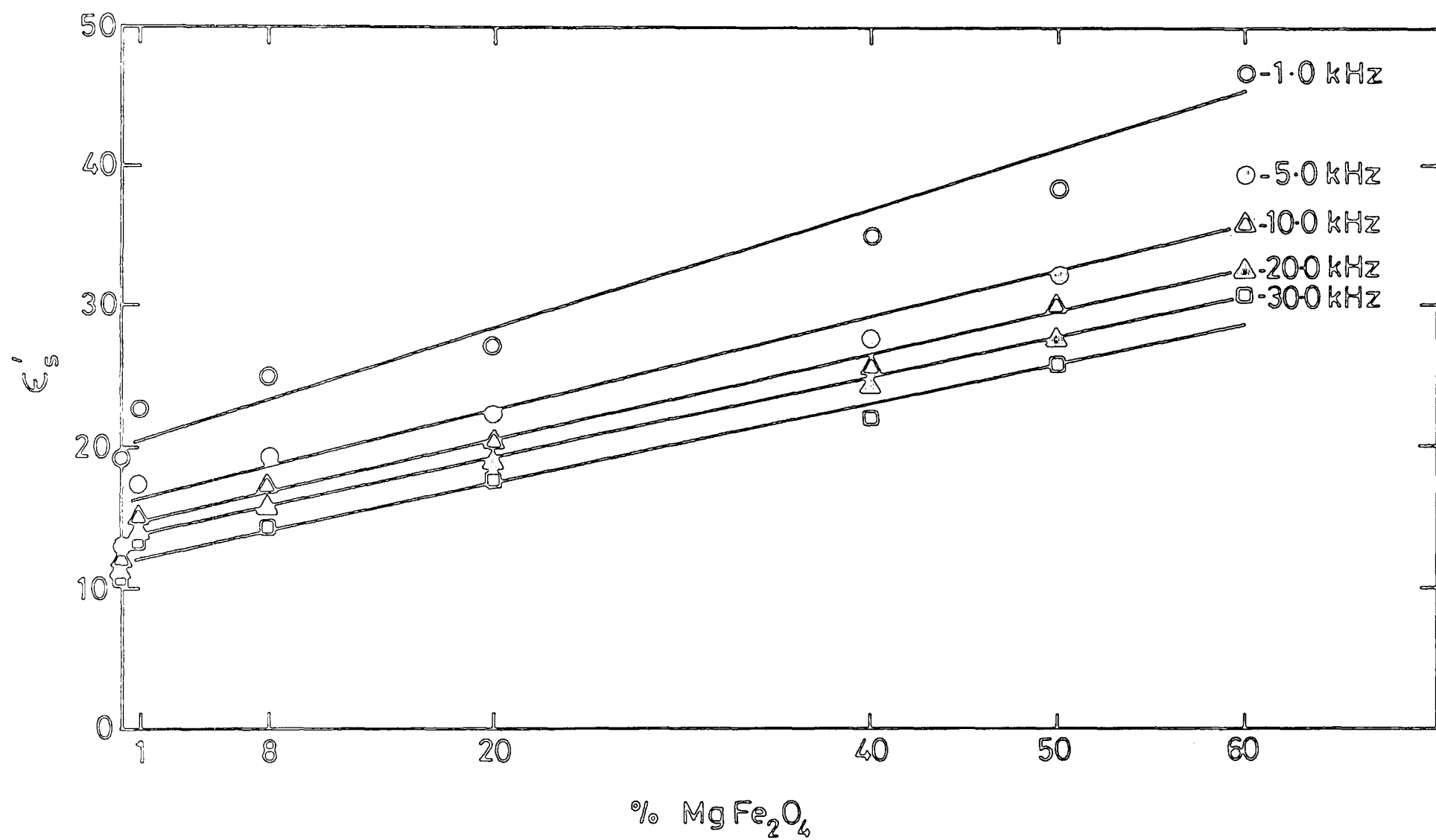


Figure 6.8. The permittivity - concentration dependence of mixed $\text{MgFe}_2\text{O}_4 / \text{MgO}$ powders.

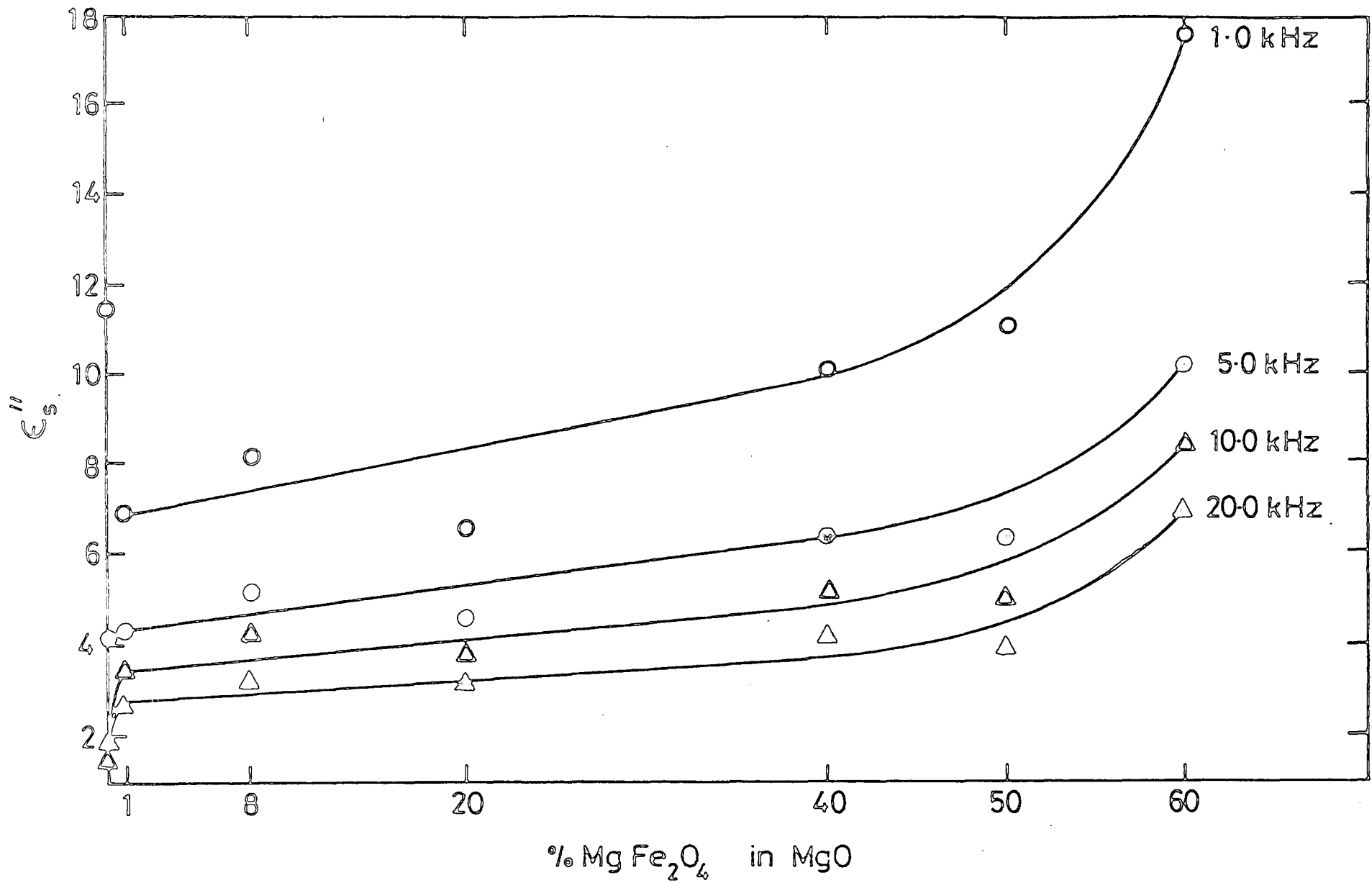


Figure 6.9. The dielectric loss - concentration dependence of mixed $\text{Mg Fe}_2\text{O}_4/\text{MgO}$ powders.

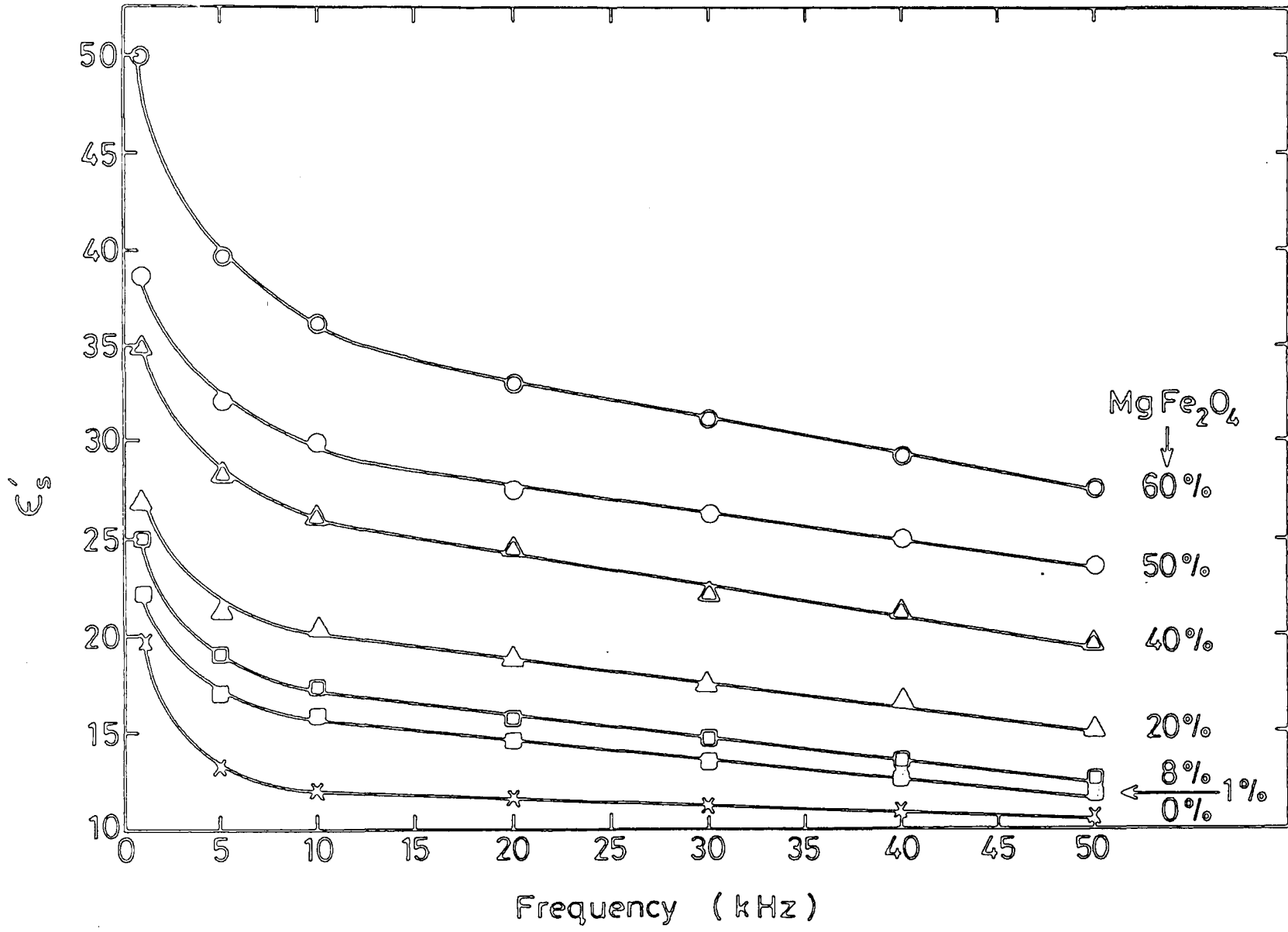


Figure 6.10. Frequency dependence of permittivity in mixed $\text{MgFe}_2\text{O}_4 / \text{MgO}$ powders.

powders there is also a very marked frequency dependence giving very high values of ϵ'' at low frequencies.

6.3 Suggestions for Future Work

Further to aid the manufacturers of magnesium oxide it would be helpful to know more detail about the magnetic phases present. In this study it has been difficult to distinguish between the various spinel structures, for example, between $\text{Mg Fe}_2\text{O}_4$ and $\text{Mn Fe}_2\text{O}_4$, from the results obtained from the techniques employed; the lattice parameters of this group are too similar to distinguish them using X-rays, and the other techniques cannot be used to identify phases. The use of techniques such as RHEED (reflection high energy electron diffraction), and Transmission Electron Microscopy (TEM) might be used to distinguish their similar lattice parameters. Electron microscopy might also be of use in determining the size of the precipitate particles formed in the iron doped magnesia samples, and perhaps to identify which if any of the commercial powders contained such a precipitate. This study could help to determine the diameters of the fusion at which the magnetic impurity was found in a less separable form. Failing that, it may be that the

ESR spectra of the two ferrites (i.e. Mg and Mn ferrite) are sufficiently different to establish which is the cause of the broad line feature seen in the commercial powders. However, to date, no source of pure $\text{Mn Fe}_2\text{O}_4$ has been found. Thus a similar experiment to that for iron doped MgO could be repeated for Manganese doped MgO.

Alternatively, those phases may be distinguishable by their Curie temperatures. To this end a sample containing magnetic impurity could be suspended between the poles of the Gouy magnetometer and the variation of force at the balance with temperature plotted. As the ferri- or ferro- magnetic reached its Curie point and became paramagnetic a discontinuity would appear on the force v. temperature plot. Nonetheless, the unambiguous interpretation of the asymmetric broad line

feature seen in the ESR spectra of some of the commercial powders could remain a problem.

The main area of interest to the commercial manufacturer is whether it is the magnetic impurities that are of prime importance, or whether there are non-magnetic impurities that are more harmful to the insulating properties of their products. For the most part their product is for use in the domestic market and therefore conductivity at 50 Hz is of most interest. Tests at that frequency on pure MgO doped or mixed with various concentrations of the pure phases identified as impurities by the X-ray diffraction would meet that point, and might also assist in determining which of the magnetic phases was the most harmful, and in what form, so that heat-treatments could be designed specifically to reduce the amounts of those impurities.

Similarly, the commercial manufacturer is most interested in the conductivity of powder. To date little or no systematic study of the effects of grain size distribution or of packing density on the electrical insulating properties of powders has been carried out.

Finally the typical operating temperatures of a domestic heating element are 800°C at the centre dropping to between about 10 to 100°C at the outer surface. Again, conductivity measurements at these temperatures would be more pertinent. Other applications of magnesia products may involve different temperatures and frequencies, and it may be found that a different set of impurities become more relevant in each different environment.



CHAPTER SIX

REFERENCES

- 6.1 A.D.Inglis, J.S.Thorp,
Jour.Mater.Sci.16, (1981), 1887.
- 6.2 A.D.Inglis, G.J.Russell, J.S.Thorp,
Jour.Mater.Sci.17, (1982), 2939.
- 6.3 E.Yamaka, K.Sawamoto,
Jour.Phys.Soc.Japan, 10, (1955), 432.
- 6.4 S.P.Mitoff,
J.Chem.Phys.31, (1959), 1261.
- 6.5 M.Pollack, T.H.Geballe,
Phys.Rev.122, (1961), 1742.
- 6.6 A.K.Jonscher,
Jour.Phys.C.Sol.St.Phys.6, (1973) L 235.
- 6.7 A.K.Jonscher,
Nature, 267, (1977), 719.
- 6.8 I.G.Austin, N.F.Mott,
Adv.Phys.18, (1969), 41.
- 6.9 J.S.Thorp, N.E.Rad,
Jour.Mater.Sci.16, (1981), 255.
- 6.10 L.Hartshorn, W.H.Ward
J.Inst.Elec.Eng 79, (1936), 597.
- 6.11 A.C.Lynch,
Proc.IEEE, 104B, (1957), 359.
- 6.12 A.H.Scott, H.L.Curtis,
J.Res.Nat.Bur.Stan., 22, (1939), 747.
- 6.13 I.Chamberlain, G.W.Chantry,
H.F.Dielectric Measurements Scientific Technical Press
Ltd,1972

APPENDIX

Magnesian-ferrite formation in heat-treated Fe/MgO powders

J. S. THORP, A. P. JOHNSON, C. SAVAGE

Department of Applied Physics and Electronics, University of Durham, South Road, Durham, UK

In previous studies on single crystals of iron-doped magnesium oxide (Fe/MgO), in which the phenomena of clustering [1] and magnesian-ferrite formation [2] were examined, the main experimental data were derived from electron spin resonance measurements. The use of this technique followed the original interest in the interpretation of the apparent independence of the observed ESR linewidths on iron concentration [3, 4]. In the first examination of clustering effects [3] the electron spin resonance linewidths and integrated intensities of Fe³⁺ in cubic sites in as-grown single crystal Fe/MgO were measured at 9 GHz between 293 and 90 K for iron concentrations ranging from 100 to 12 900 ppm; it was found that very little of the iron was present in cubic sites as isolated Fe³⁺ ions, which suggested a degree of clustering into non-paramagnetic complexes even at extremely low concentrations. In the later work [2] a similar range of iron-doped MgO single crystals were examined before and after heat treatment in oxygen in the temperature range 600 to 800° C. Before heat treatment the only magnetic resonance spectrum seen was due to isolated Fe³⁺ ions in cubic sites whilst electron diffraction revealed only MgO. However, after heat treatment, a strong anisotropic line was found which exhibited the characteristics of ferrimagnetic resonance and whose presence was coupled with the appearance in the electron diffraction pattern of a spinel pattern superimposed on that of the MgO. Analysis of the anisotropy of the ferrimagnetic resonance line gave values of the room temperature magnetization, first anisotropy constant and Curie temperature which, in view of their close agreement with other published data [5, 6], suggested magnesian-ferrite formation even at very low iron concentration. The present work was undertaken to confirm the formation of magnesian-ferrite by direct measurements of susceptibility. In this complementary means of examination it may be noted that both undoped MgO

and Fe/MgO (in which the iron enters substitutionally as isolated Fe³⁺ ions at cubic sites) will both be paramagnetic and therefore have magnetic susceptibilities very low compared with that to be expected from the ferrimagnetic magnesian-ferrite. The formation of additional phases in heat treated magnesia is of relevance and importance in connection with permittivity and dielectric loss studies [7, 8] on this material which is widely used (in powder form) as an insulator in heating elements.

In contrast to the previous studies (i.e. [1, 2]), in which all the measurements were made on doped single crystals, it was decided here to use material in powder form partly because this was more convenient for the Gouy magnetometer available and partly to enable a comparison with bulk single crystal material to be made. However, in order to preserve the benefit of having well characterized starting material, each specimen was prepared by grinding single crystal chippings of the same composition and growth batch as the corresponding doped single crystal. The single crystal chippings, grown by electro-fusion by W & C Spicer Ltd. (Cheltenham), had iron concentrations ranging from 2300 ppm to 12 900 ppm as determined by atomic emission or X-ray fluorescent analysis. The measurements were made at room temperature using conventional Gouy balance techniques, i.e. the force (F) exerted on a volume susceptibility (χ_v) was derived from the relation

$$F = \frac{1}{2} \chi_v \alpha (H_A^2 - H_B^2) (\rho_1 / \rho_2)$$

where H_A and H_B refer to the field values at the ends of the specimen, α is the cross-sectional area of the specimen and ρ_1 and ρ_2 represent the packing density of the powder and the density of magnesium oxide, respectively. Corrections were made for the small susceptibility of the glass specimen tube and the overall accuracy of the measurements was estimated to be about $\pm 5\%$. The ageing heat treatment consisted of heating the powdered

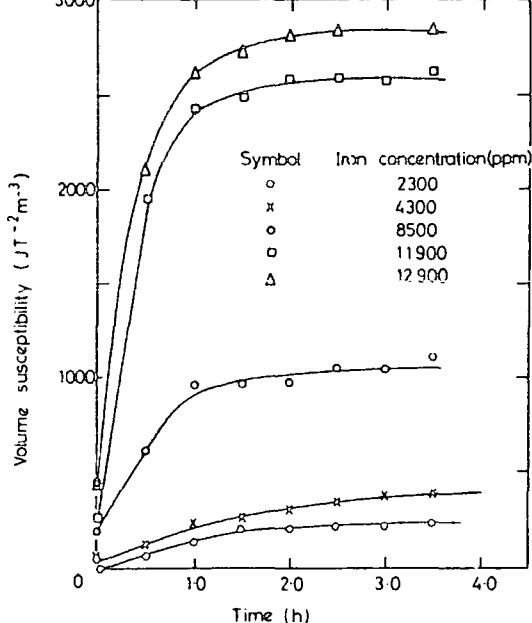


Figure 1 Variation of volume susceptibility with length of heat treatment.

specimens in oxygen at 800°C for successively longer periods of time; this heat treatment had been shown previously [2] to correspond to the conditions necessary for the formation of the ferrimagnetic resonance line. The magnetic susceptibility was measured before heat treatment and at intervals during ageing; ageing times of up to four hours were used since preliminary experiments showed that there were no pronounced changes subsequently.

The collected results for the iron-doped magnesia powders examined are shown in Fig. 1 in which the susceptibility is plotted as a function of ageing time for each level of iron concentration. In Fig. 1 several points may be noted. For each specimen, corresponding to a particular doping level, there is a marked increase in susceptibility with time; the rate of increase is largest in the initial stages of ageing and subsequently decreases to zero so as to give a constant value of susceptibility after about 2 h ageing; this plateau region extends to the maximum ageing times used (about 4 h). Comparison of the behaviour of the different specimens shows that the susceptibility values in the plateau regions increase successively with increasing iron concentration although the times taken for the various specimens to reach the plateau region are approximately constant. The data given in Fig. 1 provides direct evidence for the formation of a

high-susceptibility magnetic phase after heat treatment and the occurrence of a plateau in each instance implies that all the available iron has been converted. The higher values of resultant susceptibility after ageing for the higher iron concentrations are to be expected on the grounds that more iron is available for conversion. Examination of the data for the specimens in the "as-grown" state, i.e. before ageing, also shows that whereas the susceptibility of the specimen with the lowest doping level (2300 ppm Fe) is comparable with that of pure (undoped) MgO, there is a significant increase in initial susceptibility with concentration. Although even in the extreme case of the 12900 ppm Fe specimen this initial increase (to $0.4 \times 10^3 \text{ JT}^{-2} \text{ M}^{-3}$) is still quite small in comparison to the much greater increase (to $2.8 \times 10^3 \text{ JT}^{-2} \text{ M}^{-3}$) after 4 h ageing, this result provides confirmation of the deduction from magnetic resonance Fe^{3+} spin-count data [1] that in the as-grown crystals not all of the iron is in the Fe^{3+} state.

The validity of a two-phase model for the system may be assessed by examining the variation of this resultant susceptibility with iron concentration in terms of the applicability of Weidemann's law. If one postulates a two phase system consisting of the pure MgO (or MgO containing Fe^{3+} substituted as isolated ions at cubic sites) and a single magnetic phase, the magnesioferrite phase, the overall resultant susceptibility will be given by

$$\chi_T = C_1 \chi_{\text{MgO}} + C_2 \chi_{\text{Magnesioferrite}}$$

where C_1 and C_2 are the respective weight fractions of the two phases. Here $\chi_{\text{MgO}} \ll \chi_{\text{Magnesioferrite}}$ so to a good approximation the resultant susceptibility should vary linearly with iron concentration. When the equilibrium value data from Fig. 1 are used to show the variation of resultant susceptibility with iron concentration the plot of Fig. 2 is obtained. Up to concentrations of 8300 ppm Fe a reasonable fit to a linear variation is obtained but it is noticeable that the points corresponding to the two higher concentrations depart considerably from the extrapolation of the line fitting the lower concentration data. This suggests the possibility of the breakdown of the two phase model and the occurrence of an additional magnetic phase at high doping levels. It is interesting to note also that the magnetic resonance data [2] showed that an

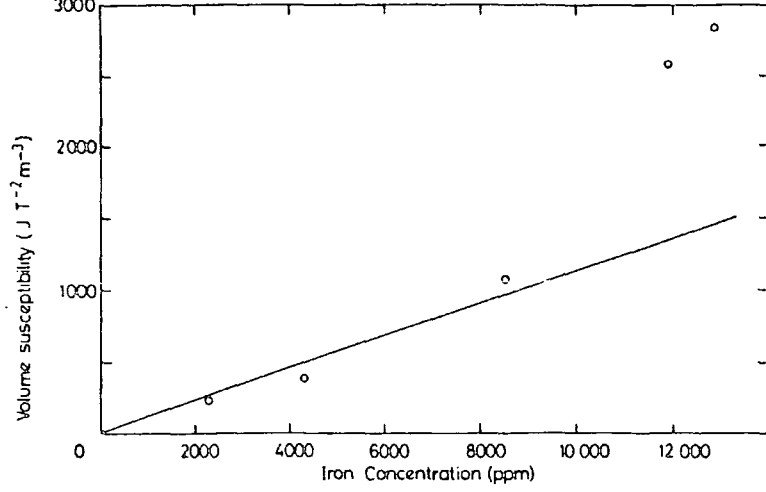


Figure 2 Variation of volume susceptibility with iron concentration.

intermediate state characterized by a strong isotropic ESR line, exists as a precursor to the formation of fully ferrimagnetic material and the present work suggests that the use of a combination of susceptibility and ESR measurements would be a fruitful method of making a more detailed examination of the Fe/MgO system.

References

1. A. D. INGLIS and J. S. THORP, *J. Mater. Sci.* 16 (1981) 1887.
2. A. D. INGLIS, G. J. RUSSELL and J. S. THORP, *Ibid.* 17 (1982) 2939.

3. J. S. THORP, R. A. VASQUEZ, C. ADCOCK and W. HUTTON, *ibid.* 11 (1976) 89.
4. A. D. INGLIS and J. S. THORP, *ibid.* 16 (1981) 2628.
5. G. P. WIRTZ and M. E. FINE, *J. Appl. Phys.* 38 (1967) 3729.
6. R. S. DE BIASI and T. C. DEVERAS, *J. Amer. Ceram. Soc.* 59 (1976) 55.
7. J. S. THORP and N. ENAYATI-RAD, *J. Mater. Sci.* 16 (1981) 255.
8. J. S. THORP, B. L. J. KULESZA, N. E. RAD and S. V. J. KENMUIR, *ibid.* 16 (1981) 1052.

Received 12 June
and accepted 9 July 1984

